

ABSTRACT

Title of Document: Investigating the mechanism of the hydrogen peroxide photoproduction from chromophoric dissolved organic matter

Yi Zhang, Doctor of Philosophy, 2014

Directed By: Professor Neil Blough
Department of Chemistry

The photochemical pathways for H_2O_2 production from chromophore dissolved organic matter (CDOM) were investigated extensively, employing in part a selective sodium borohydride reduction method to examine the structural basis of the H_2O_2 formation. Estimates of the lifetime of possible H_2O_2 precursor(s) have been acquired by examining the dependence of H_2O_2 production rates on dioxygen concentration. The results suggest that H_2O_2 arises from intramolecular electron transfer from an excited singlet donor to a ground-state acceptor. Possible donors include substituted phenols, while possible acceptors included quinones, which unlike ketones/aldehydes are not irreversibly reduced by borohydride.

The relationship between the rate of H_2O_2 formation and the rate of formation of reducing intermediate(s) upon irradiation of CDOM was thoroughly investigated employing a molecular probe. The results obtained from the dependence of dioxygen concentration and wavelength indicate that approximate 90% of produced one-electron reducing intermediates is converted to superoxide. The stoichiometric ratio between the H_2O_2 and total reducing radicals suggests that 67% of the photochemically produced superoxide decays through oxidant sinks other than dismutation to H_2O_2 .

The effect of adding external phenol electron donors on the H_2O_2 production rate was also examined. Substantially enhanced rates of H_2O_2 production were observed, which were substantially inhibited by borohydride reduction (40-50%), similar to the loss of TMP previously reported. In addition, H_2O_2 production rate increased as the dioxygen concentration decreased, consistent with reaction with a triplet state intermediate. The results all indicate that an additional pathway of H_2O_2 formation is introduced in the presence of sufficiently high concentrations of electron donors. Reaction between the phenol electron donors and the excited triplet states of aromatic ketones/aldehydes yields a ketyl radical that subsequently react with O_2 to form O_2^- and then H_2O_2 . The enhancement generally follows the reduction potential of the added phenols, as $\text{DMOP} > \text{MOP} > \text{PHE}$, with the exception of TMP. In the case of TMP, secondary radical reactions could be the cause of this difference.

INVESTIGATING THE MECHANISM OF THE HYDROGEN PEROXIDE
PHOTOPRODUCTION FROM CHROMOPHORIC DISSOLVED ORGANIC
MATTER

By

Yi Zhang

Dissertation submitted to the Faculty of the Graduate School of the
University of Maryland, College Park, in partial fulfillment
of the requirements for the degree of
Doctor of Philosophy
2014

Advisory Committee:

Professor Neil V. Blough, Chair/Advisor

Professor Catherine Fenselau

Professor Daniel E. Falvey

Professor Alice C. Mignerey

Professor Karen L. Prestegard

© Copyright by
Yi Zhang 2014

Dedication

To my beloved family

Especially to my Dear Uncle Professor Cao, Liezhao for being standing behind me all the time

Wish you could see this from heaven

Acknowledgements

I would like to sincerely thank my advisor, Professor Neil V. Blough for his guidance, patience, encouragement, and support through my graduate career. From him, I have learned not only science knowledge, problem solving skills, but also methods of critical thinking, manner of preciseness, quality of patience and the most importantly, the spirit of pursuing for the truths, all of which will be truly valuable for my future career.

My sincere appreciation extends to my advisory committee members, Dr. Daniel Falvey, Dr. Catherine Fenselau, Professor Alice C. Mignerey and Professor Karen L. Prestegaard for their assistance and time.

I'd like to express my thanks to Dr. Mohamad Al-Sheikhly at the Department of Materials Science and Engineering, from whom I received help utilizing the Electron Paramagnetic Resonance to solve difficulties in my research.

I also would like to thank my friends and colleagues in the Blough research group, Dr. Rossana Del Vecchio, Dr. Jiahai Ma, Dr. Min Jia, Dr. Lynne Heighton, Andrea Andrew, Kelli Skiorski, Dan Baluha, Tara Schendorf, and Kevin Khoech for all the inspiring research discussions, as important as all those little causal talks keeping me fresh and alive. It meant everything for me always having your companies and supports around.

I thank my life mentor Professor Yuan Hu at USTC, China. Your excellent wisdom and generosity walk me through all the difficulties not only for my research, but life.

I thank my family and all my friends for their love and support. Thank you mother, your love and encouragement are my driving forces. This Ph. D is as much as yours as it is mine.

Table of Contents

Dedication	ii
Acknowledgements	iii
Table of Contents	iv
List of Tables	vii
List of Figure	ix
List of Scheme	xiv
List of Abbreviations	xv
Chapter 1: Introduction	1
1.1 Chromophoric dissolved organic matter (CDOM).....	3
1.2 CDOM optical properties and their structural basis	5
1.3 CDOM photochemistry and its related structural basis	9
1.4 Proposed H ₂ O ₂ production pathways though photolysis of CDOM	13
1.5 Detection methods for ROS	17
1.5.1 Detection of H ₂ O ₂	17
1.5.2: Detection of photoproducted radicals capable of reducing O ₂ to O ₂ ⁻	19
1.6 Purpose of This Study	22
Chapter 2: Investigating precursors for H ₂ O ₂ production from photochemical reaction of CDOM.....	25
2.1 Introduction	25
2.2 Materials and Method.....	27
2.2.1 Chemicals	27
2.2.2 Experiment apparatus	29
2.2.3 Borohydride reduction.....	31
2.2.4 Hydrogen peroxide photoproduction rates (HPPR)	31
2.2.5 Apparent monochromatic and polychromatic quantum yields	33
2.3 Results	35

2.3.1 Borohydride reduction.....	35
2.3.2 Effect of borohydride reduction on HPPR and apparent quantum yields	36
2.3.3 Effect of dioxygen concentration on HPPR	41
2.3.4 Effect of triplet quenchers	48
2.4 Discussion	52

Chapter 3: Molecular probe measurements of the photochemical production of one electron reducing intermediates from chromophore dissolved organic matter: relation to H₂O₂

photochemical production.	54
3.1 Introduction	54
3.2 Materials and Methods	59
3.2.1 Chemicals	59
3.2.2 Experiment Apparatus.....	59
3.2.3. Detection of photoreductants	60
3.2.4 Determination of the formation rates of photoreductants from HS	65
3.3 Results	66
3.3.1 Detection of hydroxylamine formation	66
3.3.2 Dependence of R _H on [O ₂]	70
3.3.3 Comparison between hydroxylamine and H ₂ O ₂ formation rates and quantum yields	72
3.3.5 Effect of borohydride reduction on R _H	76
3.4 Discussion	76

Chapter 4: Addition of Phenol Electron Donors Substantially Enhances the Rates of Hydrogen Peroxide Photoproduction by Humic Substances

4.1 Introduction	78
4.2 Materials and Method.....	80
4.2.1 Chemicals	80
4.2.2 Determination of hydrogen peroxide photoproduction rates (R _{H2O2}) and apparent quantum yields	81
4.3 Results	83

4.3.1 H ₂ O ₂ enhancement by addition of TMP.....	83
4.3.2 Oxygen dependence	92
Chapter 5: Summary and Future Directions.....	97
5.1 Summary	97
5.2 Future work	99
Appendix 1	101
Appendix 2	104
Bibliography.....	106

List of Tables

Table 2- 1: Values of specific absorbance coefficient at 350 nm ($a^*(350)$), spectral slope (S) for unaltered and borohydride-reduced SRFA, SRHA, LAC* and C18 extracts from fresh water (FW) and shelf station (SS) from the Delaware Bay and Mid-Atlantic Bight.....	30
Table 2- 2: Polychromatic H_2O_2 quantum yields (ϕ) and difference quantum yield ($\Delta\phi$) for untreated and borohydride reduced LAC, SRHA, SRFA, and C-18 extracts from the Fresh Water and Shelf Stations. R_{ex} is the rate of light excitation, HPPR uncertainties were standard derivation from triplet measurements and ϕ uncertainties were propagated from determination of HPPR.....	40
Table 2- 3: Parameters obtained from fits of the data in Fig.2-5 to the expression. $HPPR = aO_2b + O_2$, where $a (= kf)$ and $b (= kdkO_2)$. Lifetime of the intermediate is given by, $\tau = 1/kd = 1/b \times kO_2$, where kO_2 is assumed to be $1 \times 10^9 M^{-1}S^{-1}$ (see text) . Other conditions are as in Figure. 2-5.....	44
Table 2- 4: Hydrogen peroxide concentration and reacted $3apf$ measured after irradiation for SRFA, SRHA, LAC* and the Fresh Water station for 15 min under anaerobic condition.....	45
Table 3- 1: Parameters obtained from fits of the data in Fig. 3-6 to the expression of $R_H = A3apB + 3ap$, $A = Rf$, $B = kO_2O_2 + kdk3ap$	69
Table 3- 2: Slopes and $kO_2/k3ap$ values obtained from fits of the data in Fig. 3-7 .	72
Table 3- 3: Comparison of the R_H with $R_{H_2O_2}$ under monochromatic irradiation. R_H and $R_{H_2O_2}$ were obtained under the same irradiation conditions in the presence of 600 μM $3ap$. Ratio represents $R_H/R_{H_2O_2}$. R_H was obtained under anaerobic conditions while $R_{H_2O_2}$ obtained in the presence of 250 μM O_2	73

Table 3- 4: Polychromatic quantum yield for humic samples and the quantum yields ratio between produced hydroxylamine and H_2O_2 . STD stands for standard derivation acquired from three times measurement. 75

Table 3- 5: Effect of 500 mM NaCl on anaerobic hydroxylamine production rate for 10 mg/L SRFA spiked with [3ap] 75

Table 4-1: Wavelength dependence of the slope (S), intercept, slope ratio and % inhibition by borohydride reduction (% I) acquired from linear regressions of the data in Fig. 4-1 for untreated SRFA (Su) and borohydride-reduced SRFA (Sr). 85

Table 4- 2: H_2O_2 polychromatic quantum yields for HS only (Φ_0) and for that in the presence of Phenols (Φ_p). Y_0 is the value of $R_{H_2O_2}$ in the absence of the phenols at $[O_2] = 250 \mu M$. R_{ex} is the rate of light excitation. Φ_0 obtained from fitting value y_0 . %I is the inhibition of enhancement due to borohydride reduction. EF is the enhance factor. Φ_p , which were obtained from $\phi_0 \times EF$ 90

List of Figure

Figure 1- 1: Proposed electronic interactions between electron donor (hydroxyl-aromatic moieties) and acceptors (A) within partially oxidized lignin fragment.	4
Figure 1- 2: Proposed CT model for CDOM absorption. The shorter wavelength (<350 nm) is caused by sum of absorption of individual chromophores with the longer wavelength absorption tail (>350 nm) caused by the charge transfer interaction between donor- acceptor chromophores that produce the lower energy charge transfer bands.	8
Figure 1- 3: Possible redox reactions of quinone moieties with O_2 and O_2^- . Possible reactions depend on the structure and the reductant potentials of the quinone and semiquinone species.....	11
Figure 1- 4: Chemiluminescence reactions of acridium ester with hydrogen peroxide. (Adopted from King, D.W.) ¹⁰⁰	18
Figure 1- 5: Hydroxylamine formation via reaction of the nitroxide with photochemically generated one electron reducing-intermediates from CDOM	21
Figure 1- 6: Fluorescence change upon the nitroxide reaction with fluorescamine ...	22
Figure 2- 1: Absorption spectra of untreated and borohydride –reduced SRFA, SRHA, LAC* and C 18 extracts of Fresh Water (FW), Shelf Station (SS) obtained from Delaware Bay and Mid-Atlantic Bight. Samples are in phosphate buffer pH=7. SRFA, SRHA concentrations were 10mg L^{-1} . FW, SS and LAC* spectra are matched up with SRFA @350nm.....	28
Figure 2- 2: $R(\lambda)$ for untreated and borohydride–reduced SRFA, SRHA, LAC* and C-18 extracts for the Fresh Water and Shelf Station (SS). Samples were in 0.01 M phosphate buffer pH=7.	34



Figure 2- 3: Wavelength dependence of the H_2O_2 production rate (HPPR) for untreated () and borohydride reduced () SRFA, SRHA, and C-18 extracts from the Fresh Water and Shelf Station at equivalent mass concentration (10 mg/L for SRFA and SRHA, TOC as 3.6 and 10.68 for the Fresh Water and Shelf Stations. All samples were in 10 mM phosphate buffer, pH =7.0)..... 37




Figure 2- 4: Apparent monochromatic H_2O_2 quantum yields (ϕ) and difference quantum yields ($\Delta\phi$) () for untreated () and borohydride-reduced () 38


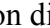
Figure 2- 5: Dependence of HPPR on dioxygen concentration for untreated () and borohydride –reduced () SRFA, SRHA, LAC* and the C-18 extract from Fresh Water station using the polychromatic source. The irradiance for LAC* and SRFA was lower than that for SRHA and the Fresh Water station. 42

Figure 2- 6: The time dependence of 3apf fluorescence increase ($\Delta F = F(t) - F(0)$) following the anaerobic addition of 3apf to SRFA, SRHA, LAC*, and the Fresh Water station, which had been previously irradiated for 15 min under anaerobic conditions. $F(0)$ represents fluorescence of the 3apf and sample prior to irradiation, while $F(t)$ is the fluorescence observed following addition of 3apf to the irradiated samples under anaerobic conditions (left panels). In control experiments (right panels), air was introduced for 2 mins prior to the addition of 3apf to the anaerobically-irradiated samples. 47


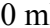



Figure 2- 7: Effects of sorbic acid (0 mM (); 1mM (); 5 mM ()) on H_2O_2 photo-production for untreated and borohydride reduced SRFA and SRHA under aerobic conditions employing the polychromatic source 49

Figure 2- 8: Effects of triplet quencher Cl ( 500mMCl-) and Br- ( 500mM) on H_2O_2 aerobic photo-production for untreated and borohydride-reduced SRFA


under aerobic conditions using the polychromatic source,() is the control without triplet quenchers..... 51

Figure 3- 1: Hydroxylamine formation via reaction of the nitroxide with photochemically-generated one electron reducing-intermediates within CDOM 57

Figure 3- 2: Fluorescence change upon the nitroxide reaction with fluorescamine ... 57

Figure 3- 3: EPR spectra of 3cp (top) and 3ap (bottom) (left panel) and the calibration curves constructed from the normalized double integral value (DI/N) (right panel). Both concentration of 3cp and 3ap were first determined from mass base. Because 3cp can be readily dried while 3ap is highly hydroscopic, 3cp was used as a primary standard. The 3ap concentration was then determined by DI/N comparison with the 3cp calibration..... 62

Figure 3- 4: HPLC chromatography of hydroxylamine production upon dithionite titration (left panel) and hydroxylamine calibration curves constructed from peak height (right panel). Top panels provide the chromatograms and calibration curve using dithionite as limiting reaction reagent, and the bottom panels from using 3ap as limiting reagent. 64

Figure 3- 5: Increase in hydroxylamine following irradiation of an anaerobic solution containing 10 mg/L SRFA and 600 μ M 3ap. Left: black, before irradiation, red after 15 min irradiation. Right: Increase in R_H with increasing [3ap] for 10 mg/L SRFA employing a 15 min anaerobic irradiation. 66

Figure 3- 6: Dependence of R_H (nM/s) on [3ap] for 5mg/L and 10 mg/L SRFA, SRHA and their corresponding borohydride reduced samples..... 67

Figure 3- 7: Dependence of R_H on $[O_2]$ in the presence of 600 μ M 3ap. 70

Figure 3- 8: Dependence of the ratio R_f/R_H on $[O_2]$ for untreated and reduced SRFA and SRHA in the presence of 600 μ M 3ap. 71

Figure 4- 1: Wavelength dependence of $R_{H_2O_2}$ in the absence and presence of increasing $[TMP]$ for untreated (black) and borohydride-reduced (red) SRFA. Samples were irradiated with a polychromatic source employing long-pass filters (325, 355 and 385 nm). Samples contained 10 mg/L SRFA in 10 mM phosphate buffer, pH =7.0. Error bars represent the standard derivation acquired from at least three measurements..... 84

Figure 4- 2: Dependence of $R_{H_2O_2}$ on phenol concentration in air ($[O_2]$ =250 μ M) for untreated (\bullet) and borohydride –reduced (\circ) SRFA, SRHA, and the C-18 extract from Lower Delaware Bay station using the polychromatic source. Error bars represent the standard derivation acquired from at least three measurements for SRFA SRHA and lower Bay sample. 87

Figure 4- 3: Values (y_0 , A and B) from the fits of the data from Fig. 4-2 using kinetic equation: $y=y_0+Ax/(B+x)$. y_0 stands for the $R_{H_2O_2}$ in the absence of phenols. A stands for the enhanced $R_{H_2O_2}$ in the presence of $[phenol]$; B is the concentration of phenol at which $R_{H_2O_2}$ reaches half its maximal value. Left panel: A (black; untreated, red; reduced) and y_0 (green; untreated, yellow; reduced). Right panel: B values (black; untreated, red; reduced). Errors are obtained from Fig. 4-2. 89

Figure 4- 4: Dependence of $R_{H_2O_2}$ on dioxygen concentration for untreated (Black) and borohydride-reduce (Red) SRFA at the presence of 100 μ M TMP using the polychromatic source. Controls: Green and yellow lines are $R_{H_2O_2}$ for SRFA and reduced SRFA respectively in the absence of TMP. 93

Figure 4- 5: Dependence of $R_{H_2O_2}$ at fixed $[TMP]$ = 100 μ M for both untreated and borohydride reduced SRFA, SRHA, Lower Bay samples. Data were fit to the

equation 4-9 employing a nonlinear least-squares fitting routine using fixed values of
 $k_T = 6.6 \times 10^4 \text{ s}^{-1}$; $k_Q = 2.0 \times 10^9 \text{ M}^{-1} \text{ s}^{-1}$; $k_{\text{TMP}} = 2.5 \times 10^9 \text{ M}^{-1} \text{ s}^{-1}$ 95

List of Scheme

Scheme 1- 1: Proposed CDOM primary and secondary photochemical reactions of CDOM. (Adapted from Sharpless and Blough) ⁶⁴	10
Scheme 1- 2: The reactions (Rxn 2-6) from proposed precursors for superoxide and hydrogen peroxide formation ⁸⁶ . ¹ CDOM* and ³ CDOM* represent excited singlet and triplet states, respectively, of either electron donors (D) or acceptors (A) within the CDOM, while CDOM [±] represents a charge-separated species (D ⁺ A ⁻) formed by electron transfer from a donor to an acceptor, and ¹ CDOM [±] represents the charge transfer states.	14
Scheme 1- 3: Possible superoxide and hydrogen peroxide production pathways in the presence of iron.....	16
Scheme 1- 4: Comparison between the reactions of nitroxides and O ₂ with excited states and radicals. From reference 103. ¹⁰¹	20
Scheme 2- 1: The proposed precursors and reactions (Rxn 2-6) for superoxide and hydrogen peroxide formation ⁸⁶	26
Scheme 3- 1: Comparison between the reactions of nitroxides and O ₂ with excited states and radicals. From reference 103.....	56

List of Abbreviations

DOM	dissolved organic matter
CDOM	chromophoric dissolved organic matter
HS	humic substance
SRFA	Suwannee River Fulvic Acid
SRHA	Suwannee River Humic Acid
LAC	lignin, alkali-treated, carboxylated
LAC*	fraction of LAC having some retention time with SRFA
FW	fresh water
SS	shelf station
LB	lower bay
P	external electron donor
PHE	phenol
MOP	4-methoxyphenol
DMOP	3,4-dimethoxyphenol
TMP	2,4,6-trimethoxyphenol
EI	electronic interaction model
CT	charge transfer model
LMCT	ligand to metal charge transfer
SMIR	superoxide-mediated iron reduction
FIA	flow injection analysis
HPLC	high pressure liquid chromatography
EPR	electron paramagnetic resonance

DI/N	normalized double integral
STD	standard derivation
SOD	superoxide dismutase
AE	acridinium carboxylate trifluoromethane sulfonate
3ap	3-aminomethyl-2,2,5,5,-tetramethyl-1-pyrrolydinyloxy
3apf	fluorescamine derivatized 3ap
3cp	3-carbamoyl--2,2,5,5,-tetramethyl-1-pyrrolydinyloxy
DMSO	dimethyl sulfoxide
Br ⁻	bromide ion
Cl ⁻	chloride ion
ϕ	apparent quantum yield
$\Delta\phi$	difference apparent quantum yield
R _{ex}	rate of light excitation
I(λ)	irradiance at wavelength λ
a(λ)	absorbance coefficient
a*(λ)	specific absorbance coefficient
HPPR	hydrogen peroxide production rate
R _H	hydroxylamine production rate
R _{H₂O₂}	hydrogen peroxide production rate
k _{O₂}	rate constant for reaction with with dioxygen
R _f (k _f)	rate constant for intermediates formation
k _d (k _t)	rate constant for relaxation to ground state
k _{3ap}	rate constant for reaction with 3ap

PO_2^-	percentage of superoxide decay via other oxidation pathway
k_p	rate constant for physical quenching of triplet with external donor
k_c	rate constant for chemical quenching of triplet by external donor
k_Q	rate constant for quenching of triplet by dioxygen
k_{rec}	rate constant for recombination of radical species
k_{rxn}	rate constant for reaction to form products
ROS	reactive oxygen species
$^1\text{O}_2$	singlet oxygen
O_2^-	superoxide
H_2O_2	hydrogen peroxide
RO_2	peroxy radical
$\cdot\text{OH}$	hydroxyl radical
e^-	hydrated electron
$^1\text{CDOM}^{\pm\cdot}$	CT states
$\text{CDOM}^{+/-\cdot}$	charge separated state
$^1\text{CDOM}^*$	excited singlet state
$^3\text{CDOM}^*$	excited triplet state
$\text{CDOM}\cdot$	CDOM radical

Chapter 1: Introduction

Hydrogen peroxide (H_2O_2), one of the most common reactive oxygen species (ROS) formed in aquatic systems, is known to initiate radical/redox reactions either as an oxidant or a reductant. Using a sensitive scopoletin-peroxidase based fluorescence method, hydrogen peroxide in seawater was first reported in 1966 by Van Baalen and Marler.¹ Later, the occurrence and concentration of H_2O_2 have been investigated extensively in rainwater, coastal and open-ocean waters, freshwaters and ground waters.²⁻¹⁰ Its ubiquitous presence in the aquatic environment can have substantial impacts on aquatic ecosystems, including: 1) influencing the cycling of carbon, sulfur, nitrogen within the hydrosphere, 2) altering biological accessibility of the trace metals,¹¹⁻¹³ 3) removing aquatic pollutants^{14,15} and 4) converting pollutants into more toxic substance.¹⁶

Because of its relatively small degradation rates (biological and the metal-mediated redox reactions) as compared with its larger photo-production rates, H_2O_2 usually accumulates to relatively high steady-state concentrations (nM in seawaters and μM in freshwaters),^{10, 17,18} and is thus widely employed as an indicator of the photochemical reactivity of chromophoric dissolved organic matter (CDOM) within natural waters. The significant impact of H_2O_2 on the chemistry of natural water has lead to many studies over the past three decades, with great deal of effort devoted to understanding the mechanisms of its photochemical production in natural waters.

The fact that H_2O_2 in natural waters increases dramatically after brief exposure to sunlight indicates that this species is primarily produced through photochemical reactions of the light-absorbing component of dissolved organic

matter (DOM), known as chromophoric dissolved organic matter (CDOM).^{17,19}

Observed linear correlations between the level of detected H_2O_2 and the CDOM absorbance provided evidence that photochemical reactions of CDOM are a primary source of H_2O_2 .^{20,21,17} Other, more minor contributions have been found from such sources as wet deposition^{22,23} and microbial production.^{24,25} However, the nature of the photo-produced intermediates that reduces the dioxygen to form H_2O_2 is still an open question. A thorough understanding of the mechanism(s) of H_2O_2 photoproduction by CDOM in aquatic systems is essential.

In this thesis, H_2O_2 photochemical generation pathways from CDOM are thoroughly investigated. The structural basis for H_2O_2 photoproduction by CDOM is proposed, in which the CDOM photochemical properties and their relation to CDOM optical properties were examined by a selective chemical reduction method. To obtain a better understanding of the nature of the H_2O_2 precursors, the lifetimes of the intermediates were examined by measuring the $[\text{O}_2]$ dependence of H_2O_2 production rates. A molecular probe for detecting radical/reducing intermediates was employed to estimate the production rates of the reducing intermediates acting as dioxygen reductants. The ratio between the levels of the detected one-electron reducing intermediates to photoproduced H_2O_2 was examined to investigate the overall stoichiometry between the production of radical/reducing intermediates and the formation of H_2O_2 . The effects of adding external phenol electron donors on H_2O_2 production rates were further examined.

1.1 Chromophoric dissolved organic matter (CDOM)

CDOM, also known as gelbstoff or yellow substance, is the light absorbing and emitting component of bulk dissolved organic matter (DOM).²⁶ It is a complex mixture of organic compounds formed via the degradation of terrestrial plant materials (primarily lignins, polyphenols, and tannins) and from aquatic sources.^{27,28} In fresh and coastal waters, terrestrially-derived humic substances (fulvic and humic acids) are thought to be the dominant CDOM component,²⁹ flowing through rivers and estuaries into coastal shelves and then open oceans.^{30,31} Upon light absorption, the light absorbing moieties within CDOM serve as good shuttles, transferring either energy or electrons to the dissolved dioxygen to form reactive oxygen species (ROS),³²⁻³⁴ such as singlet oxygen ($^1\text{O}_2$, energy transfer³⁵) or superoxide (O_2^- , electron transfer³⁶). CDOM photolysis can also act to degrade refractory organic pollutants,³⁷⁻³⁹ to mediate trace metal redox reactions,⁴⁰ and to degrade into inorganic carbon thus influencing the carbon cycle.⁴¹⁻⁴³

To gain a better understanding of structural basis of the photochemical reactions of CDOM, numerous spectroscopic techniques have been employed to probe the CDOM structures at molecular level, including pyrolysis-mass spectrometry, high and ultrahigh-resolution mass spectroscopy, ^{13}C nuclear magnetic resonance spectroscopy, electron spin resonance spectroscopy, acidimetric titration, and electrochemistry.⁴⁴⁻⁵⁴ The results reveal that CDOM contains a diverse set of organic moieties including carboxylic acids and substituted phenols, aromatic ketones/aldehydes, quinones, carbohydrates, carboxyl-rich alicyclic molecules, as well as N-containing species.

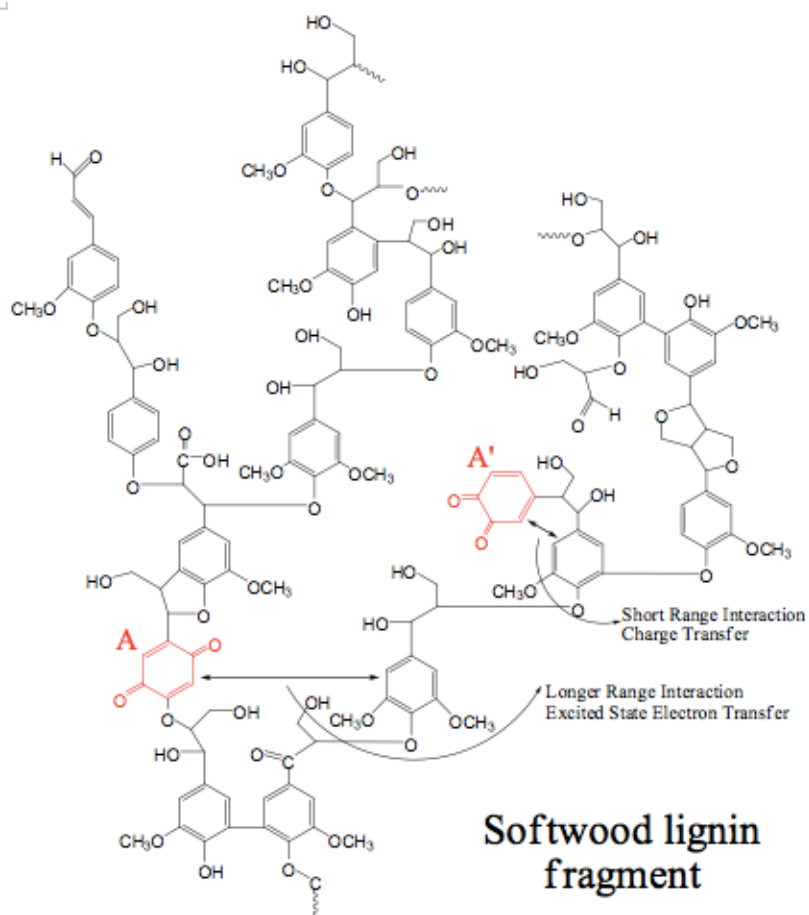


Figure 1- 1: Proposed electronic interactions between electron donor (hydroxyl-aromatic moieties) and acceptors (**A**) within partially oxidized lignin fragment.
 (Long range interaction- excited state electron transfer;
 Short range interaction- charge transfer)

1.2 CDOM optical properties and their structural basis

A fundamental tenet of photochemistry is that light must first be absorbed for a photochemical reaction to be initiated. Thus knowledge of the absorption spectra of CDOM is essential for an understanding of its photochemical reactions.

Terrestrial and marine CDOM both display rather unique absorption spectra that increase approximately exponentially toward shorter wavelengths with no discernible peaks. Spectra are often fitted to an exponential equation of the form $\alpha(\lambda) = \alpha(\lambda_0)e^{-S(\lambda-\lambda_0)}$. The exponent of this fit, spectra slope, S , characterizes how rapidly the absorption decreases with increasing wavelength.

Higher S values indicate a more rapid decline in absorption with increasing λ and a lower absorption contribution in the visible wavelengths. Another indicator of this decline is $E2/E3$ ratio, which represents the ratio of absorption at 254 nm to 365 nm.⁵⁵ These CDOM optical indices have been used to relate the change in optical properties to changes in structure. For example, it has been shown that S usually increases with decreasing molecular size of CDOM.⁵⁶ Photobleaching of CDOM in surface water also usually increases S and $E2/E3$ values, which suggests that photochemical reactions convert higher molecular weight CDOM into lower molecular weight species.⁵⁵⁻⁵⁸

Two distinct structural models have been invoked to explain the observed optical spectra and photochemistry of CDOM, namely a superposition model^{59,60} and an electronic interaction model.⁶¹⁻⁶³ A superposition model proposes that the optical properties derive from a simple sum of the absorption and emission spectra of an ensemble independent chromophores (electronically isolated) existing within CDOM.

In contrast, the electronic interaction model argues that the electronic interactions between chromophores give rise to the distinct optical properties of CDOM.

However, the superposition model cannot easily explain many of the observed optical and photochemical properties,⁶⁴ including the exponentially decreasing long wavelength absorption tail, the continuously red-shifting fluorescence emission maxima, the monotonically decreasing fluorescence quantum yields and lifetimes across the visible wavelengths, and dependence of S on the molecular size.^{61, 65, 60}

In contrast, the electronic interaction model (EI) can largely account for the observed CDOM optical and photochemical properties; within this model, short-range charge transfer interactions between chromophores are of particular importance for CDOM optical properties (charge transfer model, CT). The CT model proposes that the short-wavelength absorbance (< 350) results primarily from the superposition of the donor and acceptor absorption, and the long-wavelength near UV and visible absorption tail results from short-range charge transfer interactions between the electron donors and acceptors to form charge transfer bands (>350 nm, Fig. 1-1 and Fig. 1-2).⁶⁶ Possible electron acceptor moieties are carbonyl-containing species such as quinones and aromatic ketones/aldehydes arising from the partial oxidation of lignin precursors (A in Fig. 1-1), while possible electron donor moieties are hydroxy/methoxy-aromatic moieties.

The continuous red-shifting fluorescence emission maxima in the visible has been attribute to charge recombination luminescence arising from an ensemble of low-energy CT states populated by near UV and visible absorption. The monotonically decreasing fluorescence quantum yields and lifetimes with increasing

wavelength can be attributed to successively lower CT energies, in which the rate of non-radiative relaxation increases relative to the radiative rates thus leading to the lower fluorescence quantum yields and lifetimes.⁶⁷ In addition, the decrease in S with increasing molecular size can be explained as resulting from the larger number of CT contacts that could form statistically within larger molecules of the size ensemble. Further, the increase of S produced by partial photobleaching can be attributed to the destruction of electron donors and acceptors contributing to the CT transitions.

Many of the photochemical properties of CDOM also can be interpreted readily within the CT model as discussed further below.

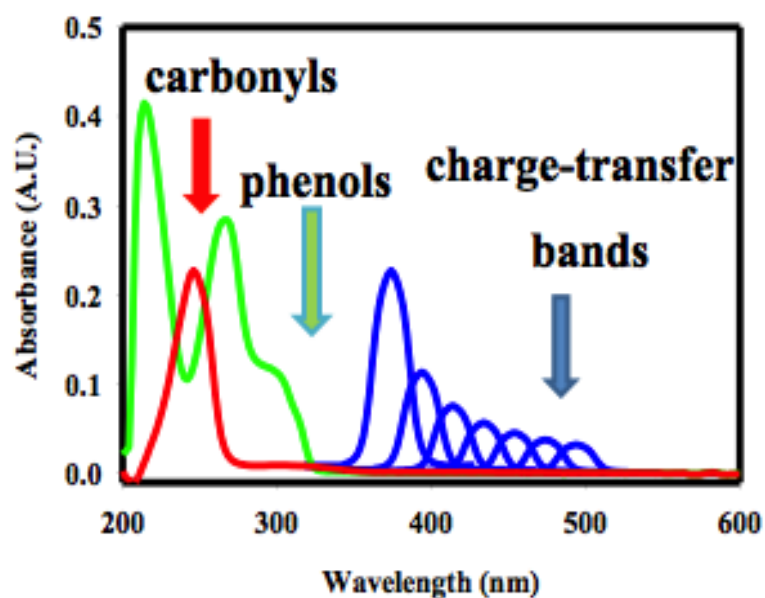
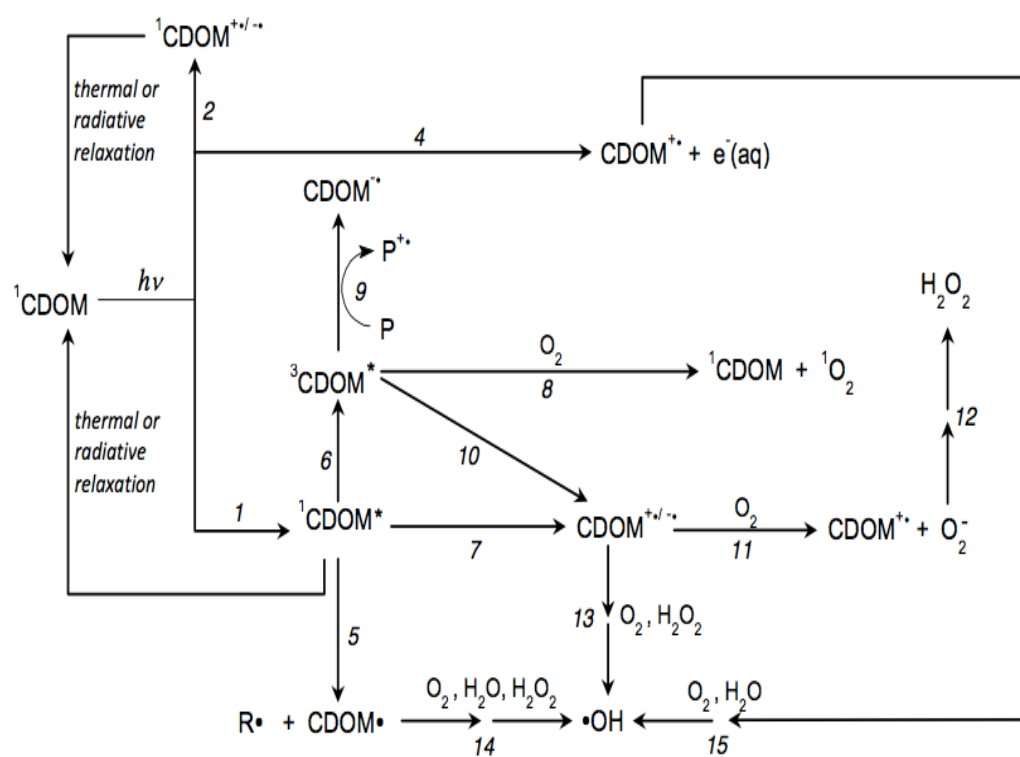


Figure 1- 2: Proposed CT model for CDOM absorption. The shorter wavelength (<350 nm) is caused by sum of absorption of individual chromophores with the longer wavelength absorption tail (>350 nm) caused by the charge transfer interaction between donor- acceptor chromophores that produce the lower energy charge transfer bands.

1.3 CDOM photochemistry and its related structural basis

Since the 1980's, numerous studies have shown that CDOM can act as a photochemical source of singlet dioxygen ($^1\text{O}_2$), superoxide (O_2^-), hydrogen peroxide (H_2O_2), aqueous electron (e^-), hydroxyl radical ($\cdot\text{OH}$) and organic radicals.^{68,69} These reactions are summarized in Scheme 1-1.⁶⁴ Following the ground state excitation of CDOM, possible primary photochemical events include: 1) direct ejection of electrons, 2) formation of CT states ($^1\text{CDOM}^{+/-\cdot}$), or 3) formation of excited singlet states CDOM ($^1\text{CDOM}^*$). In competition with recombination back to ground state CDOM, $^1\text{CDOM}^*$ can undergo homolytic cleavage to either CDOM radicals ($\text{CDOM}\cdot$), undergo electron transfer to form a charge separated state ($\text{CDOM}^{+/-\cdot}$) or undergo intersystem crossing to form the triplet CDOM ($^3\text{CDOM}^*$). $^3\text{CDOM}^*$ can further undergo electron transfer to form a charge separated states ($\text{CDOM}^{+/-\cdot}$), react with external donor (P) to relax back to the ground states.

The CDOM intermediates formed include $\text{CDOM}\cdot$, $\text{CDOM}^{+/-\cdot}$ and $^3\text{CDOM}^*$, which are unstable and will react further with ambient redox species to initiate various photochemical reactions. In our case, these intermediates can react with dioxygen to produce various reactive oxygen species such as $^1\text{O}_2$, O_2^- , H_2O_2 , $\cdot\text{OH}$, and peroxy radical (RO_2). It has already been shown that $^1\text{O}_2$ is the product of the energy transfer between $^3\text{CDOM}^*$ and dioxygen. However, the exact intermediates and pathways giving rise to O_2^- and subsequently H_2O_2 through O_2^- disproportion is still not clear.



Scheme 1- 1: Proposed CDOM primary and secondary photochemical reactions of CDOM. (Adapted from Sharpless and Blough)⁶⁴

Quinones within CDOM are frequently cited as important organic moieties responsible for its redox properties.⁷⁰⁻⁷⁴ Evidence for the presence of quinone moieties with CDOM include electron paramagnetic resonance (EPR) detection of semiquinone radicals and the results of the electrochemical measurements.^{71,75}

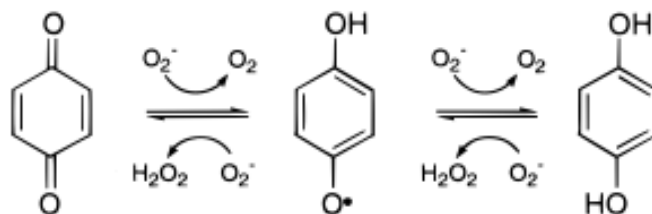


Figure 1- 3: Possible redox reactions of quinone moieties with O_2 and $O_2^{\cdot -}$. Possible reactions depend on the structure and the reductant potentials of the quinone and semiquinone species.

Garg et al employed disodium anthraquinone-2-6-disulfonate as model quinone sensitizer to simulate the H_2O_2 production from aquatic CDOM.⁷⁶ However, different H_2O_2 production behavior was observed between irradiated humic substance and model quinones in the presence of DMSO, a hydroxyl radical scavenger. This result implies that the H_2O_2 production mechanism is far more complex for humic substance than for simple quinone compounds.⁷⁷

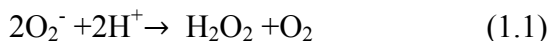
In order to test for the possible involvement of quinone and other carbonyl-containing moieties, such as (aromatic) ketones/ aldehydes as electron acceptors, as well as test for their possible involvement in CT transitions, reduction with sodium borohydride has been employed. Sodium borohydride can selectively reduce the carbonyl –containing electron acceptors within CDOM under anaerobic conditions.^{73,78,79}

For a variety of humic substance standards as well as natural water samples, the elimination of carbonyl containing groups by borohydride reduction leads to preferential loss of visible absorption that has been attributed to the elimination of the low energy CT transitions. In addition, substantially enhanced, blue-shifted fluorescence emission is observed after borohydride reduction, suggesting that the removal of electron acceptors eliminates donor quenching thereby increasing the local donor fluorescence.⁷⁸

Similar to CDOM optical absorption, apparent quantum yields and the rates of H₂O₂ photoproduction determined for both natural waters and humic substance decrease rapidly with increasing wavelength, with the majority of H₂O₂ production occurring at wavelengths between 290 and 400 nm²¹. A linear relationship was found between the quantum yields of H₂O₂ and CDOM photobleaching for Elizabeth River samples,²¹ implying an intrinsic connection between the H₂O₂ photoproduction and CDOM optical properties.⁶⁶ The much faster decrease of H₂O₂ photoproduction rates compared to the decrease of CDOM absorption indicates that the shorter wavelengths are far more efficient at photochemical producing ROS, hence higher apparent quantum efficiencies. However, a better understanding of the structural basis of CDOM optical properties, photochemical properties and the connection between the two is desirable.

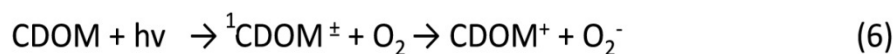
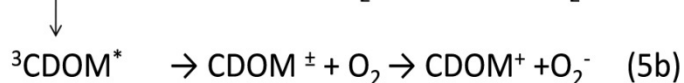
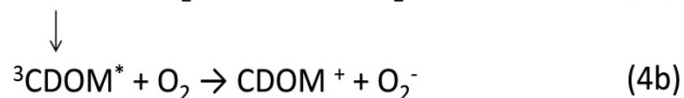
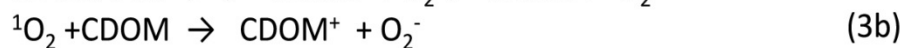
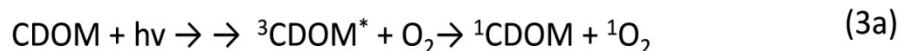
1.4 Proposed H₂O₂ production pathways through photolysis of CDOM

Over the past twenty years, evidence has shown that the photoproduction of H₂O₂ by CDOM primarily arises from the formation of O₂⁻ and its subsequent dismutation (eqn. 1.1).



Superoxide is thought to be formed via reaction between photochemically produced reductants and O₂.^{17,36,80,81} However, the nature of the reductants giving rise to O₂⁻, and thus H₂O₂, remains unclear. The possible photochemical pathways giving rise to the reductants from CDOM are proposed and discussed below (Scheme 1-2).

Both Darper and Crosby⁶ and Cooper and Zika⁸² have pointed out that photoproduction of hydrated electrons from CDOM could produce H₂O₂ in both freshwaters and seawaters (Rxn. 2a,2b). However, work by Zepp⁸² at first indicated that hydrated electrons are not produced at rates sufficient to account for the production of H₂O₂ detected in aquatic environment. Later, Thomas-Smith and Blough⁸³ employing a steady state scavenger method provided further evidence that the low rates of production of hydrated electron is not sufficient for the overall production of H₂O₂ in most natural waters at wavelengths above ~ 315 nm, thus also excluding the hydrated electron as major precursor for H₂O₂.⁸³



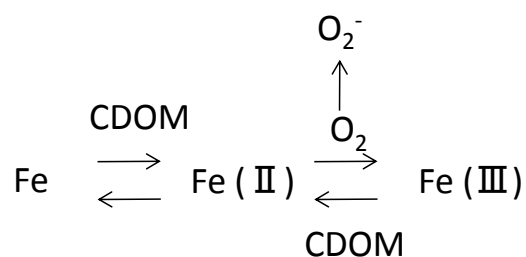
Scheme 1- 2: The reactions (Rxn 2-6) from proposed precursors for superoxide and hydrogen peroxide formation⁸⁶. $^1\text{CDOM}^*$ and $^3\text{CDOM}^*$ represent excited singlet and triplet states, respectively, of either electron donors (D) or acceptors (A) within the CDOM, while CDOM^\pm represents a charge-separated species (D^+A^-) formed by electron transfer from a donor to an acceptor, and $^1\text{CDOM}^\pm$ represents the charge transfer states.

Singlet dioxygen (94 kJ/mol), formed via energy transfer from the excited triplet states of CDOM ($^3\text{CDOM}$) to ground state dioxygen ($^3\text{O}_2$) (Rxn. 3a), was proposed as a possible precursor for O_2^- (Rxn 3b).⁸⁴ The quantum yields (ϕ) for both $^1\text{O}_2$ and O_2^- exhibit a similar spectral dependence, but the $\phi_{\text{H}_2\text{O}_2}$ is reported to be 100 times smaller than $\phi_{^1\text{O}_2}$.²¹ Dalrymple^{85,86} et al. provided further evidence that the maximum contribution from $^1\text{O}_2$ to the total photoproduction of H_2O_2 was no more than 6%, indicating $^1\text{O}_2$ is largely unimportant as a H_2O_2 source.

Other possible pathways include: 1) direct electron transfer to dioxygen from excited singlet (Rxn. 4a) or triplet states (Rxn. 4b), although reaction 4a is exceedingly unlikely due to the very short lifetimes of the singlet states,⁶⁷ 2) the formation of reducing radical intermediates (A^\cdot) through electron transfer between excited singlet (Rxn. 5a) or triplet state electron donors or acceptors (Rxn. 5b),^{32, 87, 3} the formation of reducing radical intermediates formed through direct excitation of charge-transfer transitions (Rxn. 6).^{66, 67, 78, 88, 89} In chapter 2, those possible reaction intermediates to O_2^- and thus H_2O_2 are examined.

Metals, such as Fe, are also a very common species in natural waters, and can have a significant impact on the aquatic redox environment.^{90, 91} Metal ions can be reduced from a higher to lower redox states through two primary mechanisms: ligand-to-metal charge transfer (LMCT) and direct electron transfer from excited states.^{12, 92,}⁹³ Other possible reduction pathways could come from interaction with oxidant ROS such as superoxide. In presence of superoxide, Fe (II) could rapidly be oxidized with a half-life of several minutes in oxic marine waters to Fe (III).^{94, 95} Fe (III) could further reduce back to Fe (II) via photochemical superoxide-mediated iron

reduction (SMIR) or ligand- to metal charge transfer (LMCT) (Scheme 1-3). The oxidation process occurred between steady state Fe (II) with an oxidant, such as dioxygen, could produce superoxide as well as H₂O₂. However, for the studies reported in this thesis, only trace amounts of metal ions exist within the samples (< 1 μM), generation of H₂O₂ production from metal-related pathways is minor and is considered negligible in these studies.



Scheme 1- 3: Possible superoxide and hydrogen peroxide production pathways in the presence of iron.

1.5 Detection methods for ROS

1.5.1 Detection of H₂O₂

The detection of ROS is extremely challenging due to their reactivity, and thus in many cases, short lifetimes. Among all the aquatic ROS, H₂O₂, with lifetimes ranging from minutes to days and concentrations ranging from 10's of nM to 10's of μ M, is considered the most stable. To measure H₂O₂, an acridinium ester (AE) based chemiluminescence method was employed.⁹⁶ This method allows detection of H₂O₂ at nM to μ M levels and excludes the possible fluorescence interference from naturally occurring chromophores, fluorophores, and organic peroxides, which is inevitable using the traditional colorimetric and fluorometric methods.^{97,98}

The mechanism of reaction of AE with H₂O₂ is shown in Figure 4.⁹⁶ AE (I) is stable in acidic solutions, but rapidly hydrolyzes in base. In the presence of the peroxide anion (HOO⁻), AE forms an unstable dioxetane compound IV, which decays yielding N-methylacridone (V) and the emission of light at 470 nm, which is detected employing a photomultiplier tube (PMT). The H₂O₂ sample is introduced by a flow injection analysis (FIA) system. The linear range for FIA method covers the H₂O₂ concentrations ranging from ten's of nM to μ M. Catalase can be added to the analysis solutions 12 hrs before measurement to eliminate the possible background H₂O₂.⁹⁶

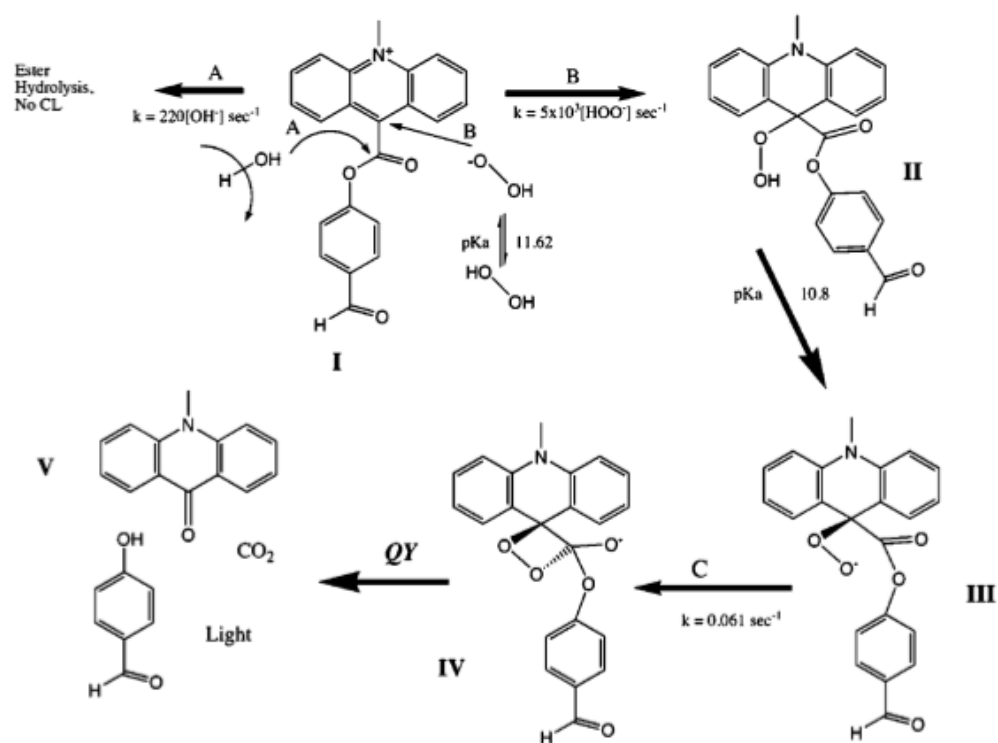


Figure 1- 4: Chemiluminescence reactions of acridium ester with hydrogen peroxide.

(Adopted from King, D.W.)⁹⁶

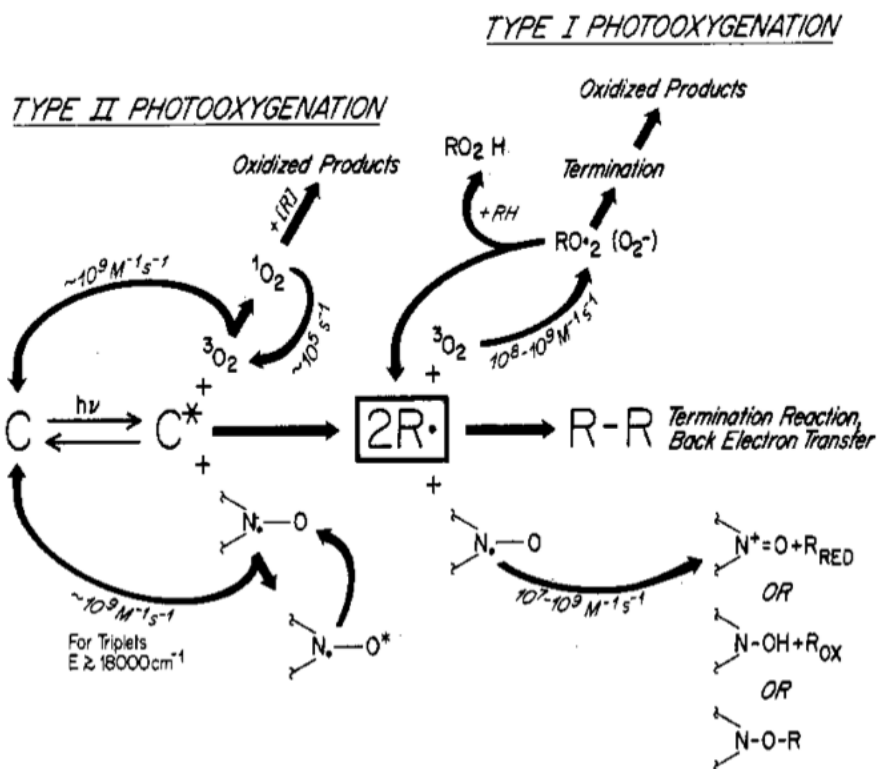
1.5.2: Detection of photoproduced radicals capable of reducing O_2 to O_2^-

The relative stability of H_2O_2 endows it as one reliable probe for estimating the net transfer of electrons from CDOM to dioxygen in natural waters. However, Zika and Petasne presented qualitative evidence that 24% to 41% of the photochemical produced O_2^- does not lead to H_2O_2 formation.³⁶ They employed the enzyme superoxide dismutase (SOD), which competes with other non-dismutation decay pathways, and favors the superoxide dismutation pathway.

Waite and Garg⁷⁷ also provided evidence that significant fraction of the photoproduced O_2^- is most likely lost through oxidation of O_2^- to O_2 via other oxidative pathways in competition with the dismutation to H_2O_2 .⁷⁷ Understanding the stoichiometry between the H_2O_2 production and the photo-reductant production would provide key insights into O_2^- formation and decay pathways and the factors affecting the net formation of H_2O_2 . However, unlike H_2O_2 which is relatively stable, photoproduced reductants are highly reactive, giving rise to short lifetimes and low steady-state concentrations. Thus steady-state concentrations are often too low to be measured by spectroscopic methods (such as electron paramagnetic resonance spectroscopy), and their short lifetimes preclude measurement by direct chemical methods.

Indirect measurement of reducing intermediates using radical molecular probes is developed in this thesis (chapter 3). Di-tert-alkyl nitroxides are a very common class of molecular probes particularly suitable for examining the production of the radicals involved in CDOM photoreactions.⁹⁹⁻¹⁰¹ These stable nitroxide radicals can react rapidly with one-electron reductants with a high reaction constant ($\sim 10^8$

to $10^9 \text{ M}^{-1} \text{ s}^{-1}$).¹⁰² In addition, having similar reactants potentials to dioxygen, nitroxides can compete with dioxygen for the photochemically-generated reducing species.⁹⁹



Scheme 1- 4: Comparison between the reactions of nitroxides and O_2 with excited states and radicals. From reference 99.⁹⁹

In contrast to reaction with O₂, the product of this reaction is the relatively stable hydroxylamine. This one-electron reduction product can be sensitively monitored by the electron paramagnetic resonance spectrometry (EPR) via the loss of spin caused by the reduction of the paramagnetic nitroxide to the diamagnetic product.¹⁰³

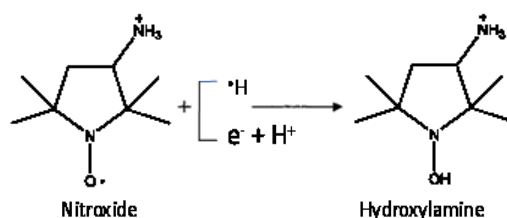


Figure 1- 5: Hydroxylamine formation via reaction of the nitroxide with photochemically generated one electron reducing-intermediates from CDOM

The sensitivity of the nitroxide method can be substantially improved by covalently linking the nitroxide to a fluorophore.¹⁰⁴ Due to efficient intramolecular quenching of the fluorophore by the nitroxide, the fluorescence yield of the fluorophore is very low when coupled to the nitroxide. However, the intramolecular quenching is eliminated when the nitroxide is converted to a diamagnetic product through radical reactions, thus greatly enhancing the fluorescence (Figure 6). The enhanced fluorescence can thus be used as a very sensitive measure of radical scavenging, and when coupled with HPLC, offers better selectivity for detection of reducing-radicals.¹⁰³

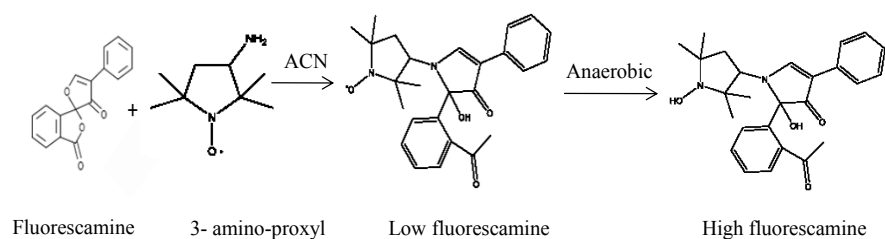


Figure 1- 6: Fluorescence change upon the nitroxide reaction with fluorescamine

1.6 Purpose of This Study

Despite almost three decades of research, the precise mechanisms by which H_2O_2 is photoproduced by CDOM remain unclear. The aim of this thesis was to investigate the nature of the reducing intermediate(s) photochemically generated from CDOM in aqueous solutions and delineate the pathways of electron transfer between CDOM and ambient dioxygen that ultimately leads to the production of H_2O_2 .

To achieve those objectives, a selective reduction method employing sodium borohydride was employed to probe the importance of (aromatic) ketone/aldehydes on H_2O_2 production. Removal of aromatic ketone/aldehydes moieties by borohydride reduction has been shown to change CDOM optical properties, such as decreasing the long wavelength absorption tail and cause a blue shift in the wavelength of fluorescence emission. If the aromatic ketone/ aldehydes electron acceptors have significant role in H_2O_2 production, the removal of such species would be expected to greatly reduce the H_2O_2 production rates.

The results of borohydride reduction on H_2O_2 production rate are presented in Chapter 2. Borohydride reduction did not greatly affect on H_2O_2 indicating that CT

transitions and aromatic ketone/ aldehydes do not play a significant role in H_2O_2 production.

The dependence of H_2O_2 photoproduction rates on dioxygen concentration can provide information on the lifetimes of the reducing intermediates. Within this model, O_2^- (and thus H_2O_2 via dismutation) could be produced through three possible pathways: 1) a very low efficiency reaction of O_2 with the short-lived charge-separated intermediates, 2) reaction of O_2 with a smaller fraction of longer-lived charge separated intermediates populated in competition with rapid recombination and, 3) reaction of O_2 with long-lived acceptor radicals (eg. semiquinone or ketyl) produced intramolecularly by electron- or hydrogen atom-transfer from excited states of endogenous (donor). In chapter 2, the trend of increasing H_2O_2 photoproduction with increasing $[\text{O}_2]$, with rate saturation above $[\text{O}_2]$ 250 μM suggests that it is more likely excited singlet state of electron donors transferring electrons to acceptors, with the reduced acceptors transferring the electrons to the ambient dioxygen, forming superoxide, and subsequently hydrogen peroxide.

Chapter 3 provides evidence that 3ap and dioxygen compete for similar pool of one electron reductants produced photochemically within HS. Evidence supporting this idea includes 1) proportional decrease in R_{H} and $R_{\text{H}_2\text{O}_2}$ with increasing wavelength (Table 3-3), 2) suppression of R_{H} with increasing $[\text{O}_2]$ due to competition for common intermediates, 3) largely unaffected ($R_{\text{H}_2\text{O}_2}$) or increase (R_{H}) rates upon borohydride reduction, indicating that charge transfer states or aromatic ketones/aldehydes are not directly involved in the formation of these reductants.

Rates and rate ratios of $R_H/R_{H_2O_2}$ were also examined. The ratio of $R_H/R_{H_2O_2}$ for untreated SRFA and SRHA employing monochromatic irradiation were 6, indicating a significant portion (67%) of O_2^- will decay by other oxidative sinks, such as light generated intermediates or CDOM itself. The observed higher $\phi_H/\phi_{H_2O_2}$ ratio (13) employing polychromatic irradiations could be explained either as enhanced efficiency for hydroxylamine formation at longer wavelengths or use of polychromatic light could “activate” additional pathways for O_2^-/H_2O_2 removal. More work need to be done for the detailed explanation.

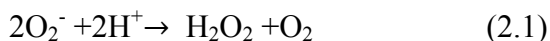
In chapter 4, the effect of adding an external phenol electron donor on the rate of H_2O_2 production was examined. Addition of phenols at concentrations in the 10's to 100's of micromolar substantially enhanced the rate of H_2O_2 production. Borohydride reduction significantly inhibited this enhancement. Decreasing $[O_2]$ to $\sim 60 \mu M$ enhanced the rate of H_2O_2 production. Those results are consistent with the reaction of the electron donor with the excited triplet state of aromatic ketones/aldehydes to form a ketyl radical that subsequently reacts with O_2 to form O_2^- and then H_2O_2 . Those results also indicated that an additional pathway of H_2O_2 formation is introduced in the presence of sufficiently high concentrations of electron donors of the appropriate redox potential.

Chapter 5 summarizes the results of this work and suggests future of the research

Chapter 2: Investigating precursors for H₂O₂ production from photochemical reaction of CDOM

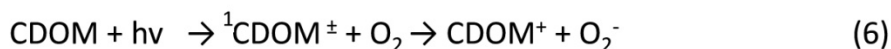
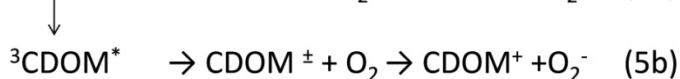
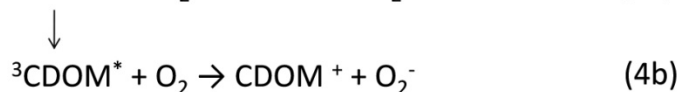
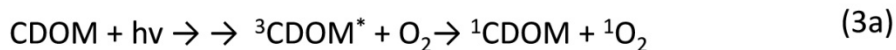
2.1 Introduction

Light absorption by humic substances (HS) and chromophoric dissolved organic matter (CDOM) has long been known to generate hydrogen peroxide (H₂O₂) in natural waters.^{1,17,19,32, 105-107} Current evidence indicates that the photochemical formation of H₂O₂ arises primarily through the one-electron reduction of O₂ by photo-produced intermediates to produce superoxide (O₂⁻)^{32,33} which subsequently undergoes dismutation, either catalyzed or un-catalyzed, to form H₂O₂ (Eqn.2.1).¹⁰⁸



These two reactive oxygen species, O₂⁻ and H₂O₂, can play a critical role in environmental redox reactions and metal ion speciation in natural waters,^{11,13,109,110} as well as in the production of hydroxyl radical (·OH) through Fenton chemistry.¹¹¹⁻¹¹⁵

Despite extensive research over the last 30 years, the mechanism by which O₂ is reduced photochemically to O₂⁻ by HS and CDOM is still not known with certainty. A variety of possibilities exist in scheme 2-1.



Scheme 2- 1: The proposed precursors and reactions (Rxn 2-6) for superoxide and hydrogen peroxide formation⁸⁶

Previous work has shown that photo-ionization to produce the hydrated electron (e^-) cannot account for the magnitude of the H_2O_2 production (Rxn. 2), at least for wavelengths in the UV-A and visible.^{105,8,116,82} Similarly, work by Sharpless et al.⁸⁵ and Cory et al.¹¹⁷ have shown that only a minor amount of H_2O_2 is produced through the reduction of singlet dioxygen by CDOM (Rxn. 3), precluding the possibility that ${}^1\text{O}_2$ serves as a major O_2^- precursor.

Here we attempt to distinguish among the possible pathways by examining the effect of $[\text{O}_2]$ and borohydride (NaBH_4) reduction on the rates and quantum yields of H_2O_2 photo-production. Our results indicate that H_2O_2 is most likely formed through a low efficiency intramolecular excited-state electron transfer process that produces

reducing radical intermediates, which then react with O_2 to produce O_2^- and subsequently H_2O_2 (Rxn. 5a).

2.2 Materials and Method

2.2.1 Chemicals

Boric acid (99.999%), sodium chloride, sodium bromide, sodium phosphate, sodium dihydrogen phosphate, sodium carbonate, phosphoric acid, alkali extracted and carboxylated lignin (LAC), Sephadex G-10, G-25 and catalase were purchased from Sigma-Aldrich. Sodium dithionite and fluorescamine were purchased from Acros. Hydrogen peroxide (30%) and 3-amino-2,2,5,5,-tetramethyl-1-pyrrolidinyloxy (3ap) were purchased from Fisher. Fluorescamine-derivatized 3ap (3apf) was synthesized as previous reported.^{100,101,118} Suwannee River fulvic acid (SRFA) and Suwannee River humic acid (SRHA) were obtained from the International Humic Substance Society. Solid phase C-18 extracts from the Delaware River station (Fresh Water; 39.9N, -75.1 W), and shelf of the Middle Atlantic Bight (Shelf Station; 38.4N, -74.9W) were obtained in December 2006 and processed as previously reported.^{67, 119} A fraction of LAC (LAC*) that had the same retention time as SRFA when passed through Sephadex G-25 column was also employed.

Concentrations of SRFA and SRHA used in this work were 10 mg/L. The C_{18} extracts and LAC* samples were matched to the absorbance of a 10 mg/L SRFA at 350 nm (Fig 2-1). Water was obtained from a Milli-Q (MQ) purification system. All samples were prepared in 0.01M phosphate buffer (pH=7).

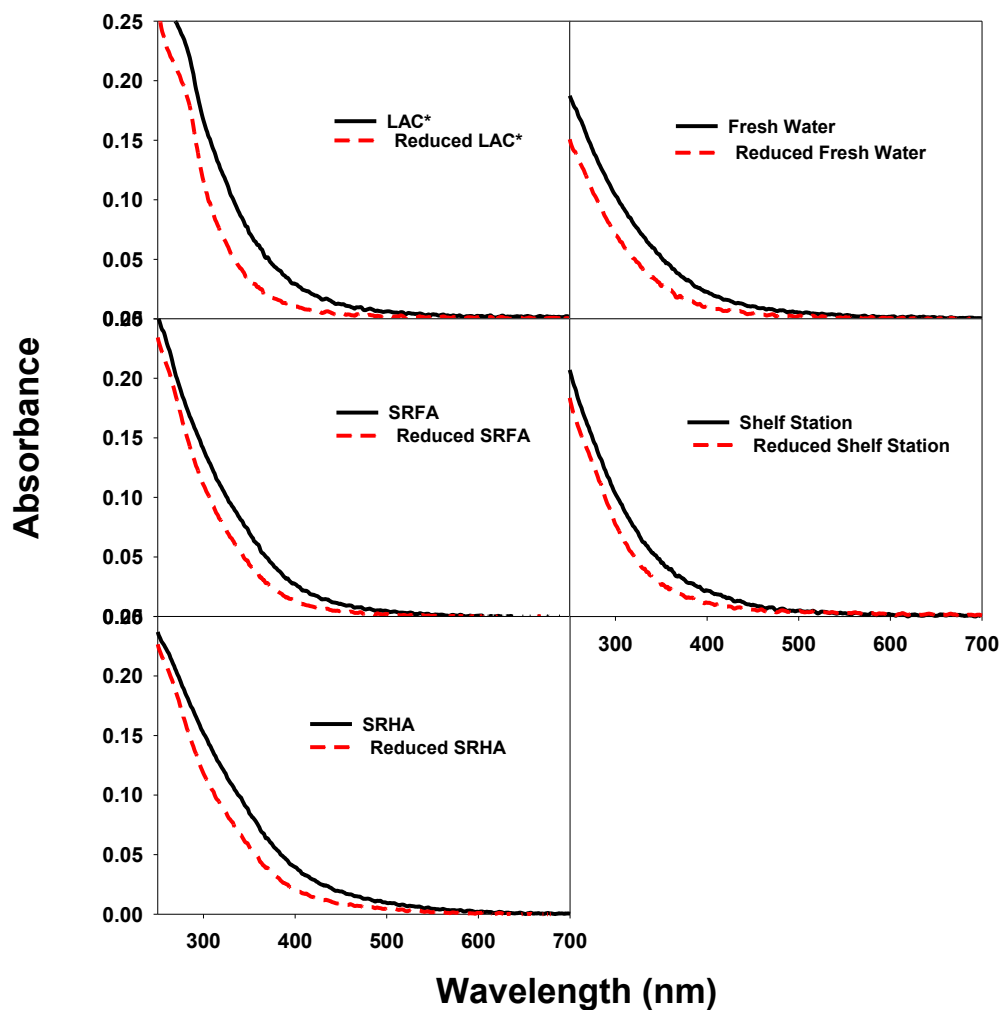


Figure 2- 1: Absorption spectra of untreated and borohydride –reduced SRFA, SRHA, LAC* and C 18 extracts of Fresh Water (FW), Shelf Station (SS) obtained from Delaware Bay and Mid-Atlantic Bight. Samples are in phosphate buffer pH=7. SRFA, SRHA concentrations were 10mg L^{-1} . FW, SS and LAC* spectra are matched up with SRFA @350nm.

2.2.2 Experiment apparatus

Either a Hewlett- Packard 8425A or a Shimadzu 2401-PC spectrophotometer was employed to acquire UV-VIS absorption spectra. Absorption spectra for 10 mg/L samples, which were prepared in the pH 7 phosphate buffer solutions, were recorded using 1 cm cuvette over the range from 190 nm to 820 nm. All spectra were baseline subtracted from MQ water. A SLM Aminco AB2 spectrofluorometer was used to collect the 3apf emission spectra. The excitation wavelength was set at 390 nm and emission collected from 400-700nm employing a 4 nm bandpass on both excitation and emission monochromators. A Shimadzu total organic analyzer (TOC-5000A) was employed to determine total organic carbon content. Specific absorption coefficients a^* were obtained by normalizing absorption coefficient $a(\lambda)$ to organic carbon concentrations,

$$a(\lambda) = \frac{2.303 \times A(\lambda)}{b} \quad (7)$$

$$a^*(\lambda) = \frac{a(\lambda)}{c} \quad (8)$$

where $A(\lambda)$ is the absorbance at a given wavelength, b is the pathlength in meters and C is the concentration of total organic carbon (TOC) in mg carbon L^{-1} . a^* for all samples used in this study are provided in Table 2-1.

Table 2- 1 Values of specific absorbance coefficient at 350 nm ($a^*(350)$), spectral slope (S) for unaltered and borohydride-reduced SRFA, SRHA, LAC* and C18 extracts from fresh water (FW) and shelf station (SS) from the Delaware Bay and Mid-Atlantic Bight.

Irradiated samples	$a^*(350)$ $\text{m}^{-1} \text{mg}^{-1} \text{C L}^{-1}$	$\text{TOC} = 2.303 \cdot A / (0.01 \times a^*)$ mg C /L	$S(\text{nm}^{-1})$
LAC*	2.55	6.48	0.015
RELAC*	1.07	7.02	0.02
SRHA	3.0	6.40	0.012
RESRHA	1.76	7.40	0.015
SRFA	3.44	4.69	0.014
RESRFA	1.95	5.11	0.016
FW	3.28	3.60	0.013
REFW	1.758	3.60	0.016
SS	0.97	10.68	0.015
RESS	0.52	11.74	0.020

2.2.3 Borohydride reduction

Borohydride reduction was performed as described below. Known concentration of humic substance was transferred into a 1 cm cuvette (3 mL) and sparged with ultrapure N₂ for 10 minutes (anaerobic reduction). 25 fold mass excess sodium borohydride was added into the humic substance solution under continuously N₂ purging for 45 minutes. Maximum reduction (absorbance loss) is accomplished over this time period. The reduced sample was kept airtight (under anaerobic conditions) for 24 hours. During this time, the absorption spectra (loss) were continuously monitored by obtaining absorption spectra at various time intervals. The reduction was considered to be complete when no further change absorption spectra were observed.

2.2.4 Hydrogen peroxide photoproduction rates (HPPR)

A chemiluminescence-based flow injection analysis (FIA) was employed to determine [H₂O₂].¹²⁰ The chemiluminescence reagent, acridinium ester 10-methyl-9(p-formylphenyl)-acridiniumcarboxylatetetrifluoromethanesulfonate (AE) was provided by Waterville Analytical Company. A 0.1 M Na₂CO₃ solution (pH= 11.2) was employed as previously recommended.⁹⁶ The buffer solution, carrier water and AE were introduced into the reaction vessel using a peristaltic pump with flow rate of 10.9 ml/min, while samples for H₂O₂ analysis were introduced with plastic syringe. Mixing of AE and H₂O₂ samples in the reaction vessel yielded chemiluminescence signals, which were converted to H₂O₂ concentration employing a H₂O₂ calibration curve. The calibration curve was prepared daily and constructed from a stock 30% H₂O₂ solution, whose concentration was determined by H₂O₂ molar absorptivity,¹²⁰

and confirmed by a titrimetric method using KMnO_4 .⁹⁶ H_2O_2 concentration in the blank was recorded and subtracted from the reported values. Catalase was added to solutions after irradiation to test whether the observed signal was arising from H_2O_2 alone. All samples contacted only glass and Teflon to avoid possible contamination by adventitious trace metals. The H_2O_2 production rate (HPPR) was calculated from a linear regression of H_2O_2 yield over a 15 min irradiation.

For aerobic polychromatic irradiations, samples were held in 1 cm pathlength quartz cuvette and irradiated with a 300 watt xenon lamp employing a 325 nm long-pass cutoff filter. A 20 cm water jacket was placed between the sample cuvette and the light source to remove the IR. For monochromatic irradiations, the output of a 1000 W Hg-Xe lamp was passed through a Spectra Energy GM 252 monochromator (10 nm bandpass), and directed onto a 5 cm pathlength quartz cuvette containing the samples.

Anaerobic samples were held in 1 cm cuvette capped tightly with a Teflon lid and Critoseal, and prepared by bubbling N_2 into samples for 20 min, with the headspace then purged for 10 min prior to a 15min irradiation. A dioxygen scrubber was mounted on N_2 tank to remove possible traces O_2 in N_2 tank.

Sodium dithionite ($\text{Na}_2\text{S}_2\text{O}_4$) was employed to check for O_2 leaks within this system. Using a gas tight syringe, 200 μM $\text{Na}_2\text{S}_2\text{O}_4$ was injected into 4 mL of anaerobic MQ water in the 1 cm cuvette, with the characteristic 315 nm absorption band of $\text{Na}_2\text{S}_2\text{O}_4$ monitored over time. Reaction of dioxygen with dithionite leads to the loss of this band, with this loss used as a sensitive monitor of O_2 leaks.

3apf was employed for quantifying the amount of radicals or reducing species remaining following irradiation under anaerobic conditions.^{99, 104, 121,102,103} A 300 μM 3apf stock was prepared by dissolving 3apf in 50 mM pH 8.4 boric buffer. Two hundred micro liters of the stock 3apf was injected with a gas tight syringe into samples (4 mL) immediately following irradiation, with fluorescence then monitored. Increases in fluorescence signal was converted to concentrations of reacted 3apf employing a calibration curve constructed from the fluorescence increases observed following reduction of known concentrations of 3apf with excess of $\text{Na}_2\text{S}_2\text{O}_4$.¹⁰²

2.2.5 Apparent monochromatic and polychromatic quantum yields

Apparent quantum yields, ϕ , were determined separately for the polychromatic and monochromatic sources. For polychromatic irradiations, ϕ were calculated using following expression,

$$\phi = \frac{\text{HPPR}}{R_{\text{EX}}} \quad (9)$$

Where HPPR is the H_2O_2 production rate, R_{EX} is the rate of light excitation,

$$R_{\text{EX}} = \int_{190}^{820} a(\lambda) \times I(\lambda) d\lambda = \int_{190}^{820} R(\lambda) d\lambda \quad (10)$$

and $a(\lambda)$ is the absorption coefficient of the sample, and $I(\lambda)$ is the irradiance at wavelength λ at the front face of the cuvette (photons $\text{cm}^{-2} \text{s}^{-1}$), as measured with an Ocean Optics spectroradiometer.⁸⁸ (Fig 2-2) R_{EX} has been converted to mole photons $\text{L}^{-1} \text{s}^{-1}$.

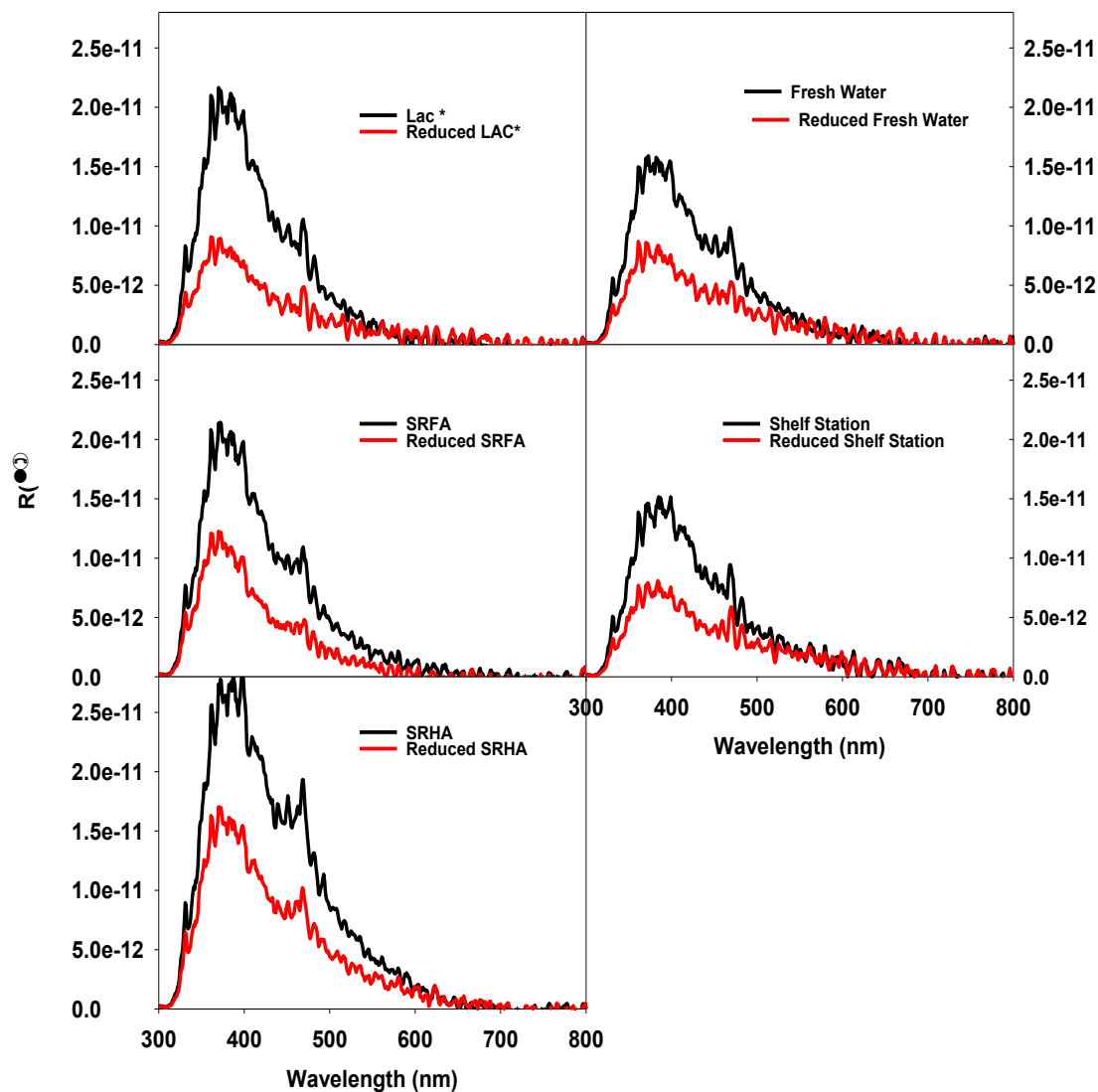


Figure 2- 2: $R(\lambda)$ for untreated and borohydride-reduced SRFA, SRHA, LAC* and C-18 extracts for the Fresh Water and Shelf Station (SS). Samples were in 0.01 M phosphate buffer pH=7.

For the monochromatic irradiations, $\phi(\lambda)$ were determined using the following equation:

$$\phi = \frac{\text{HPPR}}{R_{\text{EX}}} = \frac{\text{HPPR} \times L}{I_0(\lambda) \times (1 - 10^{-A(\lambda)})} \quad (11)$$

where L is the path length of the cell (cm), A is the absorbance, $(1 - 10^{-A})$ is the fraction of light absorbed by the sample solutions, and I_0 is the irradiance (photons $\text{cm}^{-2} \cdot \text{s}^{-1}$) acquired from the actinometric measurements. Actinometry was performed by the method of Hatchard and Parker.^{122, 123} To obtain an estimate of the apparent quantum efficiency of the species eliminated by borohydride reduction. The difference quantum yield ($\Delta\phi$) was also calculated for the polychromatic and monochromatic irradiations respectively,⁸⁸

$$\Delta\phi_{\text{polychromatic}} = \frac{(\text{HPPR}_{\text{sample}} - \text{HPPR}_{\text{reduced sample}})}{(R_{\text{EX sample}} - R_{\text{EX reduced sample}})} \quad (12)$$

$$\Delta\phi_{\text{monochromatic}} = \frac{\Delta\text{HPPR} \times L}{I_0 \times \Delta(1 - 10^{-A})} = \frac{(\text{HPPR}_{\text{sample}} - \text{HPPR}_{\text{reduced sample}}) \times L}{I_0 \times [(1 - 10^{-A_{\text{sample}}}) - (1 - 10^{-A_{\text{reduced sample}}})]} \quad (13)$$

2.3 Results

2.3.1 Borohydride reduction

Borohydride reduction was performed as previously described.^{78, 88} The borohydride-reduced samples were further passed through the Sephadex G-10 column to remove the remaining borate and borohydride ions.^{78, 88} The turmeric paper test¹²⁴ and iodate titration method¹²⁵ showed that borate ions were removed by this process, excluding possible borate ion interferences in the H_2O_2 detection. Upon re-introduction of dioxygen, any quinones previously reduced to hydroquinones by

borohydride under anaerobic conditions are expected to be reoxidized within 24 hours, and thus would not be removed by the reduction.⁷⁸ Absorption losses upon reduction were identical to those reported previously.^{78, 88} (Fig. 2-1)

The reversibility of reduction of carbonyl-containing groups was examined by re-introducing the dioxygen into the borohydride reduced samples. The results indicated that the hydroquinones are reversibly oxidized upon reintroduction of air, but not surprisingly alcohols are not. These results indicated that the aromatic ketones/ aldehydes are largely responsible for the optical changes.

2.3.2 Effect of borohydride reduction on HPPR and apparent quantum yields

As previously reported,^{78,88,126} borohydride reduction produces a substantial loss of absorption across the UV/VIS spectrum, but with preferential loss in the visible (Fig.2-1). These changes in the absorption spectra have been interpreted to result from the loss of charge transfer (CT) transitions in the visible and near-UV as a result of removing carbonyl-containing electron acceptors,^{66, 78, 88} and to the direct loss of absorption by ketone/aldehyde moieties in the ultraviolet.⁸⁸

Despite the significant losses of absorption due to borohydride reduction, HPPR at three wavelengths across the UV (302,313,and 365nm) did not change substantially following reduction, with only slight decreases observed for SRFA and SRHA (~ 15%), no apparent decrease for the Shelf Station, and a slight increase for the Fresh Water station (Fig.2-3). Thus the loss of HPPR was observed to be small or negligible as compared with the loss of absorption.

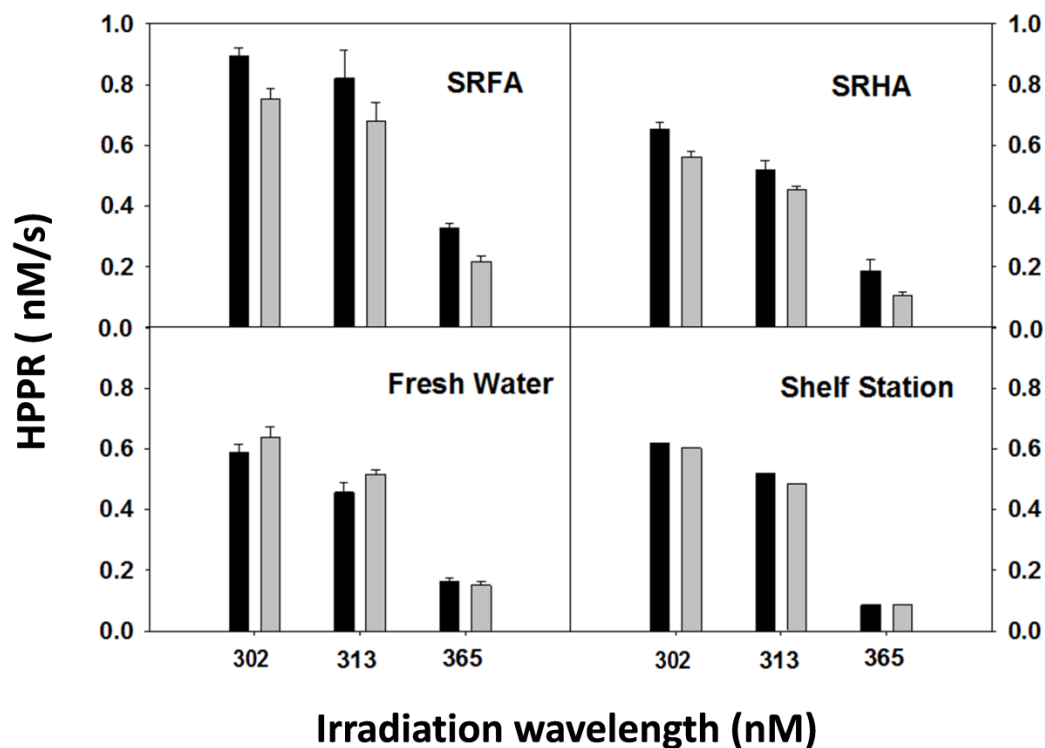


Figure 2- 3: Wavelength dependence of the H_2O_2 production rate (HPPR) for untreated (**■**) and borohydride reduced (**▒**) SRFA, SRHA, and C-18 extracts from the Fresh Water and Shelf Station at equivalent mass concentration (10 mg/L for SRFA and SRHA, TOC as 3.6 and 10.68 for the Fresh Water and Shelf Stations. All samples were in 10 mM phosphate buffer, pH =7.0)

Apparent monochromatic and polychromatic quantum yields reinforce this conclusion. Due to the small changes in HPPR and larger losses in absorption, monochromatic quantum yields at 302 nm and 313 nm increased by ~20-30 % for SRFA and the Fresh Water and Shelf Station following borohydride reduction, with smaller apparent increases in the quantum yield at 365 nm. In addition, the difference quantum yield, $\Delta\Phi$, exhibited values that were either close to zero or much smaller than the Φ of the untreated or borohydride-reduced samples, as would be expected for a loss of absorption that did not concomitantly affect HPPR (Fig. 2-4).

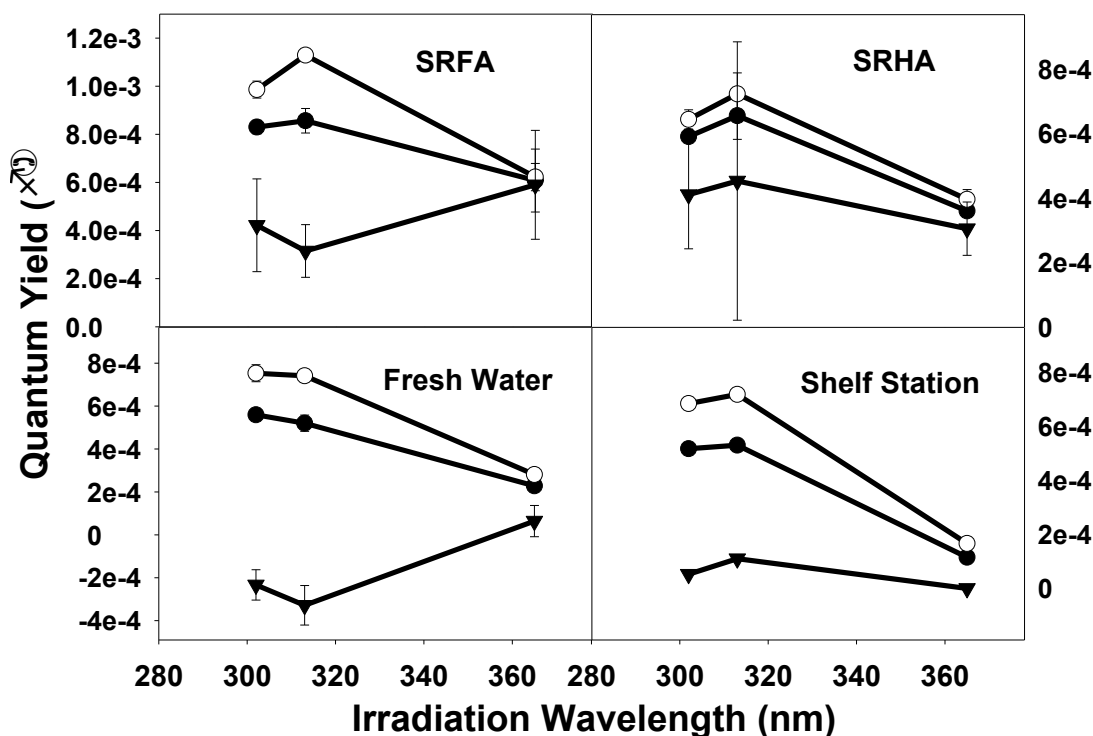


Figure 2- 4: Apparent monochromatic H_2O_2 quantum yields (Φ) and difference quantum yields ($\Delta\Phi$) (\blacktriangledown) for untreated (\bullet) and borohydride-reduced (\circ) SRFA, SRHA and C-18 extracts from Fresh Water and Shelf Station. Other conditions as in Figure 2-3.

Apparent polychromatic quantum yields exhibited even larger increases following reduction, approximately doubling in all cases (Table 2-2), while $\Delta\Phi$ was very small, indistinguishable from zero with the uncertainties of the measurements (Table 2-2). The large increases in polychromatic quantum yields following reduction are attributed to the substantial losses of absorption in the visible and near UV (Fig. 2-1), where much less or no H_2O_2 is produced in either untreated or treated samples.^{19,127,128} The lower quantum yields observed for the polychromatic (Table 2-2) as compared to the monochromatic source at short wavelengths (Fig. 2-4) is a reflection of the relatively large decrease in the monochromatic quantum yields with increasing wavelength^{19, 127, 128} (Fig. 2-4), and the $R(\lambda)$ for the polychromatic source, which is weighted to the longer wavelengths in the UV-A and visible (Fig 2-2), where again, much less or no H_2O_2 is produced.

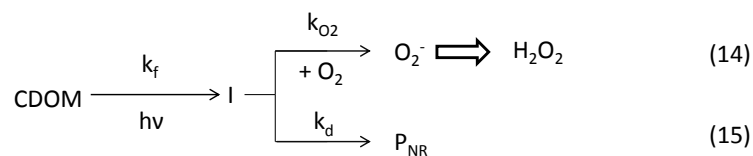
Table 2- 2: Polychromatic H₂O₂ quantum yields (ϕ) and difference quantum yield ($\Delta\phi$) for untreated and borohydride reduced LAC, SRHA, SRFA, and C-18 extracts from the Fresh Water and Shelf Stations. R_{ex} is the rate of light excitation, HPPR uncertainties were standard derivation from triplet measurements and ϕ uncertainties were propagated from determination of HPPR.

Sample	HPPR (M/s)($\times 10^{-9}$)	R_{ex} (mol/cm ³ /s) ($\times 10^{-9}$)	$\phi(\times 10^{-4})$	$\Delta\phi(\times 10^{-4})$
LAC	2.06 ± 0.27	2.29	8.99 ± 1.21	1.74 ± 2.2
REDUCED LAC	1.84 ± 0.09	1.02	18.1 ± 0.94	
SRHA	1.41 ± 0.07	3.68	3.82 ± 0.27	0.54 ± 0.72
Reduced SRHA	1.32 ± 0.05	2.14	6.18 ± 0.53	
SRFA	1.23 ± 0.07	2.43	5.08 ± 0.19	0.49 ± 0.57
Reduced SRFA	1.17 ± 0.06	1.2	9.77 ± 0.22	
Fresh Water	1.13	1.95	5.81	2.94
Reduced Fresh water	0.88	1.1	8.03	
Shelf station	0.76	1.91	4.04	-4.79
Reduced Shelf Station	1.15	1.10	10.5	

2.3.3 Effect of dioxygen concentration on HPPR

While HPPR increased with increasing $[O_2]$ at $[O_2] \leq 300 \mu\text{M}$, above $[O_2] \sim 500 \mu\text{M}$, HPPR became independent of $[O_2]$, suggesting complete reaction with the O_2 -reducing intermediates (Fig 2-4). Except for SRHA, the dependence of HPPR on $[O_2]$ was very similar for both untreated and borohydride-reduced samples, suggesting that borohydride reduction did not affect significantly the lifetime of the intermediate(s) (see below).

This kinetic behavior is consistent with the photochemical formation of an intermediate, I, formed at rate, k_f , which reacts with O_2 at rate constant, k_{O_2} , to form O_2^- (and subsequently H_2O_2), in competition with its relaxation to non-reactive species P_{NR} , formed with rate constant, k_d ,



thus leading to the following expression that relates the H_2O_2 production rate to $[O_2]$:

$$HPPR = \left[\frac{d[H_2O_2]}{dt} \right]_0 = \frac{k_f k_{O_2} [O_2]}{k_d + k_{O_2} [O_2]} = \frac{k_f [O_2]}{\frac{k_d}{k_{O_2}} + [O_2]} = \frac{a [O_2]}{b + [O_2]} \quad (16)$$

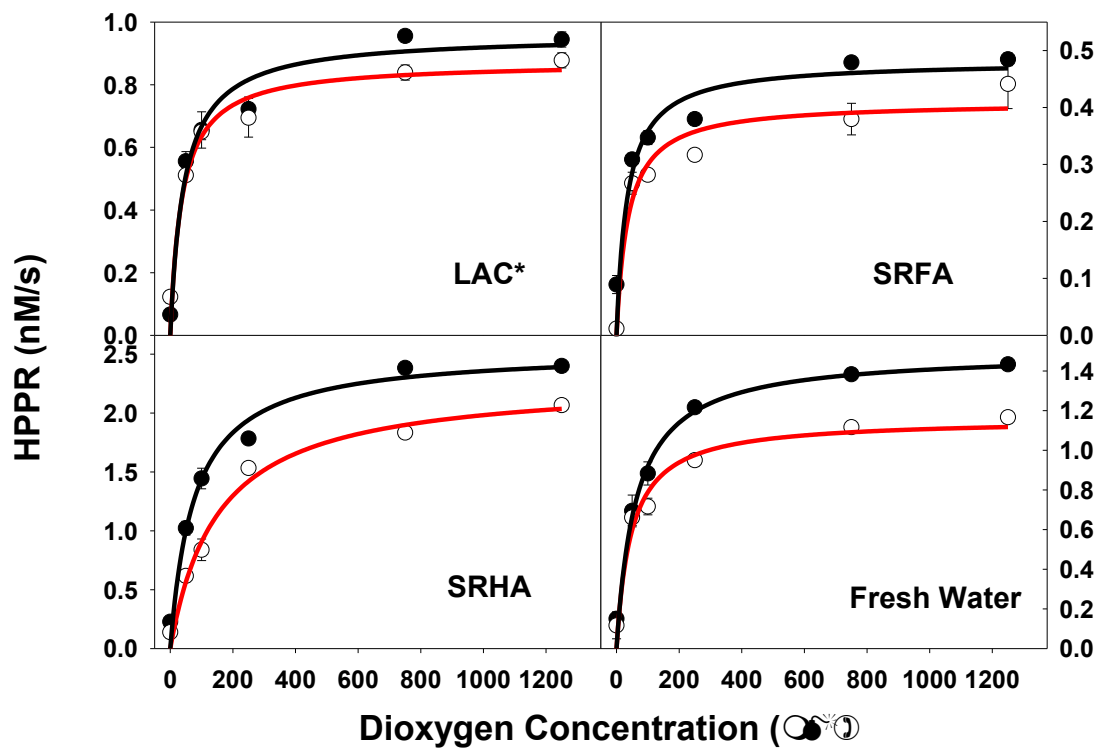


Figure 2- 5: Dependence of HPPR on dioxygen concentration for untreated (•) and borohydride –reduced (○) SRFA, SRHA, LAC* and the C-18 extract from Fresh Water station using the polychromatic source. The irradiance for LAC* and SRFA was lower than that for SRHA and the Fresh Water station.

Previous studies have provided evidence that O_2^- can back react with the HS to produce O_2 (Eqn. 14) in competition with disproportionation (Eqn. 1),^{13, 29} thus reducing the yield of H_2O_2 .

As shown in the Appendix 1, if Eqn14 and 1 are both pseudo-first order reactions, only the yield (R_f) changes and not the O_2 -dependence; the half-saturation value, k_d/k_{O_2} , remains unchanged. In contrast, if Eqn1 is a second-order reaction while Eqn 14 is a pseudo-first order reaction, the branching ratio between Eqn 14 and 1 become O_2 -dependent and an expression more complicated than Eqn. 16 is obtained (see appendix 1). However, employing previously published values of k_{dis} and k_{rec} ^{19,77} we show that this effect exerts a negligible influence on the half-saturation value and thus that Eqn. 16 remains a valid approximation.

A non-linear least-squares fitting routine was employed to fit the data in Fig. 2-5 to Eqn.16, with parameters $a (=k_f)$ and $b (= \frac{k_d}{k_{O_2}})$ provided in Table 2-3. Assuming a $k_{O_2} \approx 10^9 M^{-1} s^{-1}$, a reasonable value for reaction of O_2 with either an excited triplet state (Rxn. 4b)⁸⁸ or a reducing radical intermediate (Rxns. 5,6),¹²⁹ calculated lifetimes ranged from 10 to 30 μs , and except for SRHA, did not change significantly following borohydride reduction. If k_{O_2} for reaction with the intermediate is actually smaller, the corresponding lifetime of the intermediate clearly would be longer. Because k_{O_2} for reaction with excited triplets and reducing radicals could be similar, these data alone cannot be used to discriminate between Rxns. 4 and 5.

Table 2- 3: Parameters obtained from fits of the data in Fig.2-5 to the expression.

$HPPR = \frac{a[O_2]}{b+[O_2]}$, where $a (= k_f)$ and $b (= \frac{k_d}{k_{O_2}})$. Lifetime of the intermediate is given by, $\tau = \frac{1}{k_d} = \frac{1}{b \times k_{O_2}}$, where k_{O_2} is assumed to be $1 \times 10^9 \text{ M}^{-1}\text{S}^{-1}$ (see text) . Other conditions are as in Figure. 2-5.

$HPPR = \frac{a[O_2]}{b + [O_2]}$	$a = k_f$ (nM/min)	$b = \frac{k_d}{k_{O_2}}$ (μM)	$\tau (\mu s) = \frac{1}{b \times k_{O_2}}$
LAC*	57	43	23
Reduce LAC*	52	37	27
SRFA	28	34	29
Reduced SRFA	24	36	28
SRHA	152	76	13
Reduced SRHA	136	151	7
Fresh water	89	62	17
Reduced Fresh Water	69	46	22

Interestingly, HPPR was never completely eliminated with irradiation under N₂ (Fig.2-5), despite extensive tests employing dithionite that demonstrated anaerobic conditions were maintained. Because the introduction of O₂ during the H₂O₂ analysis could not be avoided, this H₂O₂ formation could result from the reaction of long-lived reductants formed during the anaerobic irradiation with the O₂ introduced during analysis. In fact, similar H₂O₂ concentrations were observed when the H₂O₂ analysis was performed immediately following sample irradiation and after waiting for thirty minutes under strictly anaerobic conditions, suggesting that this reductant pool was largely stable in the absence of O₂ (Table 2-4).

Table 2- 4 Hydrogen peroxide concentration and reacted 3apf measured after irradiation for SRFA, SRHA, LAC* and the Fresh Water station for 15 min under anaerobic condition.

Samples	[H ₂ O ₂] measured immediately following a 15 min irradiation under anaerobic conditions (nM)	[H ₂ O ₂] measured 30 mins after a 15 min irradiation under anaerobic conditions (nM)	Reacted 3-apf measured at 50 min following a 15 min irradiation under anaerobic conditions (nM)
SRFA	234 ±35	257	322
SRHA	201±46	298	400
Fresh Water	214±40	284	476
LAC *	351±70	253	392

To test this possibility further, we employed the nitroxide, 3apf. Nitroxides have been shown previously to compete with O₂ for reducing radicals.^{99, 102, 103} Introduction of 14μM 3apf into anaerobic samples following irradiation lead to a significant fluorescence increase over the course of 50 minutes, indicative of a nitroxide reaction to produce a diamagnetic product.^{104,130} In contrast, introduction of air for 2 minutes prior to the introduction of 3apf eliminated this fluorescence increase (Fig 2-6). Further, no changes in fluorescence were observed following the addition of 3apf to un-irradiated samples either in the presence or absence of air.

Based on the observed fluorescence increases after 50 minutes (Fig.2-6), estimates of the reductant levels produced following 15 minutes of irradiation under anaerobic conditions were obtained (Table 2-4) and were found to be in similar magnitude to the H₂O₂ concentrations measured under those same conditions (200 to 300 nM).

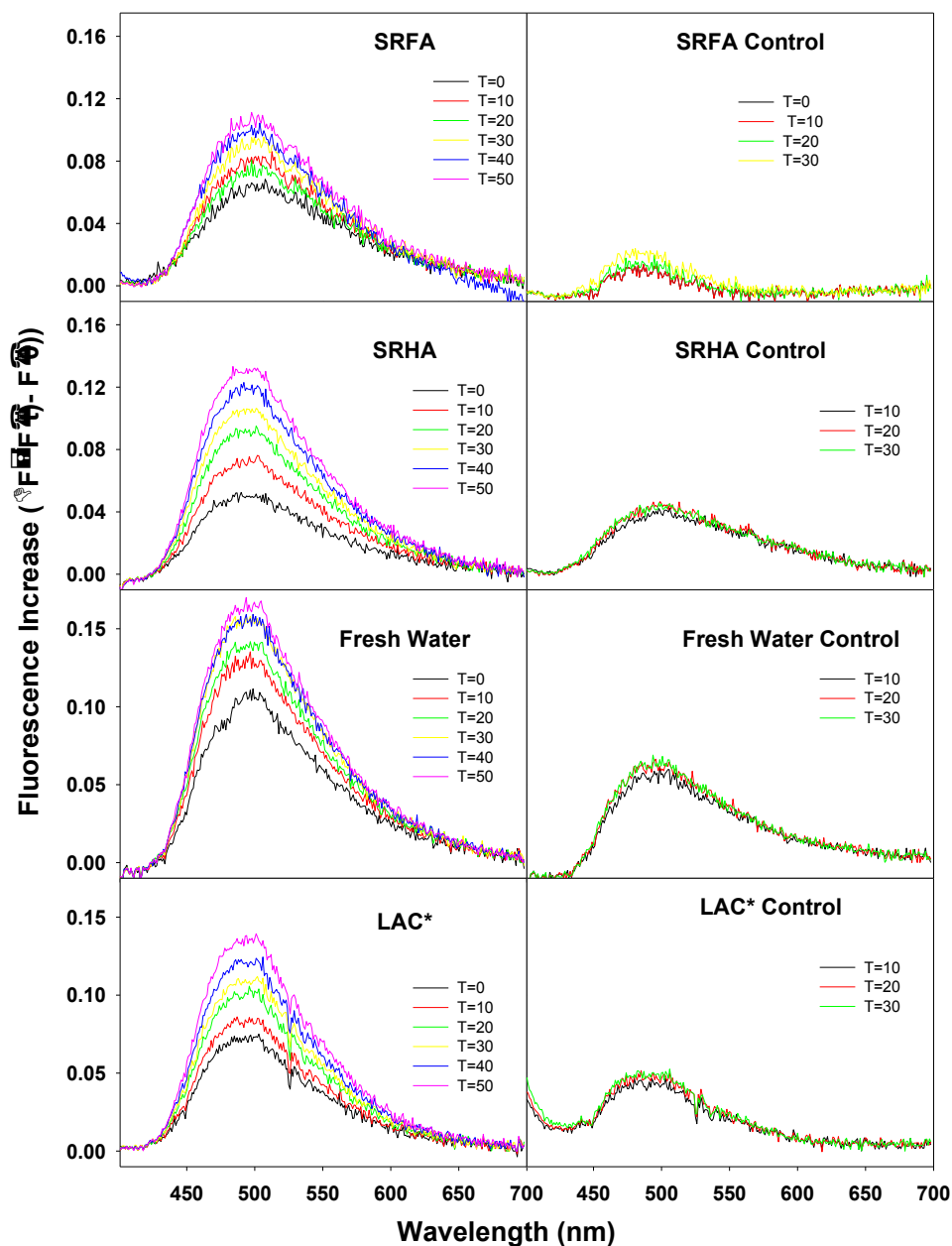


Figure 2- 6: The time dependence of 3apf fluorescence increase ($\Delta F = F(t) - F(0)$) following the anaerobic addition of 3apf to SRFA, SRHA, LAC*, and the Fresh Water station, which had been previously irradiated for 15 min under anaerobic conditions. $F(0)$ represents fluorescence of the 3apf and sample prior to irradiation, while $F(t)$ is the fluorescence observed following addition of 3apf to the irradiated samples under anaerobic conditions (left panels). In control experiments (right panels), air was introduced for 2 mins prior to the addition of 3apf to the anaerobically-irradiated samples.

2.3.4 Effect of triplet quenchers

To test directly for the involvement of excited triplet states³⁵ in the formation of H₂O₂ (Rxn. 4b), the triplet quenchers Cl⁻ and Br⁻¹³¹⁻¹³⁶ and sorbic acid^{35, 137, 138} were employed. Adding sorbic acid up to a concentration of 5 mM produced at best only ~25% decrease in H₂O₂ production for both untreated and borohydride-reduced samples (Fig. 2-7). Assuming a rate constant of $3.6 \times 10^9 \text{ M}^{-1} \text{ s}^{-1}$ for triplet quenching by sorbic acid,¹³⁷ the lifetime of the triplet would be reduced to 56 ns at a sorbic acid concentration of 5 mM. This lifetime is ~400-fold lower than the estimated lifetime of the intermediate (~20 μs , see above), and thus complete loss of HPPR would be expected under this condition, if the direct reaction of excited triplet states with dioxygen was the principal pathway producing O₂⁻ (Rxn. 4b).

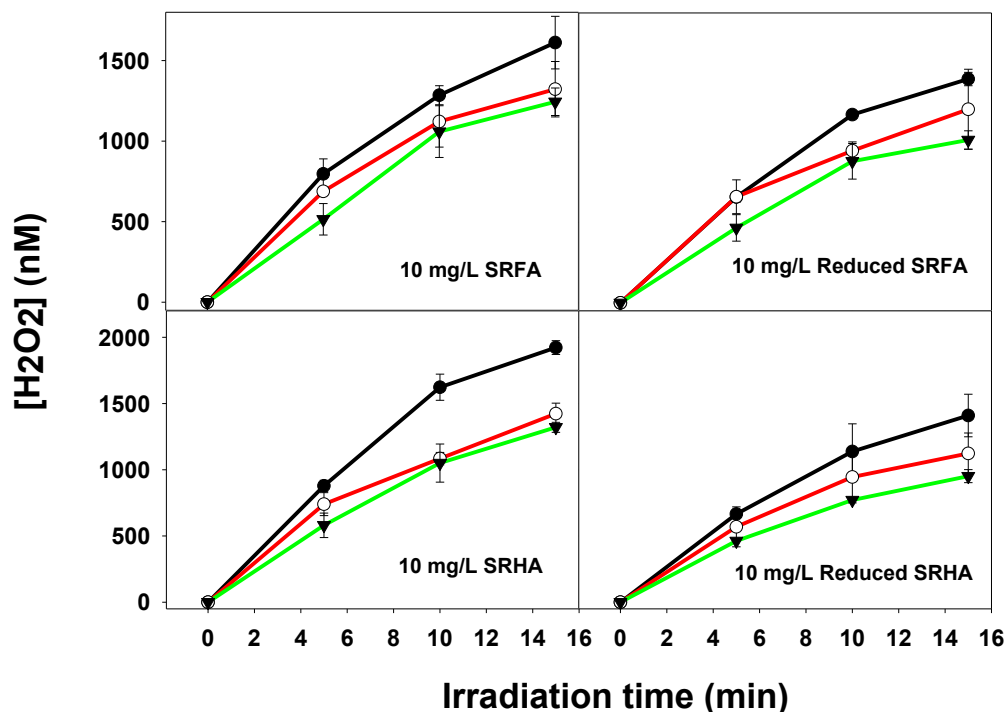
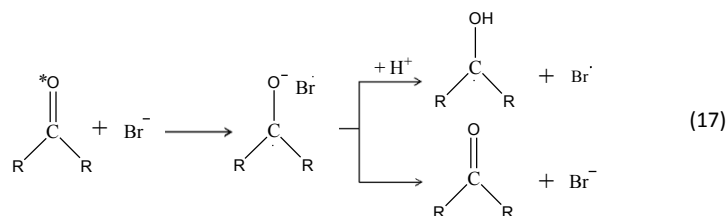
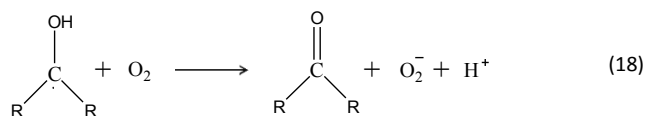


Figure 2- 7: Effects of sorbic acid (0 mM (\bullet); 1mM (\circ); 5 mM (\blacktriangledown)) on H_2O_2 photo-production for untreated and borohydride reduced SRFA and SRHA under aerobic conditions employing the polychromatic source

The conclusion that Rxn 4b is not a significant source of H_2O_2 was also supported by the results of Br^- and Cl^- addition. In fact, addition of Cl^- and Br^- at 500 mM to untreated SRFA lead to an ~20% and 50% increase in H_2O_2 production, respectively, while the borohydride-reduced sample showed no change (Figure. 2-8). Chloride and particularly bromide ions are known to quench effectively oxidizing triplets such as those of ketones through a CT mechanism.¹³² Because no enhancement of H_2O_2 production was observed following borohydride reduction, we speculate that this enhanced production, particularly in the case of Br^- , arises through the reaction of aromatic ketone triplet states with Br^- to form the ketyl radical,¹³²



which subsequently reacts with O_2 to form O_2^- :



Although most quinone triplets are also quenched effectively by Cl^- and Br^- ,^{131,139,140} and at least in some cases, appear to produce the semiquinone at high halide concentrations,¹³¹ the absence of HPPR enhancement following borohydride reduction, in which any hydroquinones formed are expected to be reversibly oxidized to quinones,^{78,141} suggests that quinones do not contribute to this process (Eqns. 17, 18)

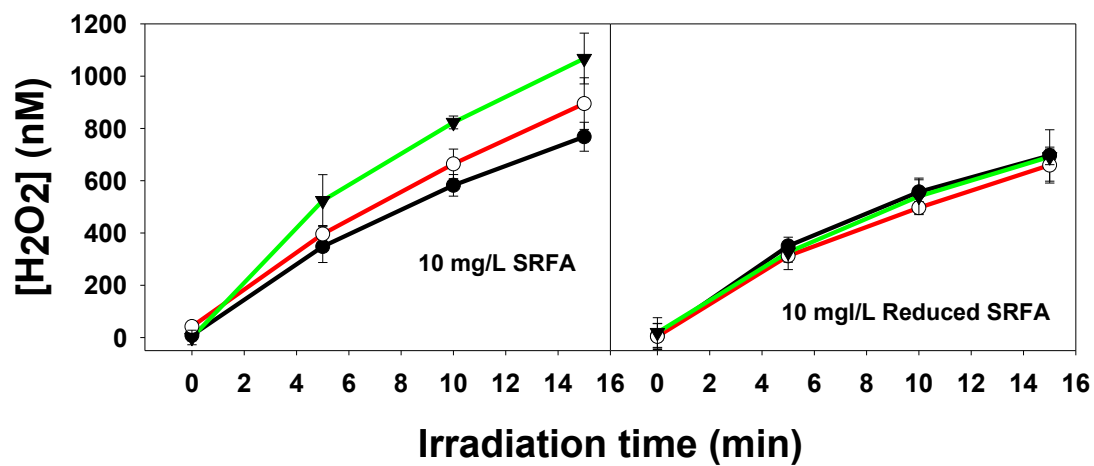


Figure 2- 8: Effects of triplet quencher Cl^- (—○— 500mM Cl^-) and Br^- (—▼— 500mM) on H_2O_2 aerobic photo-production for untreated and borohydride-reduced SRFA under aerobic conditions using the polychromatic source, (—●—) is the control without triplet quenchers

2.4 Discussion

This work clearly demonstrates that the loss of UV and visible absorption following borohydride reduction does not largely affect HPPR (Fig. 2-3, Table 2-1). Thus, monochromatic and polychromatic quantum yields for H_2O_2 photoproduction concomitantly increase (Fig. 2-4, Table 2-2). These results show that direct excitation of near-UV and visible absorption, previously assigned to CT states, does not lead to significant H_2O_2 production (Rxn.6). Instead, previous evidence suggests that these CT states relax very rapidly to the ground state through recombination, as illustrated by the exceedingly short excited state life times (sub-nanosecond) observed in the visible by time-resolved fluorescence measurements,^{67, 89} as well as by the rapid decrease in apparent H_2O_2 quantum yields with increasing wavelength^{19,127,128} (Fig 2-4). Similarly, (aromatic) ketones/aldehydes do not appear to play a significant role in H_2O_2 production, except possibly in cases where external donors (eg., Br^-) are capable of intercepting the (oxidizing) triplet states of these species¹⁴² (Fig. 2-8; see also reference 63).

A significant contribution to H_2O_2 formation through a direct reaction of O_2 with the triplet states of electron donors (Rxn. 4b) also appears highly unlikely. Although the production of H_2O_2 does decrease slightly with addition of 1 to 5 mM sorbic acid, the rates remain far higher than one would predict based on the rate constant for triplet quenching by sorbic acid¹³⁷ ($\sim 10^9 \text{ M}^{-1}\text{s}^{-1}$). Further, a past study⁹⁹ employing nitroxides, which are highly effective triplet (and singlet) quenchers^{99,143,144} as well as radical/reductant traps,¹⁰⁴ showed no evidence of a decrease in the rates of radical/reductant formation at high nitroxide and O_2

concentrations,⁹⁹ implying that the lifetimes of the excited state species giving rise to the radical/reducing intermediates are very short-lived, consistent with excited singlet states.⁹⁹ Moreover, this pathway (Rxn. 4b) cannot be operative in the formation of the long-lived radical/reducing intermediates generated under anaerobic conditions (Fig. 2-5, Table 2-3).

Instead, intramolecular electron transfer from an excited singlet donor to a ground-state acceptor appears far more likely (Rxn. 5a). Possible donors include substituted phenols, while possible acceptors included quinones, which unlike ketones/aldehydes are not irreversibly reduced by borohydride.⁷⁸ Although electron transfer to a short-lived excited state electron acceptors, eg., quinones, from a ground-state donor cannot be completely excluded, one might expect significant H₂O₂ photoproduction rates at visible wavelengths where some quinones do absorb, contrary to the experimental evidence.

In summary, this work suggests that H₂O₂ is formed primarily through a low-efficiency intramolecular excited state electron transfer process that produces reducing (radical) intermediates, which then react with O₂ to form O₂⁻ and subsequently H₂O₂. Both a shorter-lived reductant pool (10's of microseconds) and a longer-lived reductant pool (many minutes in the absence of O₂) were observed to be produced photochemically.

Chapter 3: Molecular probe measurements of the photochemical production of one electron reducing intermediates from chromophore dissolved organic matter: relation to H₂O₂ photochemical production.

3.1 Introduction

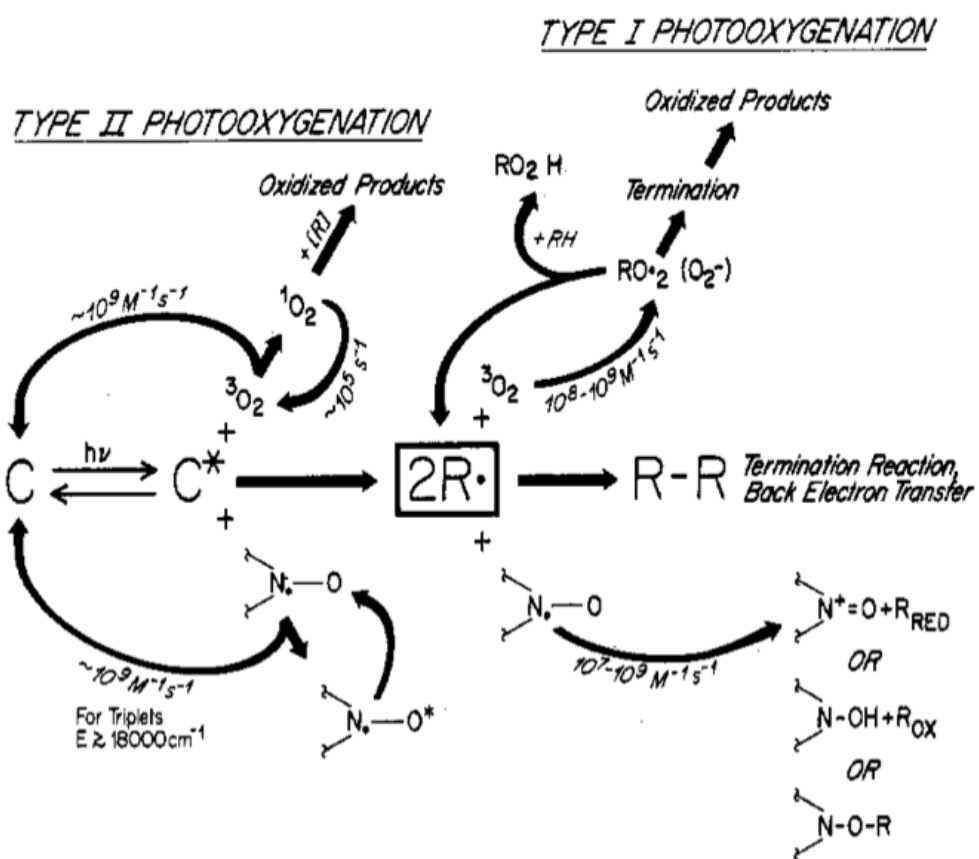
Over the past 30 years, chromophoric dissolved organic matter (CDOM) has been shown to generate a variety of reactive intermediates upon irradiation with UV and near-visible light. In aerobic waters, those species can react with dioxygen to produce various reactive oxygen species (ROS), including superoxide, hydrogen peroxide, singlet dioxygen, peroxy radicals, and organic peroxides. Among the ROS generated, the photochemical production of H₂O₂ has been one of the most intensively investigated due to its significant environmental importance. This species can affect the trace metal geochemical cycling and impact the photochemical and thermal degradation of natural and anthropogenic organic compounds in aquatic systems. In addition, as a relatively stable ROS, detection of the photoproduct H₂O₂ can serve as an informative measure of the transfer of electrons from the organic matter pool to dioxygen, allowing estimates of the net photochemical oxidation.

Past work has presented evidence that H₂O₂ primarily arises through the dismutation of superoxide, the one-electron reduction product of dioxygen.^{17,36,80,81} Petasne and Zika,³⁶ employing the enzyme, superoxide dismutase (SOD), to catalyze this dismutation, obtained evidence that 24-41% of the generated superoxide flux did not lead to the H₂O₂ formation. Waite and coworkers further argued that the

contribution of oxidative sinks of O_2^- , which do not lead to H_2O_2 production, are ~1.7-fold greater than that previously proposed by Petasne and Zika.⁷⁷ Zhang et al.¹⁴⁵ later provided evidence that superoxide is formed primarily via reactions with reduced electron acceptors within CDOM generated by intramolecular electron transfer between excited singlet-state electron donors and a ground-state electron acceptors.

A closer look at the stoichiometric relationship between H_2O_2 formation and the production of O_2^- reducing intermediates would allow a better understanding of the mechanism(s) of radical formation and the reactions leading to the net H_2O_2 production.

Here we employed the molecular probe, 3-amino-2,2,5,5-tetramethyl-1-pyrrolydinyloxy (3ap), to examine the rates of formation of one-electron reducing intermediates photochemically generated from CDOM. Having a similar reactivity to dioxygen,^{146,147} this stable nitroxide radical can react rapidly with one-electron reductants to produce a relatively stable final product, the hydroxylamine, and thus may allow quantification of the O_2^- reactive reducing intermediates in the absence of dioxygen (Scheme 3-1).⁹⁹



Scheme 3- 1: Comparison between the reactions of nitroxides and O_2 with excited states and radicals. From reference 103.

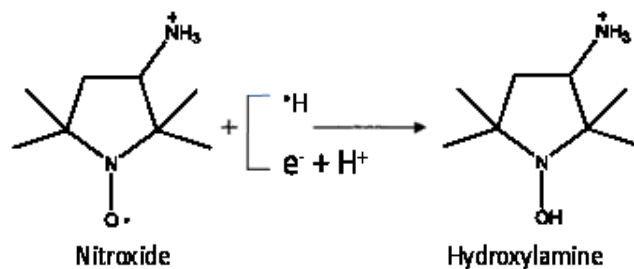


Figure 3- 1: Hydroxylamine formation via reaction of the nitroxide with photochemically-generated one electron reducing-intermediates within CDOM

For the detection of the hydroxylamine, products of the photochemical reaction are first coupled with fluorescamine.¹²¹ While the fluorescence yield of fluorescamine-derivatized 3ap is very low due to efficient intramolecular quenching,¹⁰⁴ reactions forming the hydroxylamine and other diamagnetic products eliminate this quenching and thus substantially increase the fluorescence. The enhanced fluorescence can be used as a very sensitive means of radical detection when coupled with HPLC, offers a reliable quantitative measurement of the reductant generation.¹⁰²

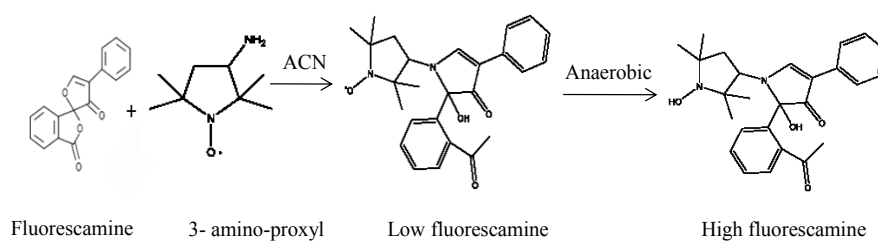


Figure 3- 2: Fluorescence change upon the nitroxide reaction with fluorescamine

If 3ap and O_2 compete for the same pool of reducing intermediates, the presence of dioxygen should lead to a decrease in the rate of hydroxylamine formation. By examining the effect of $[O_2]$ on the initial rate of hydroxylamine formation, estimates of the relative rate constants for O_2 and 3ap reaction with those reducing intermediates can be obtained, as well as estimates of the formation rates of the intermediates. These rates can then be compared with the rate of H_2O_2 formation to examine the stoichiometric relationship between the reduction of O_2^- and generated H_2O_2 formation.

3.2 Materials and Methods:

3.2.1 Chemicals

Boric acid, sodium chloride, sodium phosphate, sodium dihydrogen phosphate, fluorescamine and 3-carbamoyl-2,2,5,5,-tetramethy-1-pyrrolydinyloxy (3cp) were purchased from Sigma- Aldrich. The nitroxide probe, 3-amino-2,2,5,5,-tetramethy-1-pyrrolydinyloxy (3ap) and sodium dithionite were purchased from Acros. Acetic acid, phosphoric acid and HPLC grade methanol were obtained from Fisher. Suwannee River fulvic acid (SRFA) and Suwannee River humic acid (SRHA) were obtained from the International Humic Substance Society. Pure water for all experiments was obtained from a Millipore Milli-Q system.

3.2.2 Experiment Apparatus

Hewlett-Packard 8425A spectrophotometer was employed to acquire UV/VIS absorption spectra. Absorption spectra over the range of 190 to 820 nm for 5 and 10 mg/L samples were recorded using 1 cm cuvette referenced to the solvent. The HPLC consisted of Dionex Model P580 pump, 4 μ m C-18 reversed-phase packing column (from Waters) and a 50 μ L injection loop. All separations are performed at room temperature. The fluorescence detector used was a Hitachi model L7480 set at 390 nm (excitation) and 490 nm (emission). The mobile phase consisted of 55% methanol and 45% acetate buffer (50 mM, pH= 4.0).

EPR spectra were record on a Bruker BioSpin GmBH instrument. Standard instrument settings were: microwave frequency, 9.42 GHz; power, 2.00 mW; modulation amplitude, 1.0 G; modulation frequency 100 KHz; time constant, 10.24

ms. Samples were drawn into 50 μL capillaries, which were then sealed with Critoseal[®] and placed inside 3 mm diameter quartz EPR tubes.

Borohydride reduction of samples were performed employing a 25-fold mass excess of borohydride.¹⁴⁵ H_2O_2 measurements were performed using a chemical luminescence based flow injection method as previously described.^{129,130}

3.2.3. Detection of photoreductants

Humic substance (HS) samples at concentrations of either 5 or 10 mg/L were prepared in 50 mM borate buffer (pH =8.0), with different concentrations of 3ap added to these solutions. For the polychromatic irradiations, a 300 W xenon arc lamp combined with a 325 nm long-pass cutoff filter was employed to approximate solar spectrum. A 20 cm water jacket was placed in front of the light source to remove infrared irradiation. Monochromatic irradiations were performed using 1000 W Hg-Xe lamp and a Spectral Energy GM 252 monochromator set to a 20 nm band pass. Samples were held in a 1 cm pathlength, Teflon-capped quartz cuvette. Differing dioxygen concentrations, ranging from 0 to 1250 μM , were achieved by mixing of N_2 , O_2 or air with a rotameter, with the solutions purged with the appropriate gas mixture for 20 min prior to irradiation.

Following irradiation of 3ap, 200 μL of this solution was withdrawn with a gas-tight syringe, and derivatized via addition of 50 μL of a 5 mM stock fluorescamine solution in a Teflon container with vigorously mixing. The stock fluorescamine solution was prepared daily in acetonitrile and stored in the dark at

room temperature. The hydroxylamine was separated by HPLC and detected fluorometrically.

Because 3ap is highly hygroscopic, concentrations of 3ap were determined by paramagnetic resonance spectroscopy (EPR) using 3cp as a primary standard. The concentration of the stock 3cp solution was determined from the mass of 3cp. Lower concentrations were obtained by serial dilution of this stock. Concentrations of 3ap were first tentatively determined based on mass. The concentration was then determined accurately by the comparison of normalized double integral value (DI/N) of 3ap to that of 3cp.

The molar absorptivity of 3ap at 316 nm ($12.5 \text{ M}^{-1}\text{cm}^{-1}$) was determined by the comparison with the stock 3ap concentration, and the molar absorptivity obtained was employed to acquire 3ap concentrations. (Fig. 3-1) All the EPR solutions were prepared in pH=8 borate buffer.

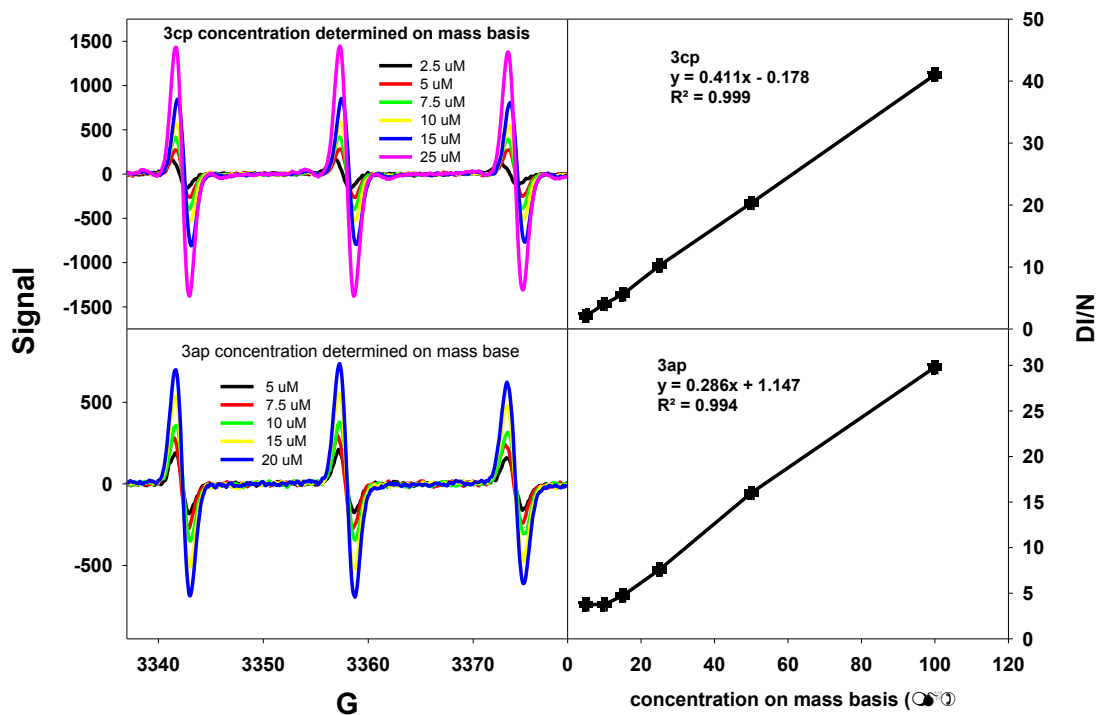


Figure 3- 3: EPR spectra of 3cp (top) and 3ap (bottom) (left panel) and the calibration curves constructed from the normalized double integral value (DI/N) (right panel). Both concentration of 3cp and 3ap were first determined from mass base. Because 3cp can be readily dried while 3ap is highly hygroscopic, 3cp was used as a primary standard. The 3ap concentration was then determined by DI/N comparison with the 3cp calibration.

The amount of hydroxylamine produced was determined from hydroxylamine calibration curves constructed through anoxic titrations employing dithionite as a reductant (Fig. 3-4). Two types of hydroxylamine calibrations were examined, with either dithionite (top left) or 3ap (bottom left) as the limiting reagent. Stock dithionite concentrations were determined from the molar absorptivity at 316 nm (8000 M cm⁻¹).^{148,149} 3ap concentrations were determined as previously described above (Fig. 3-3).

Stock concentrations of limiting reagent were determined from their molar absorptivities. Right panels are calibration curves constructed from peak height values (top dithionite $y=1607+127895x$, bottom 3ap; $y=-9494+68900x$). Because dithionite provides two reducing equivalents, the slope is twice as high when dithionite is the limiting reagent. All the curves were baseline subtracted from the control samples before reduction.

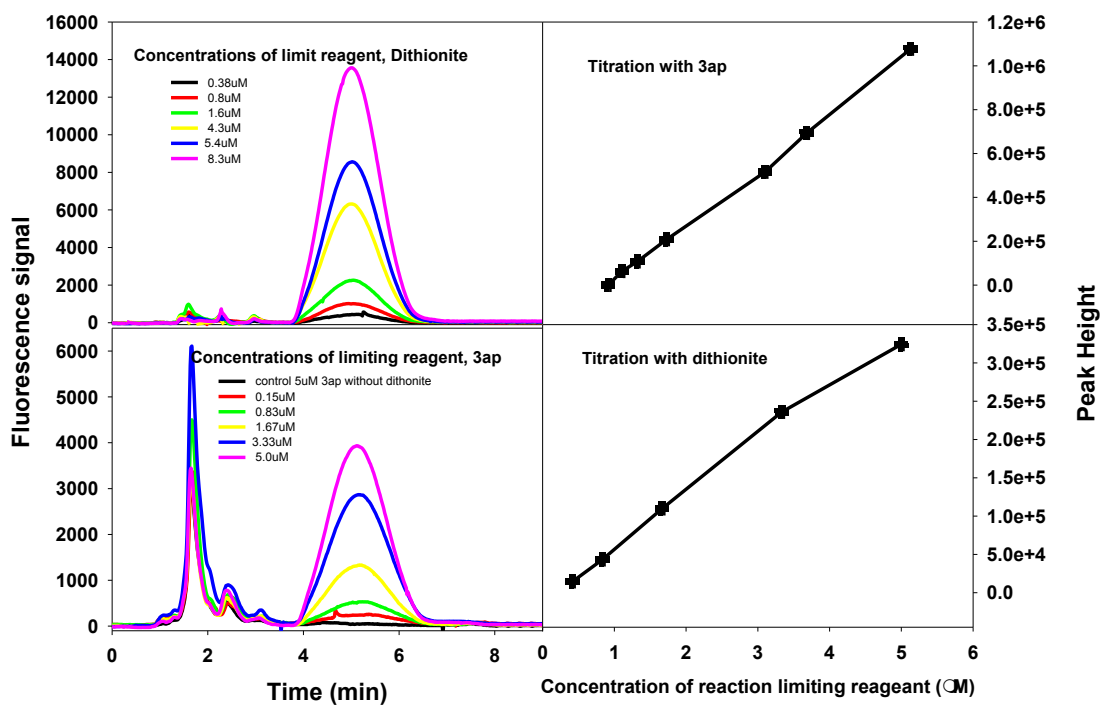


Figure 3- 4: HPLC chromatography of hydroxylamine production upon dithionite titration (left panel) and hydroxylamine calibration curves constructed from peak height (right panel). Top panels provide the chromatograms and calibration curve using dithionite as limiting reaction reagent, and the bottom panels from using 3ap as limiting reagent.

3.2.4 Determination of the formation rates of photoreductants from humic substance

The net hydroxylamine production rate (R_H) was calculated using equation 3.1,

$$R_H = \frac{T_{15} - T_0}{15 \text{ min}} \quad (3.1)$$

where T_0 is the derivatized product yield from samples of HS spiked with [3ap]

before irradiation (blank), and T_{15} is the yield at the end of 15 min irradiation.

Apparent quantum yields for polychromatic irradiations, ϕ were calculated using following expression,

$$\phi = \frac{R_H}{R_{EX}} \quad (3.2)$$

where R_{EX} is the rate of light excitation

$$R_{EX} = \int_{190}^{820} a(\lambda) \times I(\lambda) d\lambda \quad (3.3)$$

$a(\lambda)$ is the absorption coefficient of the sample, and $I(\lambda)$ is the irradiance at wavelength λ (photons $\text{cm}^{-2} \text{s}^{-1}$), as measured with an Ocean Optics spectroradiometer.

R_{EX} has been converted to mole photons $\text{L}^{-1} \text{s}^{-1}$.

For the monochromatic irradiations, $\phi(\lambda)$ were determined using the following equation:

$$\phi = \frac{HPPR}{R_{EX}} = \frac{HPPR \times L}{I_0(\lambda) \times (1 - 10^{-A(\lambda)})} \quad (3.4)$$

where, L is the path length of the cell (cm^{-1}), A is the absorbance, and $(1 - 10^{-A})$ is the fraction of light absorbed by the sample solutions.

3.3 Results

3.3.1 Detection of hydroxylamine formation

Irradiation of SRFA under anoxic condition in the presence of 3ap results in the formation of hydroxylamine, with the initial rate of hydroxylamine formation R_H , increase with increasing 3ap concentration (Fig. 3-4). The hydroxylamine was not observed in the absence of either 3ap or HS. Further, no hydroxylamine formation was observed with irradiation of 3ap in the presence of 100 mM phenol. This result excludes hydroxylamine formation through reaction with the hydrated electron from phenol photoionization under the employed light field, and also precludes hydrogen atom abstraction from phenols by the excited state nitroxide.¹⁵⁰ R_H increased in an approximately linear fashion with SRFA and SRHA concentration (Fig. 3-4 right, Fig. 3-5), indicating that the humic substances are responsible for the photo-produced hydroxylamine.

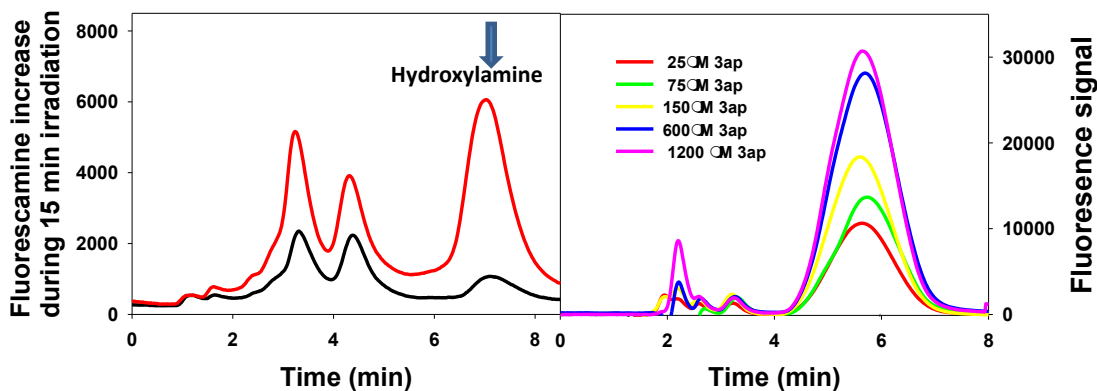


Figure 3- 5: Increase in hydroxylamine following irradiation of an anaerobic solution containing 10 mg/L SRFA and 600 μ M 3ap. Left: black, before irradiation, red after 15 min irradiation. Right: Increase in R_H with increasing [3ap] for 10 mg/L SRFA employing a 15 min anaerobic irradiation.

Above 200-300 μM 3ap, R_H appeared to saturate (Fig.3-6), suggesting complete trapping of the reducing intermediate(s). This result is consistent with a competition between the reaction of 3ap with the reducing species and their loss through recombination. (Scheme 3.2)

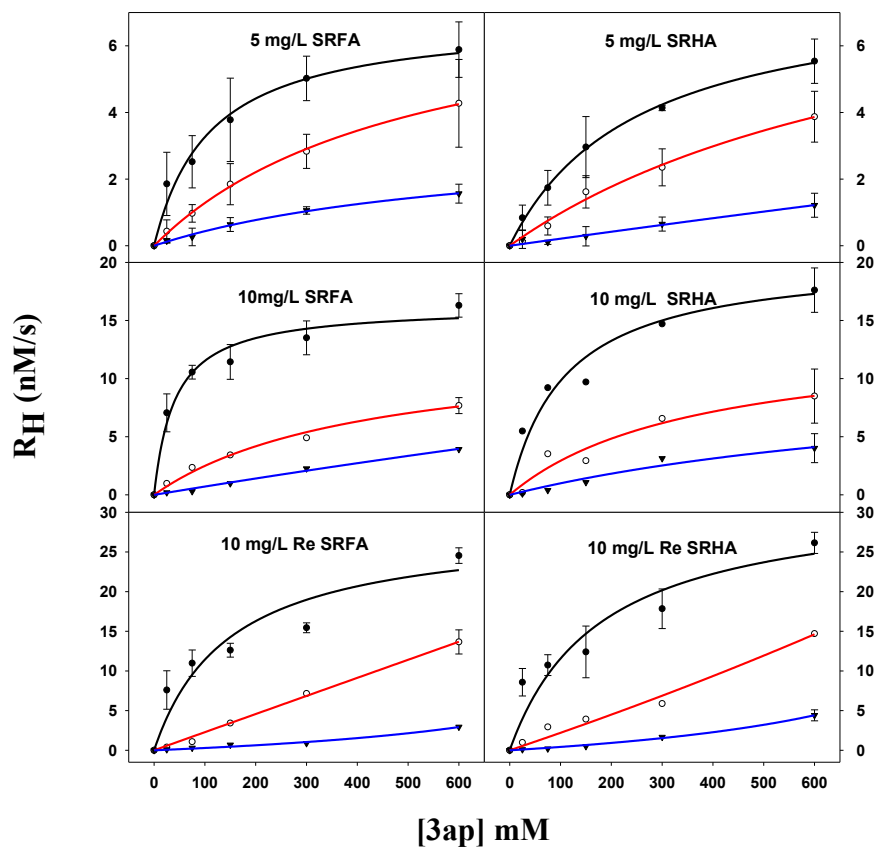
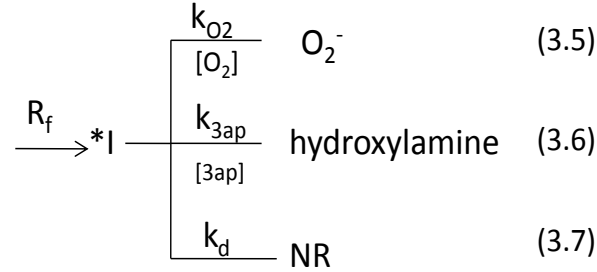


Figure 3- 6: Dependence of R_H (nM/s) on $[3ap]$ for 5mg/L and 10 mg/L SRFA, SRHA and their corresponding borohydride reduced samples (Black line: $O_2 = 0 \mu\text{M}$, Red Line $O_2 = 50 \mu\text{M}$, Blue Line $O_2 = 250 \mu\text{M}$)

At [dioxygen] = 50 μ M, R_H decreased for both SRFA and SRHA, consistent with 3ap and dioxygen competing for the same reducing intermediates. This behavior can be understood within the following simple reaction scheme:



where the dependence of R_H on [3ap] and $[O_2]$ is provided by the following expression:

$$R_H = \left(\frac{d[H]}{dt} \right)_0 = \frac{R_f[3ap]}{\left(\frac{(k_d + k_{O_2}[O_2])}{k_{3ap}} + [3ap] \right)} = \frac{ax}{b+x} \quad (3.8)$$

A nonlinear least squares fitting routine was employed to fit the data in Fig. 3-6 to Equation 3.1, with the parameter, $A = R_f$ and $B = \frac{(k_d + k_{O_2}[O_2])}{k_{3ap}}$, provided in Table 3.1.

At $[O_2] = 0$ μ M, $B_0 = k_d/k_{3ap}$, thus $k_d = B_0 \times k_{3ap}$; while at $[O_2] = 50$ μ M, $\frac{k_{O_2}}{k_{3ap}} = \frac{(B_{50} - B_0)}{50}$.

Values of $\frac{k_{O_2}}{k_{3ap}}$ for untreated SRFA and SRHA are roughly 10, implying that dioxygen reacts with the reducing intermediate much faster than 3ap (Table 3-1). Fitting R_H in the presence of 250 μ M dioxygen is far less informative, owing to the substantial quenching of intermediate(s) at this high dioxygen concentration. (See below)

Table 3- 1: Parameters obtained from fits of the data in Fig. 3-6 to the expression of $R_H = \frac{A[3ap]}{B+[3ap]}$, $A = Rf$, $B = \frac{k_{O2}[O2]+kd}{k_{3ap}}$. B values obtained at 0 and 50 μM dioxygen as $B_0 = \frac{kd}{k_{3ap}}$, and $B_{50} = \frac{k_{O2}[50]+kd}{k_{3ap}}$; k_{O2}/k_{3ap} are obtained as $\frac{B_{50}-B_0}{50 \mu\text{M}}$.

	Parameter A (nM/s)		Parameter B μM		k_{O2}/k_{3ap}
	$O_2=0$	$O_2=50$	$O_2=0$	$O_2=50$	
5 mg/L SRFA	11	13	109	515	8.1
5 mg/L SRHA	13	16	252	868	12.3
10 mg/L SRFA	29	21	67	417	7.0
10 mg/L SRHA	34	23	108	469	7.2
10 mg/L Reduced SRFA	47	215	119	5316	104
10 mg/L Reduced SRHA	54	91	119	1601	28

3.3.2 Dependence of R_H on $[O_2]$

At $[3ap] = 600 \mu M$ and $[O_2] < 250 \mu M$, R_H decreases rapidly with increasing $[O_2]$ (Fig. 3-7) further indicating a direct competition between 3ap and dioxygen for the same pool of reducing intermediates. However, significant values of R_H (2-4 nM/s) remained even under high $[O_2]$ (250-1250 μM), as can also be seen in Fig. 3-6. The remaining R_H at high $[O_2]$ ($>250 \mu M$) appears to reflect a reductant pool that is far more reactive with 3ap than with dioxygen.

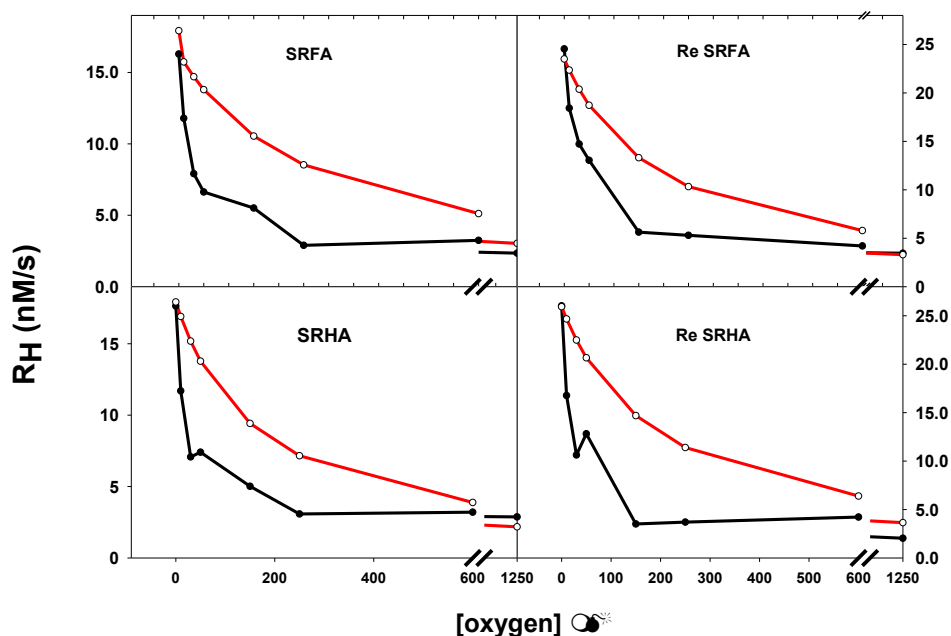


Figure 3- 7: Dependence of R_H on $[O_2]$ in the presence of 600 μM 3ap.

These two pools are more readily observed when the data are plotted in the following form, rearranged from Eqn.3.1,

$$\frac{R_f}{R_H} = 1 + \frac{k_d + k_{O_2} \times [O_2]}{k_{3ap}} \times \frac{1}{[3ap]} = 1 + \frac{k_d}{k_{3ap}[3ap]} + \frac{k_{O_2}}{k_{3ap}[3ap]} [O_2] \quad (3.2)$$

where the slope represents $\frac{k_{O_2}}{k_{3ap}[3ap]}$. (Fig. 3-8)

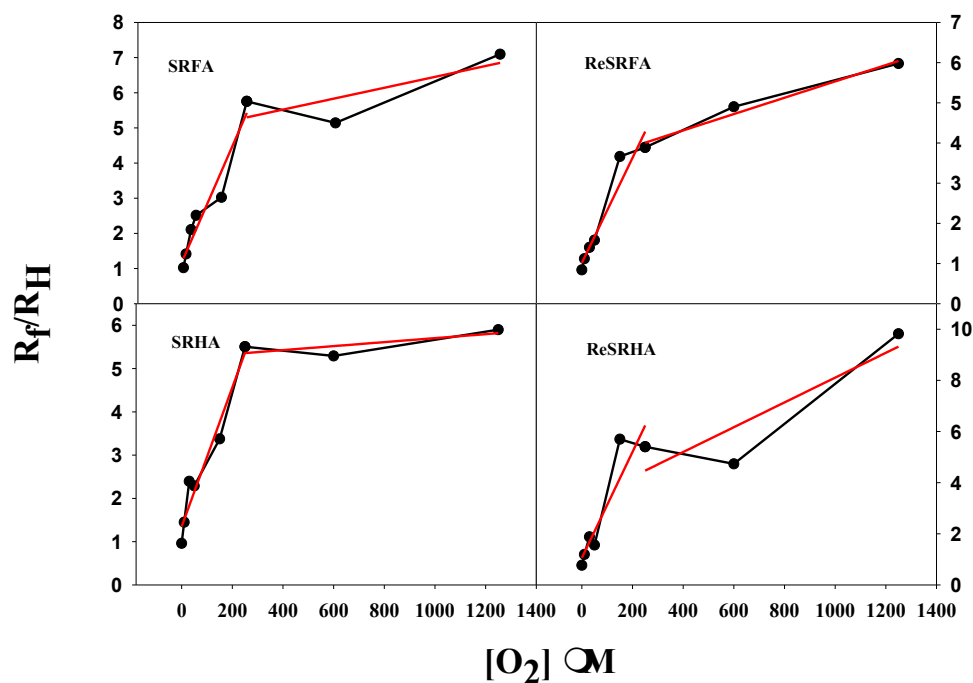


Figure 3- 8: Dependence of the ratio R_f/R_H on $[O_2]$ for untreated and reduced SRFA and SRHA in the presence of 600μM 3ap.

The slopes acquired for $[O_2] < 250 \mu\text{M}$ are clearly larger than those for $[O_2] > 250 \mu\text{M}$ (Table 3-2), indicating two pools of reducing intermediates, one of which

reacts much faster with O₂ than 3ap (< 250 μM O₂) and one that reacts with 3ap far faster than O₂ (> 250 μM).

Table 3- 2: Slopes and $\frac{k_{O_2}}{k_{3ap}}$ values obtained from fits of the data in Fig. 3-7 to the expression of $\frac{R_f}{R_H} = 1 + \frac{k_d + k_{O_2} \times [O_2]}{k_{3ap}} \times \frac{1}{[3ap]} = 1 + \frac{k_d}{k_{3ap}[3ap]} + \frac{k_{O_2}}{k_{3ap}[3ap]} [O_2]$. Slope represents $\frac{k_{O_2}}{k_{3ap}[3ap]}$, where [3ap] is 600 μM. Errors are obtained from the standard error of slope.

Rf/ RH	Slope $\times 10^{-2}$ μM^{-1}		Slope $\times 10^{-2}$ μM^{-1}	
	[O ₂] < 250 μ M	k _{O₂} /k _{3ap}	[O ₂] > 250 μ M	k _{O₂} /k _{3ap}
SRFA	1.7 ± 0.23	9.9	0.16 ± 0.12	0.93
SRHA	1.3 ± 0.20	9.7	0.2 ± 0.03	0.28
RESRFA	1.6 ± 0.18	7.9	0.05 ± 0.04	1.2
RESRHA	2.1 ± 0.4	12.6	0.48 ± 0.25	2.9

The k_{O_2}/k_{3ap} values obtained from the slope when [O₂] < 250 μM for untreated SRFA and SRHA are very similar in magnitude to the previous values obtained from the fits to the data in Fig. 3-6 (~ 10), providing further evidence that the largest pool of reductant reacts with dioxygen with rate constant that is far larger than 3ap. At [O₂] > 250 μM, the k_{O_2}/k_{3ap} are less than 1 for both SRFA and SRHA, suggesting that 3ap reacts faster with this pool than O₂.

3.3.3 Comparison between hydroxylamine and H₂O₂ formation rates and quantum yields.

In the presence of 600 μM 3ap but absence of dioxygen, R_H for untreated SRFA and SRHA decreased proportionally to R_{H₂O₂} with increasing wavelength

(chapter 2). This result is consistent with conclusion that the hydroxylamine and H₂O₂ compete for a common set of photo reductants.¹⁴⁵

Table 3- 3: Comparison of the R_H with R_{H₂O₂} under monochromatic irradiation. R_H and R_{H₂O₂} were obtained under the same irradiation conditions in the presence of 600 μM 3ap. Ratio represents R_H/R_{H₂O₂}. R_H was obtained under anaerobic conditions while R_{H₂O₂} obtained in the presence of 250 μM O₂.

	302 nm				313 nm				365 nm			
	SRFA	SRHA	RESRFA	RESRHA	SRFA	SRHA	RESRFA	RESRHA	SRFA	SRHA	RESRFA	RESRHA
H2O2 nM/s	2.2	2.0	1.8	2.1	1.7	1.4	1.3	1.8	0.4	0.3	0.4	0.5
Hydroxylamine (nM/s)	14.4	10.9	18.3	12.4	10.2	7.8	14.5	8.2	2.1	1.9	3.7	5.0
ratio	6.6	5.5	10.2	5.8	6.0	5.6	11.1	4.7	5.0	6.4	9.6	11.1

However, substantially higher values were observed for R_H than R_{H₂O₂}, producing a ratio of R_H/R_{H₂O₂} of approximately six. If every reducing equivalent trapped by 3ap was also trapped by O₂ to form O₂^{•-}, which then dismutated to H₂O₂, a ratio of two would be expected at the concentrations of 3ap and O₂ employed in this comparison (600 μM and 250 μM respectively); complete trapping of reducing equivalents by both probes would be anticipated (in this regime of rate saturation).

Thus this result implies that a significant fraction of O₂^{•-} (and possible H₂O₂) may be lost through secondary reaction pathways. In the case of O₂^{•-}, this pathway must be oxidative, because a reductive pathway would lead to H₂O₂. Assuming only this oxidative pathway of O₂^{•-}, a simple calculation is presented as below

$$\frac{R_H}{R_{H2O2}} = \frac{R_{O_2^{\bullet-}(total)}}{\frac{1}{2} [R_{O_2^{\bullet-}(total)} (1 - P_{O_2^{\bullet-}(oxidative)})]} = 6$$

where $P_{O_2^-}$ is the percentage of superoxide decay via oxidative pathway other than dismutation to H_2O_2 , which is calculated to be 67%

This value is higher than that reported by Petasne and Zika,³⁶ but is consistent with that reported by Garg et al.⁷⁷

However, a comparison between the polychromatic quantum yields obtained for the hydroxylamine (ϕ_H) and for H_2O_2 ($\phi_{H_2O_2}$) exhibits an even larger ratio with $\phi_H/\phi_{H_2O_2} \sim 13$ for untreated SRFA and SRHA. The origin of this difference between the results from the monochromatic and polychromatic experiments is still unclear. One possible explanation is that the efficiency for hydroxylamine formation extends to larger wavelength in the near UV and blue portion of this visible, where R_{EX} is larger. Alternatively, the use of polychromatic light could “activate” additional pathways for O_2^-/H_2O_2 removal. A third possibility is that 3ap is reacting with a large pool of photo-reductants that do not react with O_2 , although this seems highly unlikely on the basis of the 3ap/ O_2 competition experiments (Fig.3-6, Fig.3-7), in which $R_{H(1250)}/R_{H(0)}$ is around 0.1, indicating that about 10% of R_H maybe nonreactive with O_2 .

Table 3- 4: Polychromatic quantum yield for humic samples and the quantum yields ratio between produced hydroxylamine and H₂O₂. STD stands for standard derivation acquired from three times measurement.

polychromatic	Rate	Irradiance	Quantum yields		Φ ratio
Quantum yield	×10 ⁻⁸ M/s	×10 ⁻⁹ M/s	Φ _H ×10 ⁻³	Φ _{H₂O₂} ×10 ⁻⁴	Φ _H /Φ _{H₂O₂}
SRFA	1.6 ± 0.7	2.4E-09	6.8 ± 1.3	5.1 ± 0.2	13
SRHA	1.8 ± 0.7	4.0E-09	4.4 ± 1.2	3.8 ± 0.3	13
ReSRFA	2.5 ± 1.1	1.0E-09	25 ± 5.8	9.8 ± 0.3	25
ReSRHA	2.6 ± 0.9	2.0E-09	13 ± 4.1	6.2 ± 0.5	21

Past work has shown evidence that electrostatic effects can substantially enhance the trapping efficiency by nitroxide.⁹⁹ Because humic substances are negatively charged, while 3ap is positively charged enhanced rates of trapping can occur.⁹⁹

To test for this possibility, R_H was measured for SRFA in the presence of 500 mM NaCl at two 3ap concentrations. While R_H was only slightly reduced at 150 μM 3ap, it was almost halved at 600 μM 3ap. This electrostatic effect may explain in part the high R_H observed, although this fairly large electrostatic contribution does not show up in an obvious fashion in the data presented in Fig. 3-7.

Table 3- 5: Effect of 500 mM NaCl on anaerobic hydroxylamine production rate for 10 mg/L SRFA spiked with [3ap]

H production rate M/s ×10 ⁻¹¹	150 μM 3ap		600 μM 3ap	
	Average rate	std	Average rate	std
SRFA no salt	1.24	0.21	2.01	0.51
SRFA + salt	1.00	0.41	1.01	0.05

3.3.5 Effect of borohydride reduction on R_H

In all cases, borohydride reduction led to an approximately 20% increase in R_H , while $R_{H_2O_2}$ stayed approximate the same or slightly increased following reduction (Chapter 2). This produce a significant increase in apparent quantum yields for both processes, due to the additional loss of absorption following reduction. Thus, the removal of aromatic ketones/aldehydes and charge transfer contacts do not largely effect $R_{H_2O_2}$ and slightly enhanced R_H , indicating that these species can not involved substantially in either process.

The kinetic behavior for both untreated and reduced humic substance are consistent with reaction 3.5-3.7 which photochemical formation of intermediate I, formed at the rate of R_f , which can react either with dioxygen to form O_2^- (thus H_2O_2) or with 3ap to hydroxylamine, in competition with its relaxation to nonreactive species NR, formed with rate constant k_d .

In addition, for both SRFA and SRHA, the reduced samples displayed a similar 3ap and dioxygen as un treated samples, suggesting that reduction does not change the intermediates' lifetime dramatically, which is also similar to the H_2O_2 precursors, indicating the borohydride reduction does not largely affect the precursors for both R_H and $R_{H_2O_2}$.

3.4 Discussion

This work has provided evidence that 3ap and dioxygen compete for similar pools of one electron reductants produced photochemically within HS. Evidence that supports this idea includes 1) proportional decrease in R_H and $R_{H_2O_2}$ with increasing

wavelength (Table 3-3), 2) suppression of R_H with increasing $[O_2]$ due to competition of common intermediates, 3) largely unaffected ($R_{H_2O_2}$) or increase (R_H) rates upon borohydride reduction, indicating that charge transfer states or aromatic ketones/aldehydes are not directly involved in the formation of these photoreductants.

However, the rates and quantum efficiencies of hydroxylamine formation were significantly higher than those obtained for H_2O_2 under the same condition. The ratio of $R_H/R_{H_2O_2}$ for untreated SRFA and SRHA employing monochromatic irradiation were 6, while the ratio of $\phi_H/\phi_{H_2O_2}$ employing polychromatic irradiations were ~ 13 . Although the higher value of R_H may in part be a result of the enhanced trapping of intermediates by 3ap relative to O_2 due to an electrostatic effect, this effect could at most account for about half of the observed values. These results suggest that a significant portion of O_2^- , and possibly H_2O_2 may be lost through secondary reaction with other light generated intermediates.

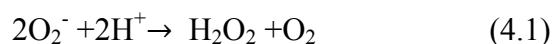
Chapter 4: Addition of Phenol Electron Donors

Substantially Enhances the Rates of Hydrogen Peroxide

Photoproduction by Humic Substances

4.1 Introduction:

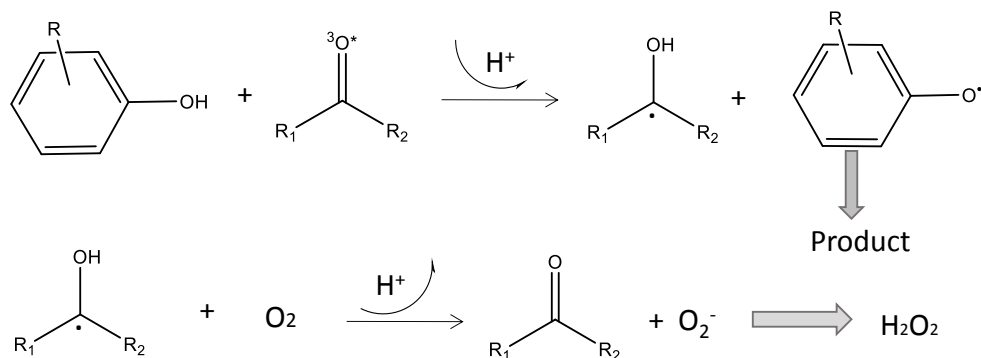
Hydrogen peroxide (H_2O_2) is found ubiquitously in surface waters where it is produced primarily via photochemical reactions of chromophoric dissolved organic matter (CDOM) and humic substances (HS).^{1,2,17} H_2O_2 has long been known to be of significant environmental importance,^{13,25,151} affecting the speciation and biological availability of metals as well as contributing to the degradation of natural and anthropogenic organic compounds.^{119,142} The photochemical formation of H_2O_2 is known to arise principally from either the catalyzed or un-catalyzed dismutation of superoxide (O_2^- , Eqn. 4.1),¹⁰⁸ which is generated through the one-electron reduction of O_2 by photoproduced intermediates within the CDOM.¹⁰⁷



Besides minor contributions from pathways involving singlet dioxygen¹¹⁷ and the hydrated electron,^{116,152,153} recent work suggests that the formation of H_2O_2 is initiated primarily through an intramolecular electron transfer reaction between short-lived excited states of electron donors, possibly phenols or methoxylated-phenols, and ground states acceptors, possible quinones or other acceptors within the CDOM.¹⁴⁵ Reaction of O_2 with the reduced acceptors then produces O_2^- , which subsequently dismutates to H_2O_2 .

However, H_2O_2 could also be formed through an additional pathway in the presence of sufficiently high concentrations of appropriate external electron donors such as phenols. Canonica et al.^{39,154} first proposed that the photochemical degradation of phenols could proceed through their reaction with excited triplet states of the aromatic ketones within the CDOM to produce initially a phenoxy radical and a ketyl radical (Scheme 4-1). Canonica et al.¹⁵⁴ further proposed that the phenoxy radical would then react to form products thus leading to the loss of the phenol, while the ketyl radical would react with ambient dioxygen and be oxidized back to the ketone while concomitantly producing superoxide and subsequently H_2O_2 through dismutation (Eqn. 4.1).

Scheme 4-1: H_2O_2 production via the photosensitized oxidation of phenols



Later work by Golanoski et al.⁸⁸ provided direct evidence that the triplet states of ketones/aldehydes were indeed involved in the photosensitized loss of 2,4,6-trimethylphenol (TMP), while a study by Auger et al.¹⁴² further indicated that these reactions could act as a photocatalytic cycle in which aromatic ketones (and possibly quinones) could act as electron shuttles for transporting electrons from appropriate donors (eg., TMP) to O_2 , thus generating H_2O_2 . Other electron donors that are capable of reacting with the oxidizing triplet states of HS could also be involved in this

reaction sequence.^{155, 156} However, direct evidence of enhanced H₂O₂ production by this mechanism has yet to be obtained.

To test this idea, we examined the effect of a series of added phenol electron donors on the rates and mechanisms of H₂O₂ formation for both untreated and sodium borohydride reduced HS samples. The results provide strong evidence that H₂O₂ can be generated through an additional pathway in presence of sufficiently high concentrations of these donors via reaction with the excited triplet states of aromatic ketones/aldehydes and possibly of other species such as quinones.

4.2 Materials and Method

4.2.1 Chemicals

Sodium phosphate, sodium dihydrogen phosphate, sodium hydroxide and Sephadex G-10 were purchased from Sigma-Aldrich. Phenol (PHE, Merck, 98%), 4-methoxyphenol (MOP, Fluka, 97%), 3,4-dimethoxyphenol (DMOP, Aldrich, 99%) and 2,4,6-trimethylphenol (TMP, Fluka, 99%) were used as received. Hydrogen peroxide (30%) was purchased from Fisher. Suwannee River fulvic acid (SRFA) and Suwannee River humic acid (SRHA) were obtained from the International Humic Substance Society. The C-18 extract from the Delaware Bay (99°N, -75.13° W) was obtained in Oct 2006 and processed as previously reported.¹⁵⁷ Sodium borohydride was obtained from Aldrich.

Borohydride reduction was performed as previously described,^{78, 88} with the exception that a 25-fold excess of borohydride was employed. For the photochemical experiments, samples were prepared in 10 mM phosphate buffer (pH=7) at a concentration of 10 mg/L for SRFA and SRHA, while the absorbance of the C₁₈

extract at 350 nm was matched to that of 10 mg/L SRFA. All phenol stock solutions were prepared fresh daily in phosphate buffer. Phenol concentrations were varied from 0 to 1000 μ M in the photochemical samples. Water was obtained from a Milli-Q purification system. A Shimadzu 2401-PC spectrophotometer was employed to acquire UV-VIS absorption spectra. Absorption spectra were recorded using 1 cm cuvette over the range from 190 nm to 820 nm. All spectra were referenced to MQ water.

4.2.2 Determination of hydrogen peroxide photoproduction rates ($R_{H_2O_2}$) and apparent quantum yields

A chemiluminescence-based flow injection analysis (FIA) was employed to determine $[H_2O_2]$.^{96, 120} The chemiluminescence reagent, acridinium ester (AE), was provided by Waterville Analytical Company. A 0.1 M Na_2CO_3 solution (pH= 11.2) was employed as reaction pH buffer. Carrier water was treated with 3 mg/L catalase over night before use to eliminate background H_2O_2 .⁹⁶ Sample H_2O_2 is unaffected by the added catalase because the reaction time for H_2O_2 and AE is less than 20 s, while the half-life of H_2O_2 in 3 mg/L catalase is \sim 15 min. The buffer solution, carrier water and AE were introduced into the reaction vessel using a peristaltic pump with flow rate of 10.9 ml/min, while samples for H_2O_2 analysis were introduced by a syringe. Hydrogen peroxide concentrations were calibrated daily by dilution of a 30% H_2O_2 stock solution, whose concentration was determined by H_2O_2 molar absorptivity,¹²⁰ and confirmed by a titrimetric method using $KMnO_4$.¹⁵⁸ Calibration curves of $[H_2O_2]$ in the presence of increasing concentrations of the phenols (0 to 1 mM) showed no evidence of significant interference. Catalase was added to solutions after irradiation

to ensure that the observed signal was arising from H_2O_2 alone. All samples contacted only glass and Teflon to avoid possible contamination by adventitious trace metals.

The output from a 300 watt xenon arc lamp, after passage through a 20 cm water jacket and a 325 nm long-pass filter (50% transmission wavelength), was employed for irradiation. Additional long-pass filters (355 and 385 nm) were employed to examine the wavelength dependence of the H_2O_2 production rate. Samples containing differing concentrations of phenols were held in 1 cm pathlength quartz cuvette. Any background of hydrogen peroxide in the phosphate buffer was subtracted. Hydrogen peroxide production rates, $R_{\text{H}_2\text{O}_2}$, were obtained from a linear regression of $[\text{H}_2\text{O}_2]$ versus time over a 10 min irradiation period employing 3 min sampling intervals (4 points). Samples containing differing phenol concentrations (up to 1 mM) in the absence of HS showed no evidence of significant dark H_2O_2 production over the 10 min irradiation period. Except for DMOP, irradiation of the phenols alone did not lead to H_2O_2 production over this same period. In the case of DMOP, the background rate was small with respect to the rates observed in the presence of the HS (<10%), and was subtracted from the observed rate for each phenol concentration.

All gases were obtained from Airgas (ultra high purity). Differing dioxygen concentrations (0 to 1250 μM) were achieved by bubbling pure N_2 , air or dioxygen gas (98%), or mixtures of these gases obtained using a rotameter, through samples contained in 1-cm cuvette capped with a Teflon lid and vented with a fine needle. Samples were first purged for 20 minutes with the desired gas or gas mixture, with the headspace then purged for an additional ten minutes prior to sealing the cuvette.

Samples were immediately irradiated for an appropriate time period and subsequently analyzed for [H₂O₂]. A dioxygen scrubber was mounted on N₂ tank to remove traces of O₂ in N₂ tank to ensure anoxic conditions were attained under N₂ purging.

Polychromatic quantum yields for H₂O₂ production in the absence of phenols, ϕ_0 , were calculated using following expression,

$$\phi_0 = \frac{R_{H_2O_2}}{R_{EX}} \quad (4.2)$$

where R_{H₂O₂} is the H₂O₂ production rate in the absence of phenols, R_{EX} is the rate of light excitation,

$$R_{EX} = \int_{190}^{820} a(\lambda) \times I(\lambda) d\lambda = \int_{190}^{820} R(\lambda) d\lambda \quad (4.3)$$

where a(λ) is the absorption coefficient of the sample, and I(λ) is the irradiance at wavelength λ at the front face of the cuvette, as measured with an Ocean Optics spectroradiometer.⁸⁸

4.3 Results

4.3.1 H₂O₂ enhancement by addition of TMP

Addition of increasing concentrations of TMP to untreated SRFA samples substantially enhanced R_{H₂O₂}, increasing this rate by as much as 2-fold by 100 μ M TMP (Fig. 4-1). At [TMP] \leq 100 μ M, R_{H₂O₂} appeared to increase linearly (Fig. 4-1). Although borohydride reduction of SRFA did not largely affect R_{H₂O₂} in the absence of TMP as was observed previously (Fig. 4-1; Table 4-1),¹⁴⁵ this treatment did substantially decrease the R_{H₂O₂} values at [TMP] \leq 100 μ M;

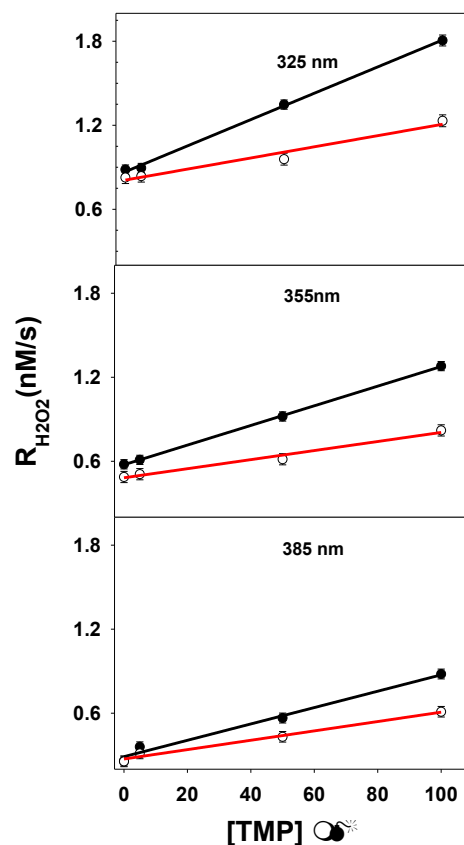


Figure 4- 1: Wavelength dependence of $R_{H_2O_2}$ in the absence and presence of increasing [TMP] for untreated (black) and borohydride-reduced (red) SRFA. Samples were irradiated with a polychromatic source employing long-pass filters (325, 355 and 385 nm). Samples contained 10 mg/L SRFA in 10 mM phosphate buffer, pH =7.0. Error bars represent the standard derivation acquired from at least three measurements.

However, the rates observed following borohydride reduction did not return to those observed in the absence of TMP. This inhibition by borohydride reduction of the enhancement of $R_{H_2O_2}$ in the presence of TMP was estimated from the expression,

$$\% I = (1 - (S_r/S_u)) \times 100 \quad (\text{eqn 4.4})$$

where S_r and S_u are the slopes obtained from Fig. 4-1 for borohydride-reduced and untreated SRFA, respectively (Table 4-1).

Table 4-1: Wavelength dependence of the slope (S), intercept, slope ratio and % inhibition by borohydride reduction (% I) acquired from linear regressions of the data in Fig. 4-1 for untreated SRFA (Su) and borohydride-reduced SRFA (Sr).

	SRFA		Reduced SRFA		Slope ratio	% I
	intercept	slope	intercept	slope	Sr/Su	
	nM/s	Su(E-5) (s-1)	nM/s	Sr (E-5) (s-1)		
325nm	0.87±0.01	0.94±0.03	0.81±0.03	0.40±0.05	0.42	57.6
355nm	0.58±0.004	0.70±0.007	0.48±0.02	0.32±0.03	0.46	53.8
385nm	0.29±0.023	0.58±0.05	0.27±0.02	0.33±0.03	0.57	42.8

The degree of inhibition following borohydride reduction (~40-60 %) is very similar to that previously observed for the inhibition of the photosensitized loss of TMP by SRFA over this same range of TMP concentration (~50%).⁸⁸ This result provides evidence that (aromatic) ketones/aldehydes are involved in the enhanced production of H₂O₂ in the presence of TMP consistent with Scheme 4-1. This result shows further that a new route for H₂O₂ photoproduction can be introduced when sufficiently high concentrations of appropriate external electron donors are present.

Evidence for two distinct mechanisms of H₂O₂ photoproduction in the presence and absence of TMP is also provided by the wavelength dependence of the slopes and intercepts, respectively (Fig.4-1, Table 4-1). In the absence of TMP, R_{H2O2} (intercepts) decrease by a factor of ~3 when the wavelength of the long-pass filter is increased from 325 to 385 nm, independent of borohydride reduction (Table 4-1). In contrast, the slopes decrease by only ~40% over this same wavelength range for the untreated sample, and by only ~18% in the borohydride-reduced sample, leading to an ~15% decrease in the % inhibition by borohydride reduction over this wavelength range (Table 4-1). These results suggest that 1) the enhanced R_{H2O2} observed in the

presence of TMP extends to longer wavelengths in the UVA than that observed for direct H_2O_2 photoproduction, and 2) there appears to be slightly less inhibition by borohydride reduction at the longer wavelengths in the UVA. Both observations provide evidence of a wavelength dependence that differs for the direct and enhanced routes of H_2O_2 photoproduction.

Substantially enhanced values of $R_{\text{H}_2\text{O}_2}$ were also observed for SRFA, SRHA and the Lower Delaware Bay sample in the presence of PHE, DMOP, MOP and TMP (Fig. 4-2). At higher concentrations of these phenols, above roughly 200-300 μM , evidence for saturation of $R_{\text{H}_2\text{O}_2}$ was observed, suggestive of a quantitative reaction of the phenols with transient intermediate(s) at high concentration, with the products of this reaction ultimately producing hydrogen peroxide (Scheme 4-1). As with SRFA (Fig. 4-1), borohydride reduction of the HS significantly decreased the values of $R_{\text{H}_2\text{O}_2}$, but clearly did not eliminate the enhancement (Fig.4-1, Fig.4-2).

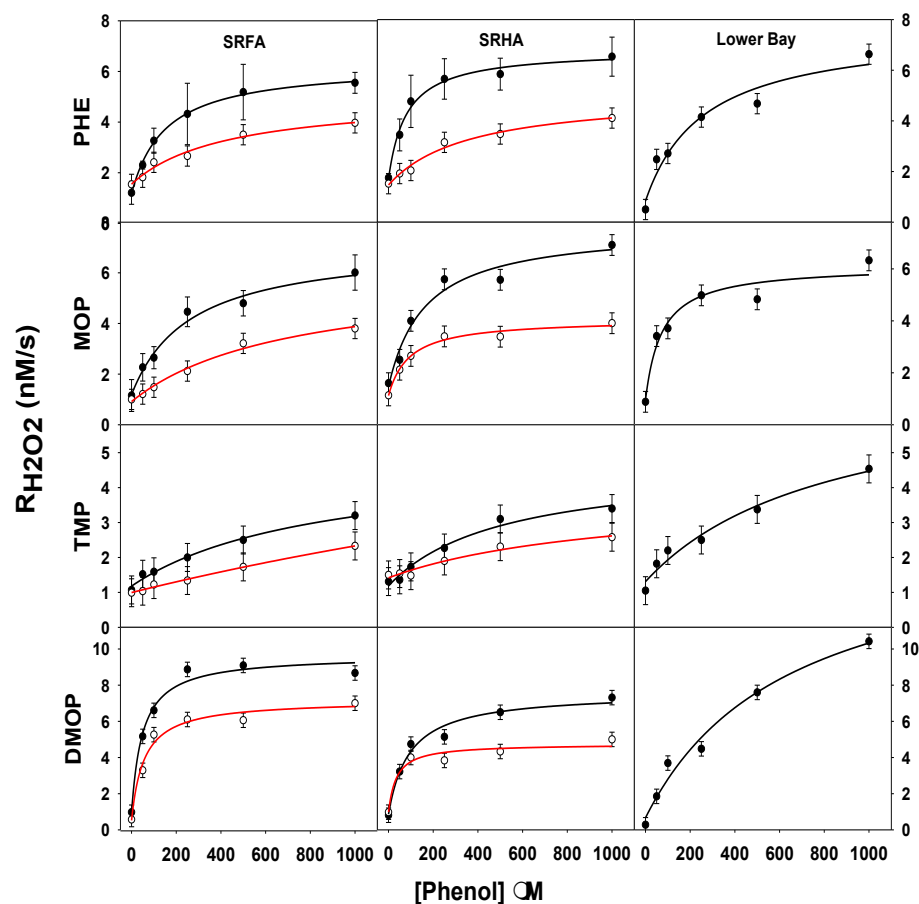


Figure 4- 2: Dependence of $R_{H_2O_2}$ on phenol concentration in air ($[O_2] = 250 \mu M$) for untreated (\bullet) and borohydride –reduced (\circ) SRFA, SRHA, and the C-18 extract from Lower Delaware Bay station using the polychromatic source. Error bars represent the standard derivation acquired from at least three measurements for SRFA SRHA and lower Bay sample.

As an empirical means of quantifying the dependencies of $R_{H_2O_2}$ on phenol concentrations, the curves in Fig. 4.2 for both untreated and borohydride-reduced samples were fit to Eqn. 4.5 using a non-linear least squares fitting routine,

$$R_{H_2O_2} = y_0 + (A[\text{phenol}]) / (B + [\text{phenol}]) \quad (4.5)$$

where y_0 is the value of $R_{H_2O_2}$ in the absence of the phenols at $[O_2] = 250 \mu M$, A is maximum value of the enhanced $R_{H_2O_2}$ attained at high phenol concentration, and B is

concentration of the phenols at which $R_{H_2O_2}$ reaches half of its maximum value (A) (Fig. 4-3). Estimates of the enhancement factor, EF , were calculated from the relation,

$$EF = A/y_0 \quad (4.6)$$

while estimates for the % inhibition of enhancement due to borohydride reduction (% I) were obtained from the relation,

$$\%I = (1 - ((A_r - y_0)/(A_u - y_0))) \times 100 \quad (4.7)$$

where A_u and A_r are the values of A for untreated and borohydride-reduced samples, respectively. Estimates of the polychromatic quantum yields under saturating [phenol], ϕ_p , were obtained from,

$$\phi_p = \phi_0 \times EF \quad (4.8)$$

where ϕ_0 is the polychromatic quantum yield for H_2O_2 photoproduction in the absence of the phenols for either untreated or borohydride-reduced samples (see Materials and Methods) (Table 4-2).

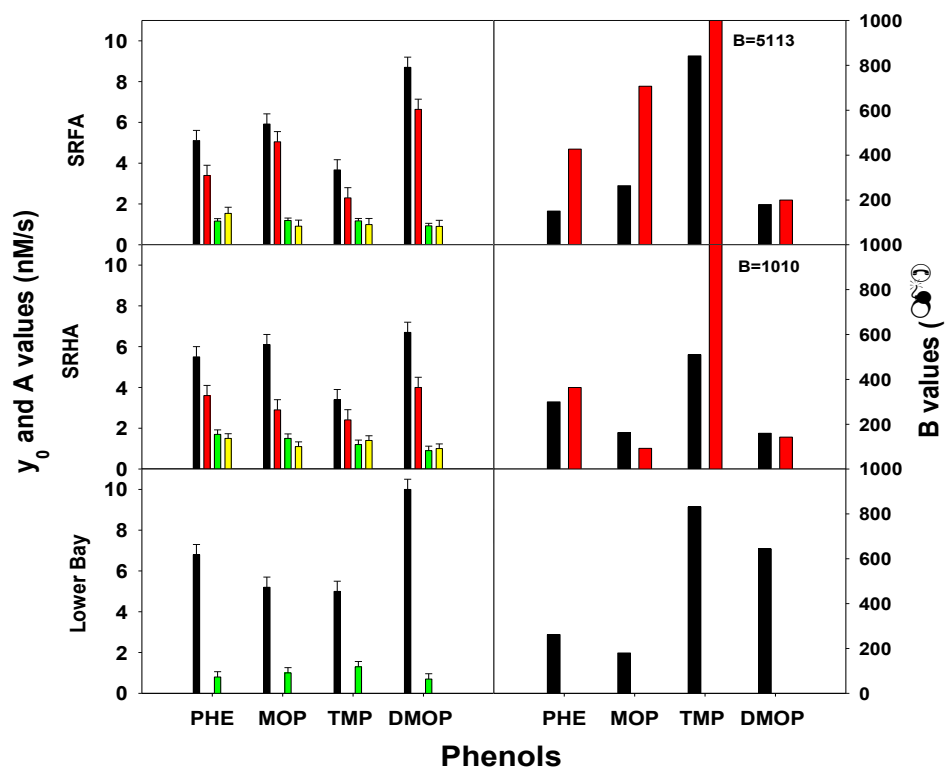


Figure 4- 3: Values (y_0 , A and B) from the fits of the data from Fig. 4-2 using kinetic equation: $y = y_0 + Ax/(B+x)$. y_0 stands for the $R_{H_2O_2}$ in the absence of phenols. A stands for the enhanced $R_{H_2O_2}$ in the presence of [phenol]; B is the concentration of phenol at which $R_{H_2O_2}$ reaches half its maximal value. Left panel: A (black; untreated, red; reduced) and y_0 (green; untreated, yellow; reduced). Right panel: B values (black; untreated, red; reduced). Errors are obtained from Fig. 4-2.

Table 4- 2: H₂O₂ polychromatic quantum yields for HS only (Φ_0) and for that in the presence of Phenols (Φ_p). Y_0 is the value of $R_{H_2O_2}$ in the absence of the phenols at $[O_2] = 250 \mu M$. R_{ex} is the rate of light excitation. Φ_0 obtained from fitting value y_0 . %I is the inhibition of enhancement due to borohydride reduction. EF is the enhance factor. Φ_p , which were obtained from $\phi_0 \times EF$.

	Y_0 E-9 M/S	R_{ex} E-6 M/s	ϕ_0 E-4		%I	EF	ϕ_p E-3
SRFA	1.1±0.1	1.8	6.2	PHE		4.4	2.7
				MOP		5.0	3.1
				TMP		3.1	1.9
				DMOP		9.4	5.8
ReSRFA	1.1±0.3	1.2	9.2	PHE	51	2.3	2.1
				MOP	35	4.4	4.1
				TMP	48	2.3	2.1
				DOMP	34	6.7	6.1
SRHA	1.3±0.4	2.6	5.0	PHE		3.2	1.6
				MOP		4.2	2.1
				TMP		2.9	1.5
				DMOP		7.8	3.9
RESRHA	1.2±0.3	1.4	8.7	PHE	54	2.2	1.9
				MOP	61	2.6	2.3
				TMP	56	1.7	1.5
				DMOP	48	4.1	3.6
LB	0.9±0.3	2.8	3.4	PHE		8.2	2.8
				MOP		5.4	1.8
				TMP		3.8	1.3
				DMOP		14.9	5.1

The values of y_0 obtained from the fitting of data in Fig. 4-2 were consistent with those acquired directly (Fig.4-1, Tables 4-1, 4-2). Values of EF ranged from a low of ~ 3 for TMP to a high of ~ 15 for DMOP, and were lower in the borohydride-reduced samples owing to the inhibition produced by reduction (Table 4-2). Values of EF increased in the order SRHA<SRFA<LB, a trend similar to that previously observed for the rates of photosensitized TMP loss.⁸⁸ Except for TMP, both untreated and borohydride-reduced samples exhibited a general trend of increasing EF and ϕ_p with decreasing oxidation potential of the phenol (Fig. 4-3, Table 4-2), suggesting higher H₂O₂ yields in the presence of better electron donors. Interestingly, the values of ϕ_p for the untreated and borohydride-reduced samples were quite similar due to an approximately proportional loss in R_{H₂O₂} and R_{ex} following borohydride reduction. Similar results have been observed previously in the sensitized loss of TMP⁸⁸ and sensitized ¹O₂ formation⁸⁵ following borohydride reduction of aquatic HS.

Except for TMP, which exhibited consistently higher values of B (Fig. 4-3), the untreated HS samples exhibited no clearly identifiable trends in B across the different phenols, with all values falling within the range from ~ 200 to $600 \mu\text{M}$. Assuming that the values of B are determined only by the competition between phenol and O₂ for reaction with the triplet states (see below),^{154, 155} dividing the value of B by [O₂] ($\approx 250 \mu\text{M}$) provides the rate constant ratio of O₂ to phenol reaction. Values of this rate constant ratio, which varies from ~ 0.8 for DMOP to ~ 3 for TMP, are within the range expected for reaction with aromatic ketone triplet states.^{154, 155}

However, these results are still somewhat surprising, since one might anticipate a systematic decrease in B with decreasing oxidation potential of the

phenol owing to more rapid reaction with the triplet relative to triplet quenching by dioxygen.^{154, 155} However, this interpretation may be too simplistic owing to potential secondary reactions of the phenoxy radicals, including possible reactions with co-produced O_2^- ¹⁵⁴ and possibly H_2O_2 . Indeed, the fact that the estimated values of ϕ_p for SRFA (1.9×10^{-3}) and SRHA (1.5×10^{-3}) in the presence of saturating [TMP] (Table 4-2) are at least 5- to 10-fold smaller than the apparent polychromatic quantum yields for the photosensitized loss of TMP (2.0×10^{-2} and 5.3×10^{-3} for SRFA and SRHA, respectively; Table 1 in Ref. 88) implies a substantial loss of O_2^- and/or H_2O_2 through secondary reactions (see further below).

As with the untreated samples, no clearly discernable trends in B were observed for the differing phenols following borohydride reduction. Borohydride reduction appeared to increase B for SRFA with some phenols, while not largely changing it for SRHA (Fig. 4-3).

4.3.2 Oxygen dependence

Further evidence for the participation of ketone/aldehyde triplet states in the enhanced photoproduction of H_2O_2 was provided by the dioxygen dependence of $R_{H_2O_2}$ in the presence of TMP (Fig. 4-4). At [TMP]=100 μ M, decreasing the $[O_2]$ from 1.2 mM to 50 μ M leads to an ~3- to 4-fold **increase** in $R_{H_2O_2}$ in all samples examined; $R_{H_2O_2}$ then dropped to near-zero under anoxic conditions. Borohydride reduction inhibited the increase in $R_{H_2O_2}$, but did not entirely eliminate it. By comparison, in the absence of phenols, $R_{H_2O_2}$ decreased with decreasing $[O_2]$ and was largely unaffected by borohydride reduction (Fig. 4-4).¹⁴⁵ Within the uncertainties, these variations with

[O₂] in the presence of TMP are essentially indistinguishable from those previously reported for the sensitized loss of TMP for untreated and borohydride reduced samples⁸⁸ and provide compelling evidence for the involvement of ketone/aldehyde triplet states in this process.⁸⁸ However, as in that study,⁸⁸ the incomplete loss of enhancement under borohydride reduction suggests that there remains another pool of oxidizing triplets.

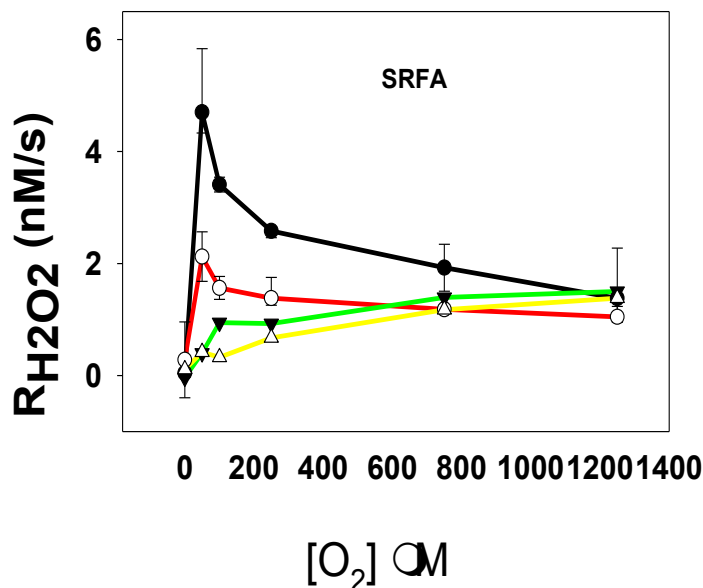
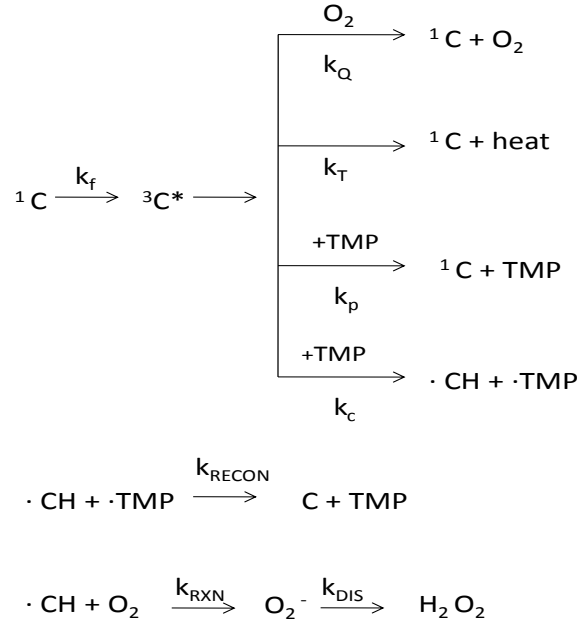


Figure 4- 4: Dependence of R_{H2O2} on dioxygen concentration for untreated (Black) and borohydride-reduce (Red) SRFA at the presence of 100 μM TMP using the polychromatic source. Controls: Green and yellow lines are R_{H2O2} for SRFA and reduced SRFA respectively in the absence of TMP.

As with the photo-sensitized loss of 2,4,6-trimethoxy phenol, those results can be understood within the following reaction scheme.



These reactions lead to the following expression that relates $R_{\text{H}_2\text{O}_2}$ to the $[\text{O}_2]$ and $[\text{TMP}]$,

$$R_{\text{H}_2\text{O}_2} = \frac{d_{\text{H}_2\text{O}_2}}{dt} = \frac{0.5k_f\phi k_{\text{TMP}}[\text{TMP}]}{(k_T + k_Q[\text{O}_2] + k_{\text{TMP}}[\text{TMP}])} \times \frac{1}{(1 + \frac{k_{\text{REC}}}{k_{\text{RXN}}} \times \frac{1}{[\text{O}_2]})} \quad (4.9)$$

where $k_c + k_p = k_{\text{TMP}}$, $\phi = k_c/(k_c + k_p)$. and $k_{\text{REC}} = k_{\text{RECOM}} [\text{TMP}\cdot]^{88}$ (see Appendix 2 for derivation).

Employing the values for the rate constants (k_T , k_Q , and k_{TMP}) and the rate constant ratio ($k_{\text{REC}}/k_{\text{RXN}}$) previously acquired by Golanoski et al.⁸⁸ through fitting of the dioxygen dependence of photosensitized TMP loss, a non-linear least-squares

fitting routine was used to fit the dioxygen dependence of $R_{H_2O_2}$, but allowing only the product, $0.5 k_f \phi$, to vary (Fig. 4.5). Considering that only one adjustable parameter was allowed, the fits are quite good and establish that one set of kinetic parameters can explain reasonably well the dependence of both H_2O_2 production and TMP loss on $[O_2]$. Note however, that the magnitudes of the product, $0.5 k_f \phi$, for H_2O_2 production are significantly smaller those found by Golanoski et al.⁸⁸ for TMP loss under comparable experimental conditions, suggesting again that a significant portion of the O_2^-/H_2O_2 produced may be consumed in secondary reactions.

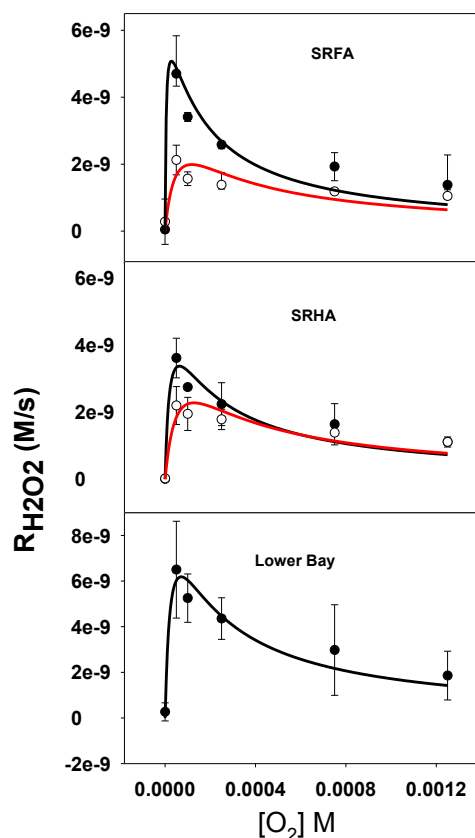


Figure 4- 5: Dependence of $R_{H_2O_2}$ at fixed $[TMP] = 100 \mu M$ for both untreated and borohydride reduced SRFA, SRHA, Lower Bay samples. Data were fit to the equation 4-9 employing a nonlinear least-squares fitting routine using fixed values of $k_T = 6.6 \times 10^4 s^{-1}$; $k_Q = 2.0 \times 10^9 M^{-1} s^{-1}$; $k_{TMP} = 2.5 \times 10^9 M^{-1} s^{-1}$.

This work has clearly demonstrated that the rate of H_2O_2 photoproduction by HS can be substantially enhanced in the presence of sufficiently high concentrations of appropriate electron donors. The effects of borohydride reduction and $[\text{O}_2]$ on $\text{R}_{\text{H}_2\text{O}_2}$ are consistent with the reaction mechanism shown in Scheme 4-1, although the incomplete loss of the enhanced $\text{R}_{\text{H}_2\text{O}_2}$ following borohydride reduction suggests that there remains another pool of oxidizing triplets as was observed previously for TMP loss.⁸⁸

Chapter 5: Summary and Future Directions

5.1 Summary

Key aspects of the mechanisms of the photochemical H_2O_2 production from aquatic humic substance have been addressed in this thesis. Borohydride reduction, which selectively removes the aromatic ketone moieties from CDOM irreversibly, does not substantially affect the ratio of H_2O_2 production, indicating that charge transfer states or aromatic ketones/aldehydes are unlikely to be directly involved with H_2O_2 production. The tens of microsecond lifetime of the H_2O_2 precursor estimated from the dioxygen dependence of $R_{\text{H}_2\text{O}_2}$ could be due to either triplet states or a reductant formed by excited state electron transfer. However, obtained evidence by the use of chloride ion and sorbic acid, triplet quenchers, indicates that triplet states are unlikely to be the precursor of produced H_2O_2 .

This work indicates that H_2O_2 is primarily formed via a low efficiency intramolecular electron transfer from excited singlet donors to ground state acceptors. Based on previous research, possible donors are substituted phenols or methoxyl phenols and possible acceptors include quinones, which unlike ketones and aldehydes, are not irreversibly reduced by borohydride.

A simple, highly-sensitive method was employed for detecting one-electron reducing intermediates produced by irradiation of CDOM. The molecular probe 3ap employed acts as one-electron acceptor similar to dioxygen, and has been shown to compete with dioxygen to form stable hydroxylamine. The rate of the photo production of the reducing intermediates can be detected by probe 3ap in the absent of dioxygen and monitored by the HPLC with a fluorescence detector when formed

hydroxylamine coupled with fluorescamine. The dependence of R_H on $[O_2]$ argues that <10% of total detected one electron reducing intermediates is nonreactive to dioxygen. Further examining on the stoichiometry ratio of indirect measurement of superoxide and direct measurement H_2O_2 monochromatically propose that 67% percentage of superoxide decay through other oxidation pathways rather than bimolecular dismutation to H_2O_2 under monochromatic irradiation conditions. This ratio is slightly higher than Waite's previous work.

The substantial enhancement of H_2O_2 production rate in the presence of added phenol donor is consistent with the reaction of the phenol with triplet states at aromatic ketone/aldehydes form ketyl radicals, which substantially react with O_2 to form superoxide. Evidence that support this interpretation includes 1) an increase in H_2O_2 production rates with decreasing $[O_2]$, 2) ability to fit the dependence of $R_{H_2O_2}$ on $[O_2]$ with parameters previously obtained from the sensitized loss of TMP, 3) a substantial loss in the rate of H_2O_2 production following borohydride reduction.

However, the incomplete loss of the enhancement in $R_{H_2O_2}$ following borohydride reduction argues that there remains another pool of oxidizing triplet as in the case of photosensitized loss of TMP.

Finally, substantial different between the quantum efficiency of the photo sensitized loss of TMP and the quantum efficiency of H_2O_2 production suggests that secondary reactions may consume a significant portion of the $O_2^{\cdot -}/H_2O_2$ that is produced.

5.2 Future work

The quantum yield of H_2O_2 monochromatic wavelength dependence has been investigated in Chapter 2. Monochromatic decreasing of the quantum yield as irradiation wavelength increase is consistent with decreasing yield of the produced excited singlet donor, which is considered as the precursor of H_2O_2 from humic substance. However, the HS photosensitization efficiency wavelength dependence for H_2O_2 production in the presence of external donor has not been investigated and need further investigation. In addition, Comparison between polychromatic H_2O_2 production quantum yields with that of monochromatic in the presence of external donors is likely to provide additional useful information.

The HS sensitized reaction between electron donor phenols to dioxygen has been investigated in Chapter 4, and the possible scheme has been proposed that the triplet states of aromatic ketones moieties are involved as electron accepting species. However, whether the aromatic ketones moieties are serving as catalytic shuttle transferring electron from external electron donating species, such as phenols, to oxidant such as dioxygen is still not known. More work need to be done to probe the redox reversibility properies of triplet states intermediates of humic substance.

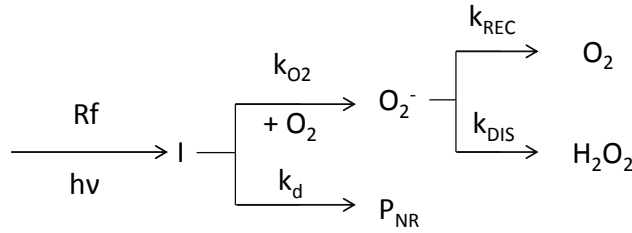
Ratasuk⁷⁴ has employed cyclic oxidation and reduction method to structurally characterize and quantify the electron carrying capacity of reversible redox sites present in humic substance. They argued that the ratio of non-quinone structure to quinone structure of redox sites is 1:2. Our results that the photosensitization capacity (H_2O_2 production) of the humic samples employed were not fully eliminated upon

borohydride reduction requires more work for probing the other possible excited redox moieties besides quinones as possible photo-reductant.

Appendix 1

The effect of O_2^- back reaction and disproportionation on the O_2^- dependence of the hydrogen peroxide production rate ($R_{H_2O_2}$)

Branching ratio effect of superoxide back reaction on the kinetic scheme of oxygen dependence of hydrogen peroxide production rate



1: Without considering branching ratio, the $R_{H_2O_2}$ is expressed as below as simple fit:

$$R_{H_2O_2} = \left[\frac{d [H_2O_2]}{dt} \right]_0 = K_r [ROS] [O_2] = \frac{R_f k_{O_2} [O_2]}{2(k_d + k_{O_2} [O_2])} = \frac{R_f [O_2]}{2\left(\frac{k_d}{k_{O_2}} + [O_2]\right)}$$

$$= \frac{a [O_2]}{2(b + [O_2])}$$

2: With considering the back reaction K_{REC} and superoxide dismutation K_{DIS} as

FIRST ORDER reaction, the is $R_{H_2O_2}$ modified as:

$$R_{H_2O_2} = \left[\frac{d [H_2O_2]}{dt} \right]_0 = \frac{K_{DIS} R_f k_{O_2} [O_2]}{2(K_{DIS} + K_{REC})(k_d + k_{O_2} [O_2])}$$

$$= \frac{K_{DIS} R_f [O_2]}{2(K_{DIS} + K_{REC}) \left(\frac{k_d}{k_{O_2}} + [O_2] \right)} = \frac{a [O_2]}{2(b + [O_2])} * \left(\frac{K_{DIS}}{(K_{DIS} + K_{REC})} \right)$$

This will not effect the oxygen dependence curve as well as half saturating concentration.

3: With considering the back reaction K_{REC} and superoxide disumuation K_{DIS} as **SECOND ORDER** reaction, the is $R_{H_2O_2}$ modified as :

$$R_{H_2O_2} = \left[\frac{d[H_2O_2]}{dt} \right]_0 =$$

$$1/2 \left[\frac{R_f k_{O_2} [O_2]}{(k_d + k_{O_2} [O_2])} + \frac{K_{REC}^2}{K_{DIS}} \left(1 - \sqrt{1 + \frac{2R_f k_{O_2} [O_2] K_{DIS}}{(k_d + k_{O_2} [O_2]) K_{REC}^2}} \right) \right]$$

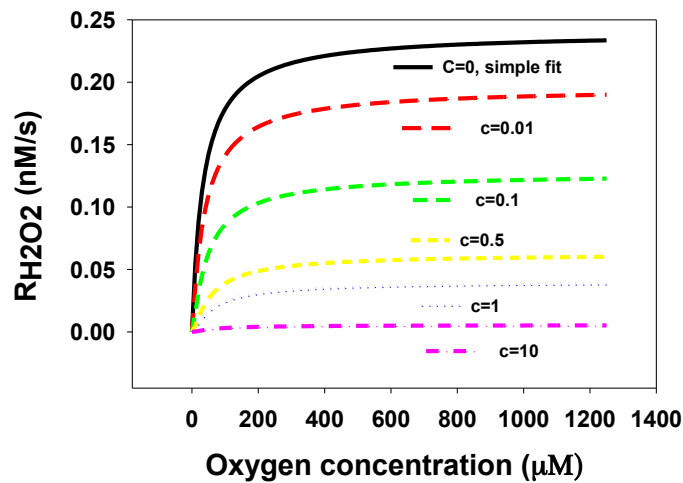
$$= 1/2 \left[\frac{a [O_2]}{(b + [O_2])} + \frac{K_{REC}^2}{K_{DIS}} \left(1 - \sqrt{1 + \frac{2a [O_2] K_{DIS}}{(b + [O_2]) K_{REC}^2}} \right) \right]$$

For sample SRFA, curve fitting provide initial value for $a=0.48$, $b=34.36$. If we

define $\frac{K_{REC}^2}{K_{DIS}}$ as c , varies c value from 0.01 to 10 to see the impact of c on the curve

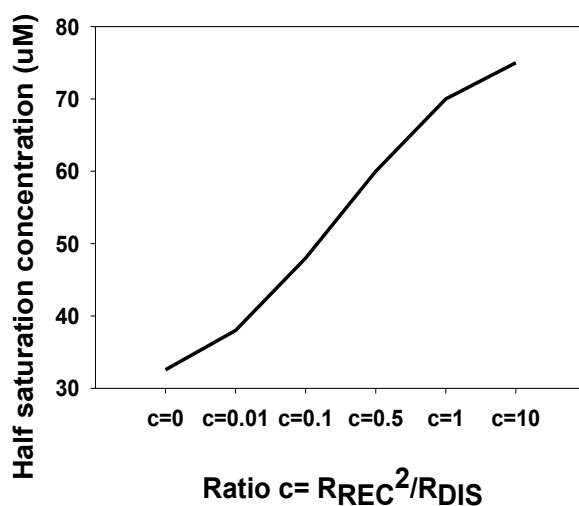
shape. The results are listed below:

SRFA oxygen dependence when chaning ratio $c = R_{REC}^2/R_{DIS}$ from 0.01 to 10



The half saturation dependence as :

Half saturation concentration dependence on ratio $c = R_{REC}^2/R_{DIS}$ from 0.01 to 10

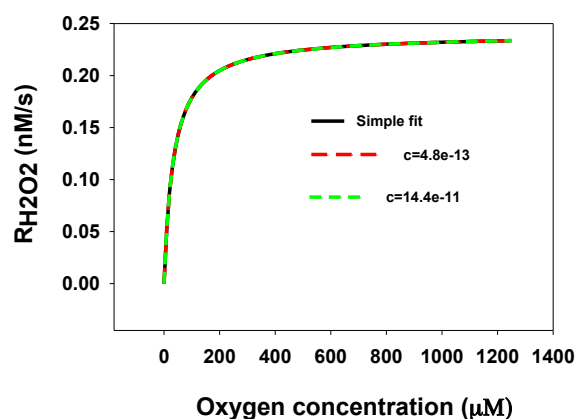


When applying the $R_{REC} = 5.4 \times 10^{-4}$ to $9.3 \times 10^{-3} s^{-1}$,^{36, 77} and $R_{DIS} = 6 \times 10^5 M^{-1} s^{-1}$ at

PH = 7¹⁹, the $\frac{K_{REC}^2}{K_{DIS}}$ is (4.86×10^{-13} - 14.4×10^{-11}). Giving the curve below when

comparing with simple fit without considering the branching ratio. Half saturation stays the same under above conditions (33uM)

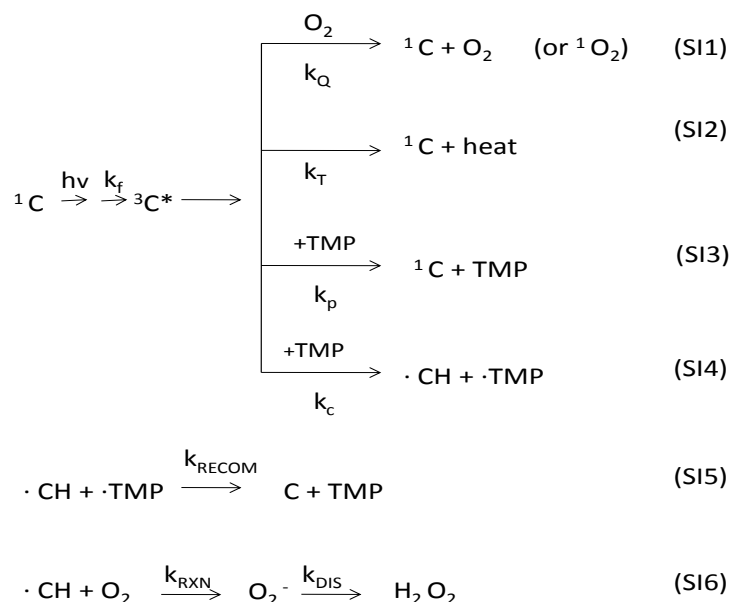
SRFA oxygen dependence simple fit and $c = R_{REC}^2/R_{DIS}$ from 4.86×10^{-13} - 14.4×10^{-11}



Since the back reaction rate constant are so small, this branching ratio does not shift the dependence as well as the half saturation with any significance.

Appendix 2

Derivation of Equation 4.9



Above scheme shows the transformation of a ground state chromophore, ${}^1\text{C}$, to a triplet excited state chromophore, ${}^3\text{C}^*$ with rate of formation of the excited triplet state k_f , under a constant flux of photons from irradiation. Transformation of ${}^3\text{C}^*$ to the ground state can occur through quenching by molecular oxygen (O_2) at rate k_Q (Eqn.SI1), radiationless transition to the ground state at rate k_T (Eqn. SI2), and physical or chemical reaction with the external donor with rate k_p and k_c , respectively (Eqn. SI3-4). The radical intermediates produced by reaction SI4 can recombine at rate k_{RECON} (Eqn.SI5) or be further oxidized by molecular oxygen to form superoxide rate k_{RXN} , and subsequently hydrogen peroxide (Eqn.SI6).

From above scheme, the $R_{\text{H}_2\text{O}_2}$ can be expressed as

$$\begin{aligned}
 R_{\text{H}_2\text{O}_2} &= \frac{d_{\text{H}_2\text{O}_2}}{dt} = 0.5 \frac{d_{\text{O}_2^-}}{dt} \\
 &= 0.5k_{\text{RXN}}[\cdot\text{CH}][\text{O}_2]
 \end{aligned} \tag{SI7}$$

The steady state concentration of the radical $[\cdot CH]$ is shown in Eqn SI8

$$0 = \frac{d[\cdot CH]}{dt} = k_C {}^3C^*[TMP][\cdot CH] - (k_{RECOM}[\cdot TMP] + Rrxn[O_2])[\cdot CH] \quad (SI8)$$

$$[\cdot CH] = \frac{k_C[TMP][{}^3C^*]}{(k_{RECOM}[\cdot TMP] + Rrxn[O_2])} \quad (SI9)$$

where the steady state concentration of the excited triplet state chromophore is given by Eqn. SI10,

$$0 = \frac{d[{}^3C^*]}{dt} = k_f - k_Q[O_2][{}^3C^*] - k_T[{}^3C^*] - k_P[TMP][{}^3C^*] - k_C[TMP][{}^3C^*] \quad (SI10)$$

$$[{}^3C^*] = \frac{k_f}{k_T + k_Q[O_2] + (k_P + k_C)[TMP]} \quad (SI11)$$

Eqn 12 is derived by substitutions of equation SI9 and SI11 into equation SI7,

$$\begin{aligned} \frac{d_{H2O2}}{dt} &= 0.5 \frac{d_{O_2^-}}{dt} \\ &= \frac{0.5k_f k_C k_{RXN}[O_2][TMP]}{(k_T + k_Q[O_2] + (k_P + k_C)[TMP])(k_{RECOM}[\cdot TMP] + Rrxn[O_2])} \quad (SI12) \end{aligned}$$

The branching ratio for the chemical and physical reaction of TMP with ${}^3C^*$ can be

represented by $= \frac{k_C}{(k_P + k_C)}$, where the sum of the reaction is defined as the total rate

constant for TMP reaction, such that $k_{TMP} = k_C + k_P$. The terms $k_{RECOM}[\cdot TMP]$ are combined into a simple lifetime term k_{REC} , with the resulting expression is shown in equation SI13.

$$\frac{d_{H2O2}}{dt} = 0.5 \frac{d_{O_2^-}}{dt} = \frac{0.5k_f \phi k_{TMP} [TMP]}{(k_T + k_Q[O_2] + k_{TMP}[TMP])} \times \frac{1}{(1 + \frac{k_{REC}}{k_{RXN}} \times \frac{1}{[O_2]})} \quad (SI12)$$

Bibliography

1. Van Baalen, C.; Marler, J. E., Occurrence of hydrogen peroxide in sea water. *Nature* **1966**, *211* (5052), 951-951.
2. Kok, G. L., Measurements of hydrogen peroxide in rainwater. *Atmospheric Environment (1967)* **1980**, *14* (6), 653-656.
3. V.E.Sinel'nikov, G. Z., W.J.Cooper, R.G.Zika, R.G.Petasne, Experimental study of separate stages in the mechanism of oxidation of organic matter in waters by a chemiluminescent method. In *American Water Works Association Conference* Miami Beach, 1971; pp 16-21.
4. Zika, R. G.; Moffett, J. W.; Petasne, R. G.; Cooper, W. J.; Saltzman, E. S., Spatial and temporal variations of hydrogen peroxide in Gulf of Mexico waters. *Geochimica et Cosmochimica Acta* **1985**, *49* (5), 1173-1184.
5. Holm, T. R.; George, G. K.; Barcelona, M. J., Fluorometric determination of hydrogen peroxide in groundwater. *Analytical Chemistry* **1987**, *59* (4), 582-586.
6. Draper, W.; Crosby, D., The photochemical generation of hydrogen peroxide in natural waters. *Arch. Environ. Contam. Toxicol.* **1983**, *12* (1), 121-126.
7. Willey, J.; Kieber, R.; Lancaster, R., Coastal rainwater hydrogen peroxide: Concentration and deposition. *J Atmos Chem* **1996**, *25* (2), 149-165.
8. Cooper, W. J.; Lean, D. R. S., Hydrogen peroxide concentration in a northern lake: photochemical formation and diel variability. *Environmental Science & Technology* **1989**, *23* (11), 1425-1428.
9. Hellpointner, E., Gab, S., Detection of methyl, hydroxymethyl and hydroxyethyl hydroperoxides in air and precipitation. *Nature* **1989**, *337* (6208), 4.

10. Miller, W. L.; Kester, D. R., Peroxide variations in the Sargasso Sea. *Marine Chemistry* **1994**, *48* (1), 17-29.
11. Moffett, J. W.; Zika, R. G., Reaction kinetics of hydrogen peroxide with copper and iron in seawater. *Environmental Science & Technology* **1987**, *21* (8), 804-810.
12. Miller, W. L.; King, D. W.; Lin, J.; Kester, D. R., Photochemical redox cycling of iron in coastal seawater. *Marine Chemistry* **1995**, *50* (1-4), 63-77.
13. Benedetti, M. F.; Van, R. W. H.; Koopal, L. K.; Kinniburgh, D. G.; Gooddy, D. C.; Milne, C. J., Metal ion binding by natural organic matter: from the model to the field. *Geochim. Cosmochim. Acta* **1996**, *60*, 2503-2513.
14. Draper, W. M.; Crosby, D. G., Solar photooxidation of pesticides in dilute hydrogen peroxide. *Journal of Agricultural and Food Chemistry* **1984**, *32* (2), 231-237.
15. Hoffmann, M.; Edwards, J. O., Kinetics and mechanism of the oxidation of thiourea and N,N'-dialkylthioureas by hydrogen peroxide. *Inorganic Chemistry* **1977**, *16* (12), 3333-3338.
16. Zika, R. G.; Cooper, W. J., *Photochemistry of environmental aquatic systems*. 1987; p Medium: X; Size: Pages: 288.
17. Cooper, W. J.; Zika, R. G., Photochemical formation of hydrogen peroxide in surface and ground waters exposed to sunlight. *Science* **1983**, *220* (4598), 711-712.
18. Zika, R.; Saltzman, E.; Chameides, W. L.; Davis, D. D., H₂O₂ levels in rainwater collected in south Florida and the Bahama Islands. *Journal of Geophysical Research: Oceans* **1982**, *87* (C7), 5015-5017.

19. Cooper, W. J.; Zika, R. G.; Petasne, R. G.; Plane, J. M. C., Photochemical formation of hydrogen peroxide in natural waters exposed to sunlight. *Environmental Science & Technology* **1988**, 22 (10), 1156-1160.
20. Gerringa, L. J. A.; Rijkenberg, M. J. A.; Timmermans, R.; Buma, A. G. J., The influence of solar ultraviolet radiation on the photochemical production of H₂O₂ in the equatorial Atlantic Ocean. *Journal of Sea Research* **2004**, 51 (1), 3-10.
21. O'Sullivan, D. W.; Neale, P. J.; Coffin, R. B.; Boyd, T. J.; Osburn, S. L., Photochemical production of hydrogen peroxide and methylhydroperoxide in coastal waters. *Marine Chemistry* **2005**, 97 (1-2), 14-33.
22. Hanson, A. K.; Tindale, N. W.; Abdel-Moati, M. A. R., An Equatorial Pacific rain event: influence on the distribution of iron and hydrogen peroxide in surface waters. *Marine Chemistry* **2001**, 75 (1-2), 69-88.
23. Kieber, R.; Cooper, W.; Willey, J.; Avery, G. B., Jr., Hydrogen Peroxide at the Bermuda Atlantic Time Series Station. Part 1: Temporal Variability of Atmospheric Hydrogen Peroxide and Its Influence on Seawater Concentrations. *J Atmos Chem* **2001**, 39 (1), 1-13.
24. Stevens, S. E.; Patterson, C. O. P.; Myers, J., The production of hydrogen peroxide by blue-green algae: a survey 1. *Journal of Phycology* **1973**, 9 (4), 427-430.
25. Xenopoulos, M. A.; Bird, D. F., Effect of Acute Exposure to Hydrogen Peroxide on the Production of Phytoplankton and Bacterioplankton in a Mesohumic Lake. *Photochemistry and Photobiology* **1997**, 66 (4), 471-478.
26. Bricaud A, M. A., Prieur L, Absorption by dissolved organic matter of the sea (yellow substance) in the UV and Visible domains. . *Limnol Oceanogr* **1981**, 26, 11.

27. Thurman, E., *Structural study of humic substances: new approaches and method*. Ann Arbor Science: Ann Arbor, 1983; p 1-23.
28. Sutton, R.; Sposito, G., Molecular Structure in Soil Humic Substances: The New View. *Environmental Science & Technology* **2005**, *39* (23), 9009-9015.
29. Aguer, J. P.; Richard, C.; Trubetskaya, O.; Trubetskoj, O.; Lévêque, J.; Andreux, F., Photoinductive efficiency of soil extracted humic and fulvic acids. *Chemosphere* **2002**, *49* (3), 259-262.
30. Del Vecchio, R.; Blough, N. V., Spatial and seasonal distribution of chromophoric dissolved organic matter and dissolved organic carbon in the Middle Atlantic Bight. *Marine Chemistry* **2004**, *89* (1-4), 169-187.
31. Kujawinski, E. B.; Longnecker, K.; Blough, N. V.; Vecchio, R. D.; Finlay, L.; Kitner, J. B.; Giovannoni, S. J., Identification of possible source markers in marine dissolved organic matter using ultrahigh resolution mass spectrometry. *Geochimica et Cosmochimica Acta* **2009**, *73* (15), 4384-4399.
32. Blough, N. V. In *Photochemistry in the sea-surface microlayer*, Cambridge University Press: 1997; pp 383-424.
33. Blough, N. V.; Zepp, R. G., Reactive oxygen species in natural waters. *Struct. Energ. React. Chem. Ser.* **1995**, *2*, 280-333.
34. Vione, D.; Falletti, G.; Maurino, V.; Minero, C.; Pelizzetti, E.; Malandrino, M.; Ajassa, R.; Olariu, R.-I.; Arsene, C., Sources and Sinks of Hydroxyl Radicals upon Irradiation of Natural Water Samples. *Environmental Science & Technology* **2006**, *40* (12), 3775-3781.

35. Zepp, R. G.; Schlotzhauer, P. F.; Sink, R. M., Photosensitized transformations involving electronic energy transfer in natural waters: role of humic substances. *Environmental Science & Technology* **1985**, *19* (1), 74-81.
36. Petasne, R. G.; Zika, R. G., Fate of superoxide in coastal sea water. *Nature (London)* **1987**, *325*, 516-18.
37. Konstantinou, I. K.; Zarkadis, A. K.; Albanis, T. A., Photodegradation of Selected Herbicides in Various Natural Waters and Soils under Environmental Conditions. *J. Environ. Qual.* **2001**, *30* (1), 121-130.
38. Hudson, N.; Baker, A.; Reynolds, D., Fluorescence analysis of dissolved organic matter in natural, waste and polluted waters—a review. *River Research and Applications* **2007**, *23* (6), 631-649.
39. Richard, C.; Canonica, S., Aquatic Phototransformation of Organic Contaminants Induced by Coloured Dissolved Natural Organic Matter. In *Environmental Photochemistry Part II*, Boule, P.; Bahnemann, D. W.; Robertson, P. K. J., Eds. Springer Berlin Heidelberg: 2005; Vol. 2M, pp 299-323.
40. Zhu, Q.; Lian, Y.; Thyagarajan, S.; Rokita, S. E.; Karlin, K. D.; Blough, N. V., Hydrogen Peroxide and Dioxygen Activation by Dinuclear Copper Complexes in Aqueous Solution: Hydroxyl Radical Production Initiated by Internal Electron Transfer. *Journal of the American Chemical Society* **2008**, *130* (20), 6304-6305.
41. Miller, W. L.; Zepp, R. G., Photochemical production of dissolved inorganic carbon from terrestrial organic matter: Significance to the oceanic organic carbon cycle. *Geophysical Research Letters* **1995**, *22* (4), 417-420.

42. Rutledge, S.; Campbell, D. I.; Baldocchi, D.; Schipper, L. A., Photodegradation leads to increased carbon dioxide losses from terrestrial organic matter. *Global Change Biology* **2010**, *16* (11), 3065-3074.
43. Anderson, T. R.; Williams, P. J. I. B., Modelling the Seasonal Cycle of Dissolved Organic Carbon at Station E1 in the English Channel. *Estuarine, Coastal and Shelf Science* **1998**, *46* (1), 93-109.
44. Fimmen, R. L.; Cory, R. M.; Chin, Y.-P.; Trouts, T. D.; McKnight, D. M., Probing the oxidation–reduction properties of terrestrially and microbially derived dissolved organic matter. *Geochimica et Cosmochimica Acta* **2007**, *71* (12), 3003-3015.
45. Abbt-Braun, G.; Lankes, U.; Frimmel, F., Structural characterization of aquatic humic substances – The need for a multiple method approach. *Aquat. Sci.* **2004**, *66* (2), 151-170.
46. Truong, H.; Lomnicki, S.; Dellinger, B., Potential for Misidentification of Environmentally Persistent Free Radicals as Molecular Pollutants in Particulate Matter. *Environmental Science & Technology* **2010**, *44* (6), 1933-1939.
47. Fiorentino, G.; Spaccini, R.; Piccolo, A., Separation of molecular constituents from a humic acid by solid-phase extraction following a transesterification reaction. *Talanta* **2006**, *68* (4), 1135-1142.
48. Vairavamurthy, M. A.; Maletic, D.; Wang, S.; Manowitz, B.; Eglinton, T.; Lyons, T., Characterization of Sulfur-Containing Functional Groups in Sedimentary Humic Substances by X-ray Absorption Near-Edge Structure Spectroscopy. *Energy & Fuels* **1997**, *11* (3), 546-553.

49. Simpson, A. J.; Simpson, M. J., Nuclear Magnetic Resonance Analysis of Natural Organic Matter. In *Biophysico-Chemical Processes Involving Natural Nonliving Organic Matter in Environmental Systems*, John Wiley & Sons, Inc.: 2009; pp 589-650.
50. Martin-Neto, L.; Milori, D. M. B. P.; Da Silva, W. T. L.; Simões, M. L., EPR, FTIR, Raman, UV–Visible Absorption, and Fluorescence Spectroscopies in Studies of NOM. In *Biophysico-Chemical Processes Involving Natural Nonliving Organic Matter in Environmental Systems*, John Wiley & Sons, Inc.: 2009; pp 651-727.
51. Redwood, P. S.; Lead, J. R.; Harrison, R. M.; Jones, I. P.; Stoll, S., Characterization of Humic Substances by Environmental Scanning Electron Microscopy. *Environmental Science & Technology* **2005**, 39 (7), 1962-1966.
52. Mobed, J. J.; Hemmingsen, S. L.; Autry, J. L.; McGown, L. B., Fluorescence Characterization of IHSS Humic Substances: Total Luminescence Spectra with Absorbance Correction. *Environmental Science & Technology* **1996**, 30 (10), 3061-3065.
53. Garrison, A. W.; Schmitt, P.; Kettrup, A., Capillary electrophoresis for the characterization of humic substances. *Water Research* **1995**, 29 (9), 2149-2159.
54. Kowalczyk, P.; Cooper, W.; Whitehead, R.; Durako, M.; Sheldon, W., Characterization of CDOM in an organic-rich river and surrounding coastal ocean in the South Atlantic Bight. *Aquat. Sci.* **2003**, 65 (4), 384-401.
55. Helms, J. R. S., A. Ritchie, J.D. Minor, E.C, Absorption spectral slopes and slope ratios as indicators of molecular weight, source, and photobleaching of chromophoric dissolved organic matter. *Limnol. Oceanogr.* **2008**, 53 (3), 14.

56. Schreiber, B.; Brinkmann, T.; Schmalz, V.; Worch, E., Adsorption of dissolved organic matter onto activated carbon—the influence of temperature, absorption wavelength, and molecular size. *Water Research* **2005**, *39* (15), 3449-3456.
57. Kowalczyk, P.; Stoń-Egiert, J.; Cooper, W. J.; Whitehead, R. F.; Durako, M. J., Characterization of chromophoric dissolved organic matter (CDOM) in the Baltic Sea by excitation emission matrix fluorescence spectroscopy. *Marine Chemistry* **2005**, *96* (3–4), 273-292.
58. Kieber, R.; Willey, J.; Whitehead, R.; Reid, S., Photobleaching of chromophoric dissolved organic matter (CDOM) in rainwater. *J Atmos Chem* **2007**, *58* (3), 219-235.
59. Boehme, J. R.; Coble, P. G., Characterization of Colored Dissolved Organic Matter Using High-Energy Laser Fragmentation. *Environmental Science & Technology* **2000**, *34* (15), 3283-3290.
60. Stedmon, C. A.; Markager, S.; Bro, R., Tracing dissolved organic matter in aquatic environments using a new approach to fluorescence spectroscopy. *Marine Chemistry* **2003**, *82* (3–4), 239-254.
61. Del Vecchio, R.; Blough, N. V., Photobleaching of chromophoric dissolved organic matter in natural waters: kinetics and modeling. *Marine Chemistry* **2002**, *78* (4), 231-253.
62. Power, J. F.; Langford, C. H., Optical absorbance of dissolved organic matter in natural water studies using the thermal lens effect. *Analytical Chemistry* **1988**, *60* (9), 842-846.
63. Ariese, F.; van Assema, S.; Gooijer, C.; Bruccoleri, A.; Langford, C., Comparison of Laurentian Fulvic Acid luminescence with that of the hydroquinone/quinone model

- system: Evidence from low temperature fluorescence studies and EPR spectroscopy. *Aquat. Sci.* **2004**, *66* (1), 86-94.
64. Sharpless, C. M.; Blough, N. V., The importance of charge-transfer interactions in determining chromophoric dissolved organic matter (CDOM) optical and photochemical properties. *Environmental Science: Processes & Impacts* **2014**.
65. Goldstone, J. V.; Del Vecchio, R.; Blough, N. V.; Voelker, B. M., A Multicomponent Model of Chromophoric Dissolved Organic Matter Photobleaching¶§. *Photochemistry and Photobiology* **2004**, *80* (1), 52-60.
66. Del Vecchio, R.; Blough, N. V., On the origin of the optical properties of humic substances. *Environmental Science & Technology* **2004**, *38* (14), 3885-3891.
67. Boyle, E. S.; Guerriero, N.; Thiallet, A.; Del Vecchio, R.; Blough, N. V., Optical properties of humic substances and CDOM: relation to structure. *Environmental Science & Technology* **2009**, *43* (7), 2262-2268.
68. Cooper, W. J.; Zika, R. G.; Petasne, R. G.; A.M., F. Sunlight-induced photochemistry of humic substances in natural waters: major reactive species *In Aquatic Humic substances* [Online], 1988.
69. Hoigne, J.; Faust, B. C.; Haag, W.; Scully, C.; Zepp, R. G. Aquatic humic substances as sources and sinks of photochemically produced transient reactants *In Aquatic Humic substances* [Online], 1988.
70. Nurmi, J. T.; Tratnyek, P. G., Electrochemical Properties of Natural Organic Matter (NOM), Fractions of NOM, and Model Biogeochemical Electron Shuttles. *Environmental Science & Technology* **2002**, *36* (4), 617-624.

71. Struyk, Z.; Sposito, G., Redox properties of standard humic acids. *Geoderma* **2001**, *102* (3–4), 329-346.
72. Scott, D. T.; McKnight, D. M.; Blunt-Harris, E. L.; Kolesar, S. E.; Lovley, D. R., Quinone Moieties Act as Electron Acceptors in the Reduction of Humic Substances by Humics-Reducing Microorganisms. *Environmental Science & Technology* **1998**, *32* (19), 2984-2989.
73. Maximov, O. B.; Glebko, L. I., Quinoid groups in humic acids. *Geoderma* **1974**, *11* (1), 17-28.
74. Ratasuk, N.; Nanny, M. A., Characterization and Quantification of Reversible Redox Sites in Humic Substances. *Environmental Science & Technology* **2007**, *41* (22), 7844-7850.
75. Paul, A.; Stosser, R.; Zehl, A.; Zwirnmann, E.; Vogt, R. D.; Steinberg, C. E. W., Nature and abundance of organic radicals in natural organic matter: Effect of pH and irradiation. *Environmental Science & Technology* **2006**, *40* (19), 5897-5903.
76. Garg, S.; Rose, A. L.; Waite, T. D., Production of Reactive Oxygen Species on Photolysis of Dilute Aqueous Quinone Solutions. *Photochemistry and Photobiology* **2007**, *83* (4), 904-913.
77. Waite, T. D.; Garg, S.; Rose, A. L., Photochemical production of superoxide and hydrogen peroxide from natural organic matter. *Geochimica et Cosmochimica Acta* **2011**, *75* (15), 4310-4320.
78. Ma, J. H.; Del Vecchio, R.; Golanoski, K. S.; Boyle, E. S.; Blough, N. V., Optical properties of humic substances and CDOM: effects of borohydride reduction. *Environmental Science & Technology* **2010**, *44* (14), 5395-5402.

79. Andrew, A. A.; Del Vecchio, R.; Subramaniam, A.; Blough, N. V., Chromophoric dissolved organic matter (CDOM) in the Equatorial Atlantic Ocean: Optical properties and their relation to CDOM structure and source. *Marine Chemistry* **2013**, *148* (0), 33-43.
80. Baxter, R. M. C., John H., Evidence for photochemical generation of superoxide ion in humic waters. *Nature* **1983**, *306* (4943), 575.
81. Bielski, B. H. J.; Cabelli, D. E.; Arudi, R. L.; Ross, A. B., Reactivity of HO₂/O⁻² Radicals in Aqueous Solution. *Journal of Physical and Chemical Reference Data* **1985**, *14* (4), 1041-1100.
82. Zepp, R. G.; Braun, A. M.; Hoigne, J.; Leenheer, J. A., Photoproduction of hydrated electrons from natural organic solutes in aquatic environments. *Environmental Science & Technology* **1987**, *21* (5), 485-490.
83. Thomas-Smith, T. E.; Blough, N. V., Photoproduction of Hydrated Electron from Constituents of Natural Waters. *Environ. Sci. Technol.* **2001**, *35*, 2721-2726.
84. Cooper William, J.; Shao, C.; Lean David, R. S.; Gordon Andrew, S.; Scully Frank, E., Factors Affecting the Distribution of H₂O₂ in Surface Waters. In *Environmental Chemistry of Lakes and Reservoirs*, American Chemical Society: 1994; Vol. 237, pp 391-422.
85. Dalrymple, R. M.; Carfagno, A. K.; Sharpless, C. M., Correlations between dissolved organic matter optical properties and quantum yields of singlet oxygen and hydrogen peroxide. *Environmental Science & Technology* **2010**, *44* (15), 5824-5829.

86. Cory, R. M.; McNeill, K.; Cotner, J. P.; Amado, A.; Purcell, J. M.; Marshall, A. G., Singlet Oxygen in the Coupled Photochemical and Biochemical Oxidation of Dissolved Organic Matter. *Environ. Sci. Technol.* **2010**, *44*, 3683-3689.
87. Garg, S.; Rose, A. L.; Waite, T. D., Photochemical production of superoxide and hydrogen peroxide from natural organic matter. *Geochimica et Cosmochimica Acta* **2011**, *75* (15), 4310-4320.
88. Golanoski, K. S.; Fang, S.; Del Vecchio, R.; Blough, N. V., Investigating the mechanism of phenol photooxidation by humic substances. *Environmental Science & Technology* **2012**, *46* (7), 3912-3920.
89. Mignone, R. A.; Martin, M. V.; Morán Vieyra, F. E.; Palazzi, V. I.; López de Mishima, B.; Mártire, D. O.; Borsarelli, C. D., Modulation of optical properties of dissolved humic substances by their molecular complexity. *Photochemistry and Photobiology* **2012**, *88* (4), 792-800.
90. Martin, J. H.; Fitzwater, S. E.; Gordon, R. M., Iron deficiency limits phytoplankton growth in Antarctic waters. *Global Biogeochemical Cycles* **1990**, *4* (1), 5-12.
91. Martin, J. H., Iron in Antarctic waters. *Nature* **1990**, *345*, 3.
92. Johnson, K. S.; Coale, K. H.; Elrod, V. A.; Tindale, N. W., Iron photochemistry in seawater from the equatorial Pacific. *Marine Chemistry* **1994**, *46* (4), 319-334.
93. King, D. W.; Lounsbury, H. A.; Millero, F. J., Rates and Mechanism of Fe(II) Oxidation at Nanomolar Total Iron Concentrations. *Environmental Science & Technology* **1995**, *29* (3), 818-824.

94. Rose, A. L.; Waite, T. D., Kinetic Model for Fe(II) Oxidation in Seawater in the Absence and Presence of Natural Organic Matter. *Environmental Science & Technology* **2002**, *36* (3), 433-444.
95. Rose, A. L.; Waite, T. D., Kinetics of iron complexation by dissolved natural organic matter in coastal waters. *Marine Chemistry* **2003**, *84* (1-2), 85-103.
96. King, D. W.; Cooper, W. J.; Rusak, S. A.; Peake, B. M.; Kiddle, J. J.; O'Sullivan, D. W.; Melamed, M. L.; Morgan, C. R.; Theberge, S. M., Flow Injection Analysis of H₂O₂ in Natural Waters Using Acridinium Ester Chemiluminescence: Method Development and Optimization Using a Kinetic Model. *Anal. Chem.* 4169-4176.
97. Miller, W. L.; Kester, D. R., Hydrogen peroxide measurement in seawater by (p-hydroxyphenyl)acetic acid dimerization. *Analytical Chemistry* **1988**, *60* (24), 2711-2715.
98. Kieber, R. J.; Helz, G. R., Two-method verification of hydrogen peroxide determinations in natural waters. *Analytical Chemistry* **1986**, *58* (11), 2312-2315.
99. Blough, N. V., Electron paramagnetic resonance measurements of photochemical radical production in humic substances. 1. Effects of oxygen and charge on radical scavenging by nitroxides. *Environ. Sci. Technol.* **1988**, *22*, 77-82.
100. Jia, M.; Tang, Y.; Lam, Y. F.; Green, S. A.; Blough, N. V., Prefluorescent nitroxide probe for the highly sensitive determination of peroxy and other radical oxidants. *Analytical Chemistry* **2009**, *81* (19), 8033-8040.
101. Li, B. B.; Gutierrez, P. L.; Blough, N. V., Trace determination of hydroxyl radical using fluorescence detection. *Method Enzymol* **1999**, *300*, 202-216.

102. Kieber, D. J.; Blough, N. V., Determination of carbon-centered radicals in aqueous-solution by liquid-chromatography with fluorescence detection. *Analytical Chemistry* **1990**, 62 (21), 2275-2283.
103. Johnson, C. G.; Caron, S.; Blough, N. V., Combined liquid chromatography mass spectrometry of the radical adducts of a fluorescamine-derivatized nitroxide. *Analytical Chemistry* **1996**, 68 (5), 867-872.
104. Blough, N. V.; Simpson, D. J., Chemically mediated fluorescence yield switching in nitroxide fluorophore adducts - optical sensors of radical redox reactions. *Journal of the American Chemical Society* **1988**, 110 (6), 1915-1917.
105. Swallow, A. J., Hydrated electrons in seawater. *Nature* **1969**, 222 (5191), 369-370.
106. Clark, C. D.; De Bruyn, W. J.; Jones, J. G., Photochemical production of hydrogen peroxide in size-fractionated Southern California coastal waters. *Chemosphere* **2009**, 76 (1), 141-146.
107. Micinski, E.; Ball, L. A.; Zafiriou, O. C., Photochemical oxygen activation: superoxide radical detection and production rates in the Eastern Caribbean. *J. Geophys. Res.* **1993**, 98 (C2), 2299-2306.
108. Petasne, R. G.; Zika, R. G., Fate of superoxide in coastal sea water. *Nature* **1987**, 325 (6104), 516-518.
109. Rose, A. L.; Waite, T. D., Reduction of organically complexed ferric iron by superoxide in a simulated natural water. *Environmental Science & Technology* **2005**, 39 (8), 2645-2650.

110. Rose, A. L.; Waite, T. D., Role of superoxide in the photochemical reduction of iron in seawater. *Geochimica et Cosmochimica Acta* **2006**, *70* (15), 3869-3882.
111. Southworth, B. A.; Voelker, B. M., Hydroxyl radical production via the photo-Fenton reaction in the presence of fulvic acid. *Environmental Science & Technology* **2003**, *37* (6), 1130-1136.
112. White, E. M.; Vaughan, P. P.; Zepp, R. G., Role of the photo-Fenton reaction in the production of hydroxyl radicals and photobleaching of colored dissolved organic matter in a coastal river of the southeastern United States. *Aquat. Sci.* **2003**, *65* (4), 402-414.
113. Vermilyea, A. W.; Voelker, B. M., Photo-Fenton reaction at near neutral pH. *Environmental Science & Technology* **2009**, *43* (18), 6927-6933.
114. Heller, M. I.; Croot, P. L., Superoxide decay as a probe for speciation changes during dust dissolution in Tropical Atlantic surface waters near Cape Verde. *Mar. Chem.* **2011**, *126*, 37-55.
115. Heller, M. I.; Croot, P. L., Superoxide decay kinetics in the Southern Ocean. *Environ. Sci. Technol.* **2010**, *44*, 191-196.
116. Thomas-Smith, T. E.; Blough, N. V., Photoproduction of hydrated electron from constituents of natural waters. *Environmental Science & Technology* **2001**, *35* (13), 2721-2726.
117. Cory, R. M.; McNeill, K.; Cotner, J. P.; Amado, A.; Purcell, J. M.; Marshall, A. G., Singlet oxygen in the coupled photochemical and biochemical oxidation of dissolved organic matter. *Environmental Science & Technology* **2010**, *44* (10), 3683-3689.

118. Li, B. B.; Gutierrez, P. L.; Blough, N. V., Trace determination of hydroxyl radical in biological systems. *Analytical Chemistry* **1997**, *69* (21), 4295-4302.
119. Kujawinski, E. B.; Del Vecchio, R.; Blough, N. V.; Klein, G. C.; Marshall, A. G., Probing molecular-level transformations of dissolved organic matter: insights on photochemical degradation and protozoan modification of DOM from electrospray ionization Fourier transform ion cyclotron resonance mass spectrometry. *Marine Chemistry* **2004**, *92* (1-4), 23-37.
120. Miller, G. W.; Morgan, C. A.; Kieber, D. J.; King, D. W.; Snow, J. A.; Heikes, B. G.; Mopper, K.; Kiddle, J. J., Hydrogen peroxide method intercomparison study in seawater. *Marine Chemistry* **2005**, *97* (1-2), 4-13.
121. Kieber, D. J.; Blough, N. V., Fluorescence detection of carbon-centered radicals in aqueous-solution. *Free Radical Res Com* **1990**, *10* (1-2), 109-117.
122. Parker, C. A., A new sensitive chemical actinometer .1. some trials with potassium ferrioxalate. *Proc R Soc Lon Ser-A* **1953**, *220* (1140), 104-116.
123. Hatchard, C. G.; Parker, C. A., A new sensitive chemical actinometer .2. potassium ferrioxalate as a standard chemical actinometer. *Proc R Soc Lon Ser-A* **1956**, *235* (1203), 518-536.
124. Scott, W. W.; Webb, S. K., Determination of minute amounts of boron in soils. *Industrial & Engineering Chemistry Analytical Edition* **1932**, *4* (2), 180-181.
125. Lytle, D. A.; Jensen, E. H.; Struck, W. A., A simple volumetric assay for sodium borohydride. *Analytical Chemistry* **1952**, *24* (11), 1843-1844.

126. Sharpless, C. M., Lifetimes of triplet dissolved natural organic matter (DOM) and the effect of NaBH₄ reduction on singlet oxygen quantum yields: implications for DOM photophysics. *Environmental Science & Technology* **2012**, 46 (8), 4466-4473.
127. Andrews, S. S., Photochemical oxygen consumption in marine waters: A major sink for colored dissolved organic matter? *Limnol. Oceanogr.* **2000**, 45 (2), 267-277.
128. Sikorski, R. J.; Zika, R. G., Modeling mixed-layer photochemistry of H₂O₂: physical and chemical modeling of distribution. *J. Geophys. Res.* **1993**, 98 (C2), 2329-2340.
129. Maillard, B.; Ingold, K. U.; Scaiano, J. C., Rate constants for the reactions of free radicals with oxygen in solution. *Journal of the American Chemical Society* **1983**, 105 (15), 5095-5099.
130. Gerlock, J. L.; Zacmanidis, P. J.; Bauer, D. R.; Simpson, D. J.; Blough, N. V.; Salmeen, I. T., Fluorescence detection of free-radicals by nitroxide scavenging. *Free Radical Res Com* **1990**, 10 (1-2), 119-121.
131. Loeff, I.; Treinin, A.; Linschitz, H., The photochemistry of 9,10-anthraquinone-2-sulfonate in solution. 2. Effects of inorganic anions: quenching vs. radical formation at moderate and high anion concentrations. *The Journal of Physical Chemistry* **1984**, 88 (21), 4931-4937.
132. Jammoul, A. S. D., S.; D'Anna, B.; and George, C., Photoinduced oxidation of sea salt halides by aromatic ketones. *Atmospheric Chemistry and Physics* **2009**, 9 (2), 7681-7706.
133. Carroll, F. A., *Perspectives on Structure and Mechanism in Organic Chemistry*. Brooks/Cole Publishing Company, Pacific Grove, CA 1998.

134. Koziar, J. C.; Cowan, D. O., Photochemical heavy-atom effects. *Accounts of chemical research* **1978**, *11*.
135. Treinin, A.; Loeff, I.; Hurley, J. K.; Linschitz, H., Charge-transfer interactions of excited molecules with inorganic anions: the role of spin-orbit coupling in controlling net electron transfer. *Chemical Physics Letters* **1983**, *95* (4–5), 333-338.
136. Grebel, J. E.; Pignatello, J. J.; Song, W.; Cooper, W. J.; Mitch, W. A., Impact of halides on the photobleaching of dissolved organic matter. *Marine Chemistry* **2009**, *115* (1–2), 134-144.
137. Grebel, J. E.; Pignatello, J. J.; Mitch, W. A., Sorbic acid as a quantitative probe for the formation, scavenging and steady-state concentrations of the triplet-excited state of organic compounds. *Water Research* **2011**, *45* (19), 6535-6544.
138. Velosa, A. C.; Baader, W. J.; Stevani, C. V.; Mano, C. M.; Bechara, E. J. H., 1,3-Diene Probes for Detection of Triplet Carbonyls in Biological Systems. *Chemical Research in Toxicology* **2007**, *20* (8), 1162-1169.
139. Gan, D.; Jia, M.; Vaughan, P. P.; Falvey, D. E.; Blough, N. V., Aqueous photochemistry of methyl-benzoquinone. *J Phys Chem A* **2008**, *112* (13), 2803-2812.
140. Goerner, H., Photoprocesses of p-benzoquinones in aqueous solution. *J. Phys. Chem. A* **2003**, *107* 11587-11595.
141. Aeschbacher, M.; Sander, M.; Schwarzenbach, R. P., Novel electrochemical approach to assess the redox properties of humic substances. *Environmental Science & Technology* **2010**, *44* (1), 87-93.

142. Aguer, J.-P.; Tetegan, D.; Richard, C., Humic substances mediated phototransformation of 2,4,6-trimethylphenol: a catalytic reaction. *Photochemical & Photobiological Sciences* **2005**, 4 (6), 451-453.
143. Green, S. A.; Simpson, D. J.; Zhou, G.; Ho, P. S.; Blough, N. V., Intramolecular quenching of excited singlet states by stable nitroxyl radicals. *J. Am. Chem. Soc.* **1990**, 112, 7337-46.
144. Herbelin, S. E.; Blough, N. V., Intramolecular quenching of excited singlet states in a series of fluorescamine-derivatized nitroxides. *J Phys Chem B* **1998**, 102 (42), 8170-8176.
145. Zhang, Y.; Del Vecchio, R.; Blough, N. V., Investigating the Mechanism of Hydrogen Peroxide Photoproduction by Humic Substances. *Environmental Science & Technology* **2012**, 46 (21), 11836-11843.
146. Hodgson, J. L.; Namazian, M.; Bottle, S. E.; Coote, M. L., One-Electron Oxidation and Reduction Potentials of Nitroxide Antioxidants: A Theoretical Study. *The Journal of Physical Chemistry A* **2007**, 111 (51), 13595-13605.
147. Ilan, Y. A.; Czapski, G.; Meisel, D., The one-electron transfer redox potentials of free radicals. I. The oxygen/superoxide system. *Biochimica et Biophysica Acta (BBA) - Bioenergetics* **1976**, 430 (2), 209-224.
148. Mayhew, S. G., The Redox Potential of Dithionite and SO₂ from Equilibrium Reactions with Flavodoxins, Methyl Viologen and Hydrogen plus Hydrogenase. *European Journal of Biochemistry* **1978**, 85 (2), 535-547.

149. Dixon, M., The acceptor specificity of flavins and flavoproteins. I. Techniques for anaerobic spectrophotometry. *Biochimica et Biophysica Acta (BBA) - Bioenergetics* **1971**, 226 (2), 241-258.
150. Leaver, I.; Ramsay, G., E.S.R. of nitroxide radicals. II. Photosensitization of indoles, phenols, and thiols by a diphenylpyrazoline. *Australian Journal of Chemistry* **1969**, 22 (9), 1899-1904.
151. Moffett, J. W.; Zika, R. G., Reaction kinetics of hydrogen peroxide with copper and iron in seawater. *Environ. Sci. Technol.* **1987**, 804-10.
152. Wang, W.; Zafiriou, O. C.; Chan, I. Y.; Zepp, R. G.; Blough, N. V., Production of hydrated electrons from photoionization of dissolved organic matter in natural waters. *Environmental Science & Technology* **2007**, 41 (5), 1601-1607.
153. Zepp, R. G.; Braun, A. M.; Hoigne, J.; Leenheer, J. A., Photoproduction of hydrated electrons from natural organic solutes in aquatic environments. *Environ. Sci. Technol.* **1987**, 21., 485-90.
154. Canonica, S.; Jans, U.; Stemmler, K.; Hoigne, J., Transformation Kinetics of Phenols in Water: Photosensitization by Dissolved Natural Organic Material and Aromatic Ketones. *Environmental Science & Technology* **1995**, 29 (7), 1822-1831.
155. Canonica, S.; Hellrung, B.; Wirz, J., Oxidation of Phenols by Triplet Aromatic Ketones in Aqueous Solution. *The Journal of Physical Chemistry A* **2000**, 104 (6), 1226-1232.
156. Canonica, S., Oxidation of aquatic organic contaminants induced by excited triplet states. *Chimia* **2007**, 61 (10), 641-644.

157. Kujawinski, E. B.; Del Vecchio, R.; Blough, N. V.; Klein, G. C.; Marshall, A. G., Probing molecular-level transformations of dissolved organic matter: insights on photochemical degradation and protozoan modification of DOM from electrospray ionization Fourier transform ion cyclotron resonance mass spectrometry. *Marine Chemistry* **2004**, *92* (1-4), 23-37.
158. Klassen, N. V.; Marchington, D.; McGowan, H. C. E., H₂O₂ Determination by the I₃- Method and by KMnO₄ Titration. *Anal. Chem.* **1994**, *66*, 2921-5.